Chemical Vapor Deposition of β–SiC Thin Films on Si(100) in a Hot Wall Reactor

by

Chienchia Chiu

Dissertation submitted to the Faculty of the
Virginia Polytechnic Institute and State University
in partial fulfillment of the requirements for the degree of

Doctor of Philosophy

in

Materials Engineering Science

APPROVED:

Seshu B. Desu, Chairman

Ronald S. Gordon

David F. Cox

William T. Reynolds, Jr.

Guo–Quan Lu

January, 1994

Blacksburg, Virginia

Chemical Vapor Deposition of β–SiC Thin Films on Si(100) in a Hot Wall Reactor

by

Chienchia Chiu

Committee Chairman: Seshu B. Desu

Materials Engineering Science

(ABSTRACT)

A systematic method was developed for the deposition of β–SiC thin films on Si(100) substrates in a hot wall reactor, using low pressure chemical vapor deposition (LPCVD). Due to poor adhesion resulting from lattice mismatch and difference in thermal expansion coefficients between the β–SiC films and the Si(100) substrates, the feasibility of forming a SiC buffer layer on the Si(100) surface before beginning the chemical vapor deposition (CVD) process was investigated. The SiC buffer layers were formed with either a smooth or porous morphology. A nonporous Si(100) substrate with a 35Å thick SiC buffer layer was formed when the Si surface was heated at 1050° C in an atmosphere of C_2H_2 and H_2. A porous surface was obtained when the Si substrate was heated at 1000° C in C_2H_2 alone. The porous defects were correlated to the out–diffusion of Si in the carburizing process.

On smooth Si(100) substrates, polycrystalline and stoichiometric β–SiC thin films with the (111) planes paralleling the Si(100) substrates were grown from a CH_3SiCl_3 (MTS)–H_2 mixture at 1050° C. At high H_2/MTS ratios and/or low deposition pressures, no etching on the Si substrates of the β–SiC films was observed, resulting in a smooth topography. Degradation in film morphology,

changes in the preferred orientation, and etching of the Si substrates were observed at higher pressures, temperatures, and H_2/MTS ratios. The etching of the Si substrate was due to the out–diffusion of Si atoms from the substrate and the presence of Cl–containing radicals, which resulted from the decomposition of MTS molecules before arriving at the substrates. A model of the deposition mechanism is proposed which predicts the deposition rates in a hot wall CVD reactor and agrees very well with the experimental data.

On the Si(100) substrate with a porous topography, epitaxial β–SiC(100) thin films were grown from MTS–H_2 at 1150° C. The crystallinity of the deposited films was influenced by the deposition time. With increasing deposition time, rotational β–SiC(100) crystals and polycrystalline β–SiC with a highly preferred orientation of (100) and/or (111) were obtained. At a lower temperature of 1100° C, poor morphology and polycrystalline β–SiC thin films were observed.

Finally, a new approach to the calculation of the local equilibrium CVD phase diagrams, which represent the most stable phases above the substrates in a hot wall reactor, for SiC deposition from the MTS–H_2 gas mixture by coupling the depletion effects to the equilibrium thermodynamic computer code SOLGASMIX–PV. The calculated CVD phase diagrams were also compared with experimental and the literature data. Although the local equilibrium CVD phase diagrams predicted the deposition of single phase SiC better than established CVD phase diagrams, the experimental regions for depositing single phase SiC are larger than those calculated from local CVD phase diagrams. This may be because of the high linear velocity of the gas flux under low pressure and the polarity of the Si–containing intermediate species.

Acknowledgments

I would like to thank my dissertation advisor, Professor Seshu B. Desu, for his advice, patience, and support throughout this work, and for giving me this opportunity to work under his guideness for five years. I am also indebted to Professor Desu for giving me the freedom to work independently.

Many thanks also to my advisory committee members: Professor R.S. Gordon, Professor D.F. Cox, Professor W.T. Reynolds, Jr., and Professor G–Q Lu, for their reviewing and assistance for this manuscript. Special thanks to : Professor D.F. Cox for his insightful suggestions on surface analysis, and Professor W.T. Reynolds, Jr. for his assistance in TEM analysis.

I am also indebted to the Center for Composite Materials and Structure (CCMS) at Virginia Tech for partially supporting this research.

I would also like to thank all my colleagues and friends, who I met throughout my career of study at Virginia Tech. Sepcial thanks go to: Steve McCartney for his help in XPS, Sean W. King for his help in the experimental work on SiC buffer layers, Gang Chen and Dr. C.K. Kwok for their works in TEM analysis, Dr. Chien H. Peng for his help in FTIR, Dr. Ching Yi Tsai for his help in kinetic model and an excellect roomate for three years, Professor Chen for making SOLGASMIX–PV so friendly for the deposition of SiC, and Dilip Vijay for his unbelievable patience in helping me praparing my publications. Special thanks to all the member of the Thin Film Laboratory at the Department of Materials Science and Engineering: Gene Li, J–F Chang, W.C. Hendricks, Jie Si, Shi Tian, Dr. In Yoo, May Nyman, Justin Gaynor, Wei Pan, Ashraf Khan, Claire Chen, Zhiqi Xing, and many others for many interesting and critical discussions and being good

friends. I also like to thank Dr. T. Sun at the Department of Materials Science and Engineering for his help and encouragement through my career at Virginia Tech.

Finally, I wish to express my deepest love and appreciation to my family. Without their support and love, I could not have finished this work.

This work is dedicated to my parents.

Table of Contents

Chapter 1: INTRODUCTION

1.1 MOTIVATION

Silicon carbide (SiC), which exhibits closed–packed structure, exhibits a special one dimensional type of polymorphism call polytypism [1,2]. The polytypes are alike in the two dimensions of close–packed planes, but have different stacking sequences in the dimension perpendicular to these planes. More than 170 polytypes have been identified. The only cubic polytype of SiC crystallizes in the zincblende structure with the stacking sequence of covalently bonded tetrahedra (either SiC_4 or CSi_4), which can be described by the ABC notation. This structure is also designated as 3C– or β–SiC, where 3 refers to the number of planes in the periodic sequence. The additional hexagonal (H) and rhombohedral (R) polytypes, whose stacking sequences are ABAB, are collectively referred to as α–SiC. In general, the most common polytypes are 3C and 6H; however, 4H, 15R, and 2H have also been identified [3].

SiC has been considered as a material for working in harsh environmental conditions because of its highly stable thermal, mechanical, chemical, and electronic properties. Table 1.1 compares SiC (β– and α– forms) with traditional semiconductor materials (*e.g.* Si), SiC possesses a wide band gaps at 27° C, high values of saturated electron drift velocity, high breakdown electric field, and high thermal conductivity [4,5,6]. In fact, the electron transport characteristics of β–SiC over the temperature range of 27° C~730° C, predicted from theoretical calculations,

Table 1.1: Comparison of silicon carbide (SiC) with silicon (Si).

	Si	β-SiC(3C)	α-SiC(6H)
Bandgap, Eg (eV), at room temperature	1.1	2.2	2.9
Maximum operation Temp. (K)	600	1200	1580
Electron Mobility ($cm^2V^{-1}s^{-1}$)	1400	1000	400
Breakdown Field, E_B ($10^5 Vcm^{-1}$)	3	40	40
Thermal conductivity, k ($wcm^{-1}k^{-1}$) at room temp.	1.5	4.9	4.9
Dielectric constant, ε_r	11.8	9.7	10.0
Saturated Electron drift velocity, Vs (10^7 cms^{-1})	1.0	2.5	2.0
Johnson's Figure of Merit $(E_B V_S/\pi)^2$ (High Frequency & High Power)	$9.0x10^{23}$	$10240x10^{23}$	$6250x10^{23}$
Keyes' Figure of Merit (Switching Speed) $k \cdot (V_{sat}/\varepsilon_r)^{1/2}$	$13.8x10^2$	$80.3x10^2$	$70.7x10^2$
Available large diameter	8 in	1.187 in	1.187 in

are significantly greater than those obtained from α–SiC due to reduced phonon scattering in the cubic material [7]. Thus there is significant interest in β–SiC thin films for device applications. The motivation for current interest in β–SiC for electronic applications is based on its use in fabrication of high–temperature, high–frequency, high–power, and light–emitting devices. Devices that can be fabricated from SiC include blue LED's [8], thermistors, metal semiconductor field–effect transistors (MESFET) [5,9], and heterojunction bipolar transistors (HBTs) [10], as well as various types of diodes. Its intrinsic resistance to oxidation, corrosion, and creep at high temperatures also makes it a desirable protective coating for devices operating at elevated temperatures. The high thermal conductivity of SiC also indicates the potential for high density integration of SiC devices.

In general, single crystal β–SiC films have been grown primarily on monocrystalline Si or α–SiC substrates with different orientations using chemical vapor deposition (CVD). However, to grow β–SiC on α–SiC, size is limited because of the difficulty in obtaining single crystal α–SiC surfaces with a sufficiently large area, as shown in Table 1.1. Furthermore, the deposition temperatures and the cost are high for using α–SiC substrates to grow β–SiC thin films [11,12]. Single crystal silicon has been widely used as the substrates to grow β–SiC due to the easy availability of high purity, high quality silicon wafers. Unfortunately, growing β–SiC on silicon substrates has been hindered by the large mismatch (20%) in lattice constants and the differences in thermal expansion coefficients between the β–SiC film and the underlying silicon substrates [13]. Also, the deposition temperatures cannot exceed 1400° C, the low melting point of silicon. Nevertheless, the processes mentioned above were performed at high temperatures and in cold

wall reactors. The advantages in using a hot wall CVD reactor include (1) the ability to deposit thin films simultaneously upon many wafers and (2) the elimination of contamination from the susceptor by using a very low pressure (LPCVD) process [14]. However, other than the deposition of Si or Si:Ge, no single crystal material has been reported deposited by using this type of reactor in an ultrahigh vacuum ($< 10^{-4}$ Torr) [15].

The purpose of this study is to develop a systematic approach to depositing β–SiC thin films on Si(100) substrates in a hot wall reactor by using low pressure chemical vapor deposition (LPCVD) with a deposition pressure ranging from 1 to 8 Torr. In this report, the deposition processes were all performed in a hot wall LPCVD reactor and included the formation of the SiC buffer layers on Si(100) surfaces with a smooth or porous topography by using C_2H_2 and/or H_2 and the subsequent LPCVD procedure to deposit β–SiC from the gaseous mixture of MTS and H_2. It was shown that a single crystal β–SiC(100) thin film with a limited thickness (< 0.2 μm) can be obtained on a Si(100) substrate with a porous topography. Therefore, in a hot wall reactor, it is possible to deposit a single crystal β–SiC(100) film with a large area on a porous Si(100) substrate, as shown in Fig. 1.1.

1.2 LITERATURE REVIEW

Chemical vapor deposition (CVD) is usually defined as a process in which gaseous precursors are introduced into a reactor and a solid is obtained by chemical reactions which are, in general, heterogeneous between the gas and the solid phases. The schematic diagram for this process is shown in Fig. 1.2. As shown in Fig. 1.2, a

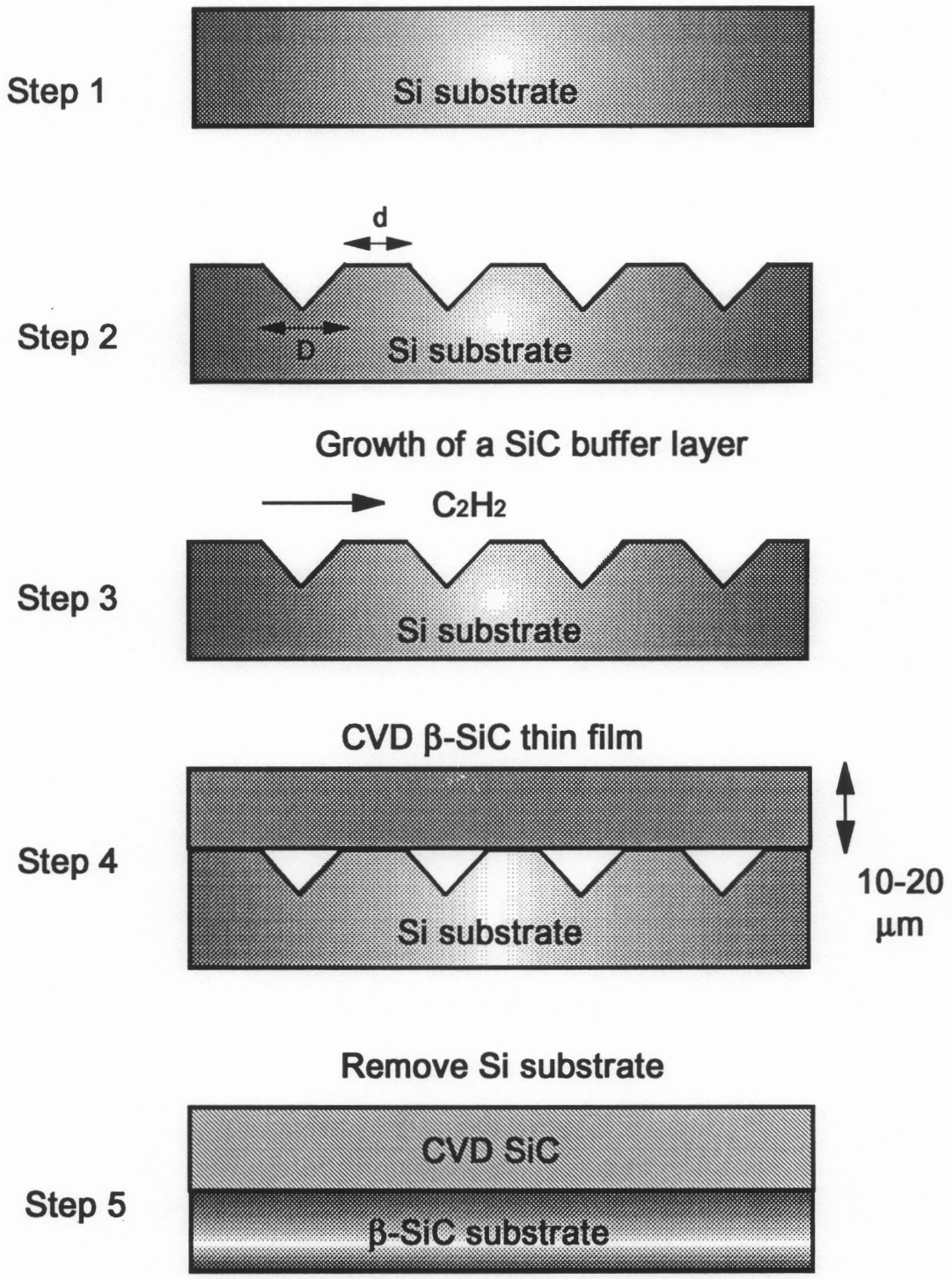

Fig. 1.1: The approach to deposit a β–SiC film with a large area.

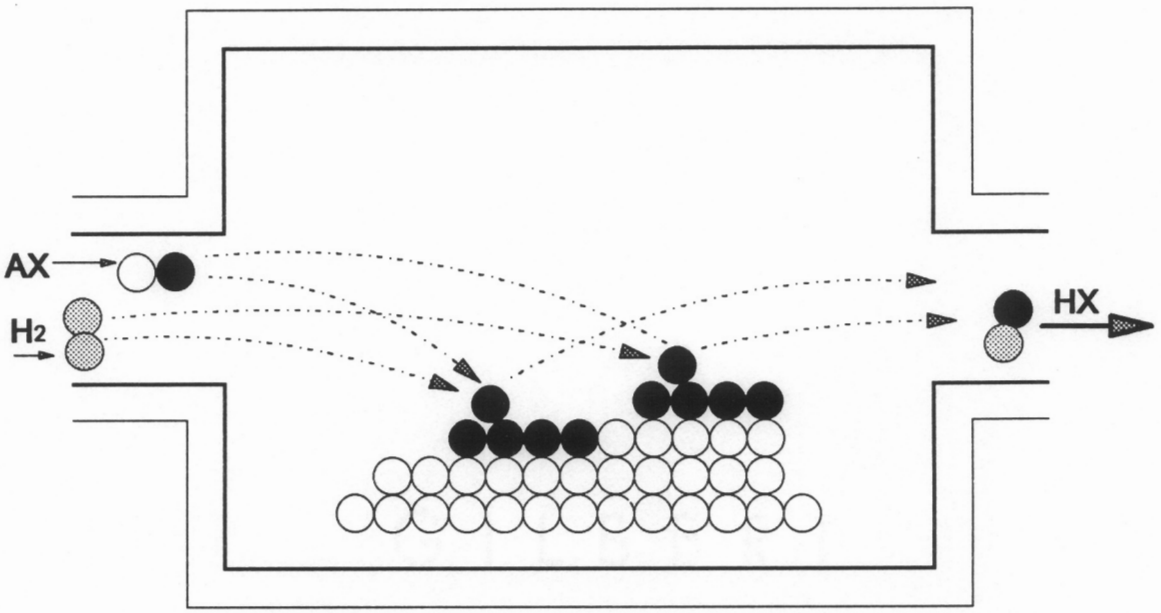

Fig. 1.2: A schematic diagram of chemical vapor deposition (CVD).

gas mixture is introduced into a reactor. Near or on the substrate surface which may be heated, a chemical reaction which yields a solid material occurs:

$$2AX_{(g)} + H_2 \longrightarrow 2A_{(s)} + 2HX_{(g)} \qquad (1.1)$$

In addition to the solid material A, volatile reaction products are formed which are exhausted from the reactor.

In a CVD process there is a complex interplay between different reactions taking place in the vapor phase, at the vapor/solid interface, at the substrate/coating interface and within the solid phases (substrate and coating). A net CVD process can be described by a series of mechanistic steps which can be described through mass and flux balances. The steps which can occur during a vapor deposition process are schematically shown in Fig. 1.3; seven steps are involved [16]:

1. Forced flow of reactant gases into the system.
2. Diffusion of reactant gases through the gaseous boundary layer to the substrate.
3. Adsorption of gases onto the substrate.
4. Chemical reactions of the adsorbed species.
5. Desorption of adsorbed species from the substrates.
6. Diffusion of product gases through the boundary layer to the bulk gas.
7. Forced exit of gases from the system.

Steps 1 and 7 are mass transport steps, with the rate of step 1 determined completely by the experimentally controlled input gas flow. Step 7 is controlled by the total gas flow rate of the system, with the chemistry of the gas determined by the nature and extent of the chemical reactions occurring in the system. Steps 2 and 6 are mass transport processes through the boundary layer with rates which can

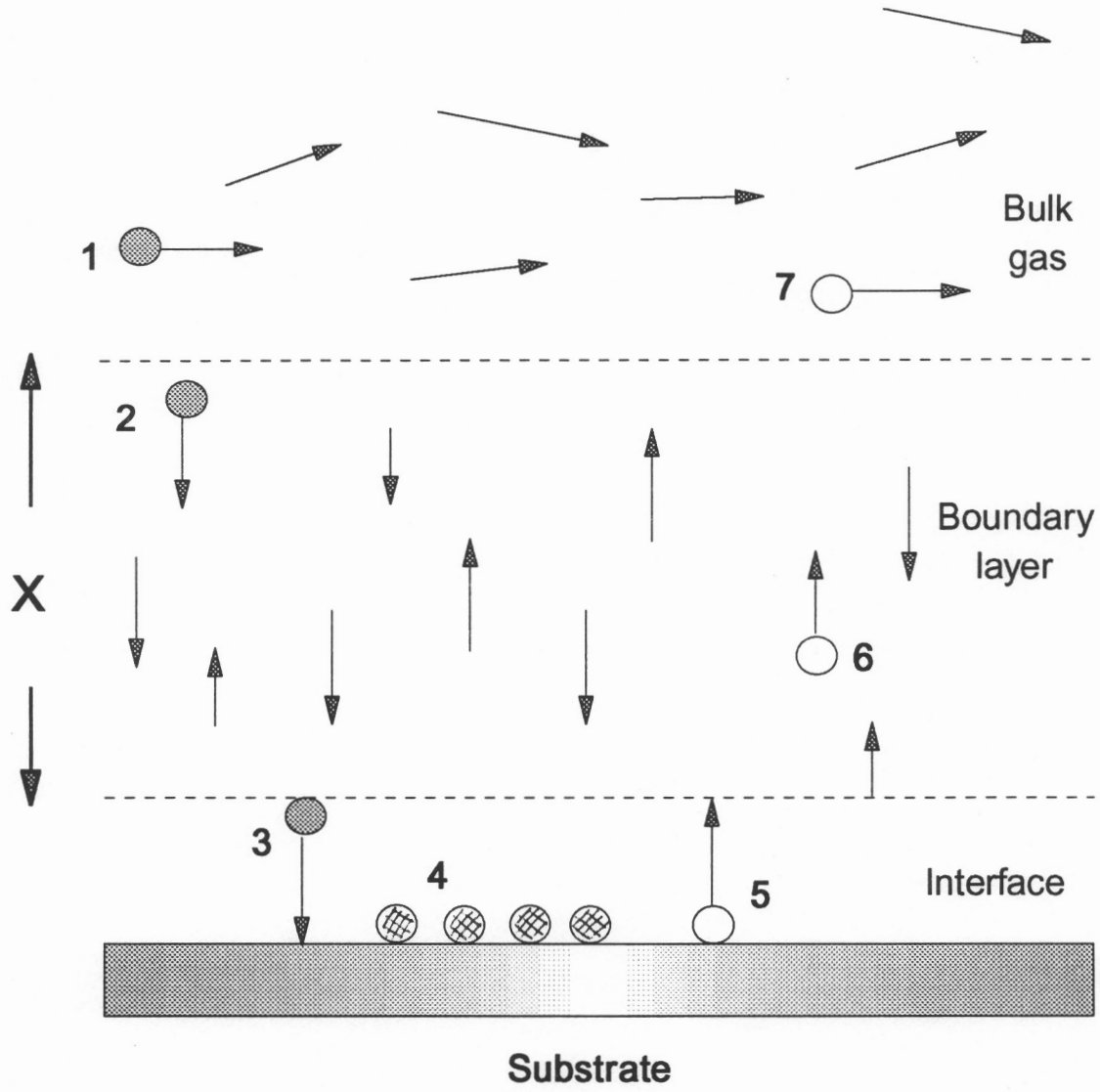

Fig. 1.3: Schematic diagram showing seven mechanistic steps which occur during a CVD process.

be described by diffusion equations [17]. Steps 3, 4, and 5 are the activated chemical processes with rate constants following an Arrhenius relationship [16].

A large variety of CVD reactors exist for depositing SiC from a gaseous precursor, but they can be placed into two broad categories: cold wall and hot wall. A detailed review of work on the chemical vapor deposition of SiC before 1980 was reported by Schlichting [18]. However, very few reports described the deposition of SiC on Si substrates for both cold and hot wall reactors. A brief review of work since 1980 on the deposition of SiC on Si substrates is given in the following two sections.

1.2.1 Chemical vapor deposition of SiC thin films on Si substrates in a cold wall reactor.

In a cold wall reactor, as shown in Fig. 1.4, the walls of the reactor are at room temperature and deposition rarely occurs on them. With a low wall temperature, the risk of contamination from vapor/wall reactions is reduced. Furthermore, the homogeneous reactions are suppressed and the importance of surface reactions is increased. As a result of a steep temperature gradient (as shown in Fig. 1.4) which introduces severe natural convection, uniformity with respect to microstructure and thickness may be difficult to control. However, a cold wall reactor has the advantage of flexibility, cleanliness, high cooling rate, and easy construction of an automated substrate handling system. The modeling cold wall reactor kinetics is also simpler since the gaseous precursors are not consumed along the reactor and are independent of the location of the substrates.

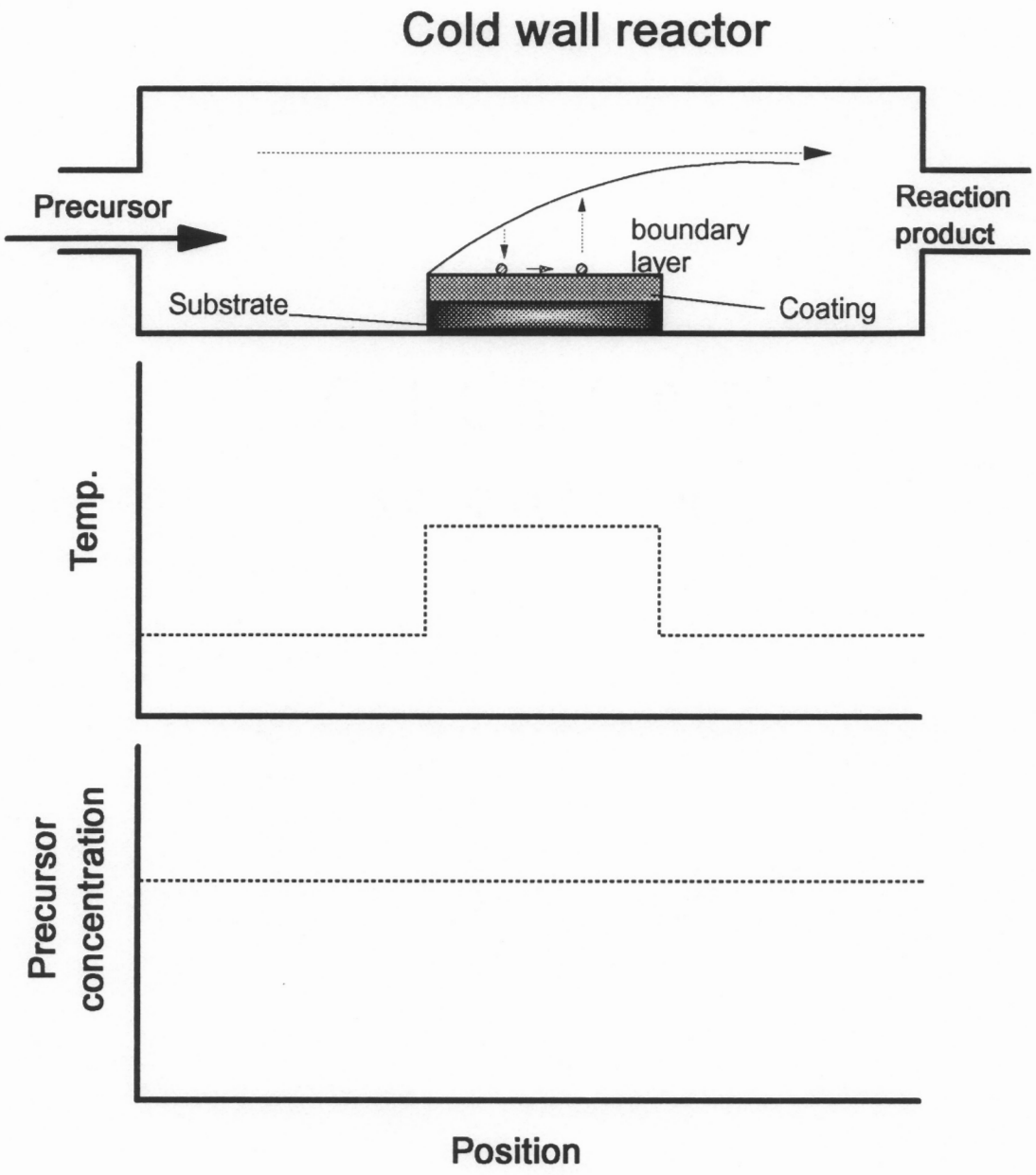

Fig. 1.4: A schematic diagram of the CVD process in a cold wall reactor.

For the deposition of SiC thin films on silicon substrates, some obstacles have been encountered because of the mismatches in coefficients of thermal expansion and lattice constants, as mentioned above. A reduction in the mismatches resulted from the initial reaction of the silicon surface with a carbon–containing gas. Relatively thick (up to 30μm), crack–free β–SiC films on the converted layer using carbon– (C_3H_8) and silicon–containing (SiH_4) gases were initially reported by Nishino et al. [19]. This procedure was followed by numerous groups in the USA and Japan [20–22]. The most intensive research has been led by Davis using C_2H_4 and SiH_4 as the SiC precursor in a cold wall, vertical barrel reactor at atmospheric pressure [20,23–25]. So far, SiC based electronic devices are fabricated by this method, either at atmospheric pressure or low pressures. In addition to the Si–C–H gas system with individual carbon– and silicon–containing gases, a single gas source containing Si and C was used [26–28]. Furthermore, some Si–C–H–Cl gas systems were utilized to deposit SiC on silicon substrates in a cold wall reactor [29–34].

1.2.2 Chemical Vapor deposition of SiC thin films on Si substrates in a hot wall reactor.

In a hot wall reactor, as shown in Fig. 1.5, the reactor is surrounded by a furnace and the substrates and reactor walls are at the same temperature. This indicates that the deposition could take place both on the substrate and inside the reactor walls. Thus, while transporting the gas mixture through the reactor, there is successive depletion of the reactants (Fig. 1.5). Such depletion effects result in different deposition conditions within the reactor. This makes the modeling of the

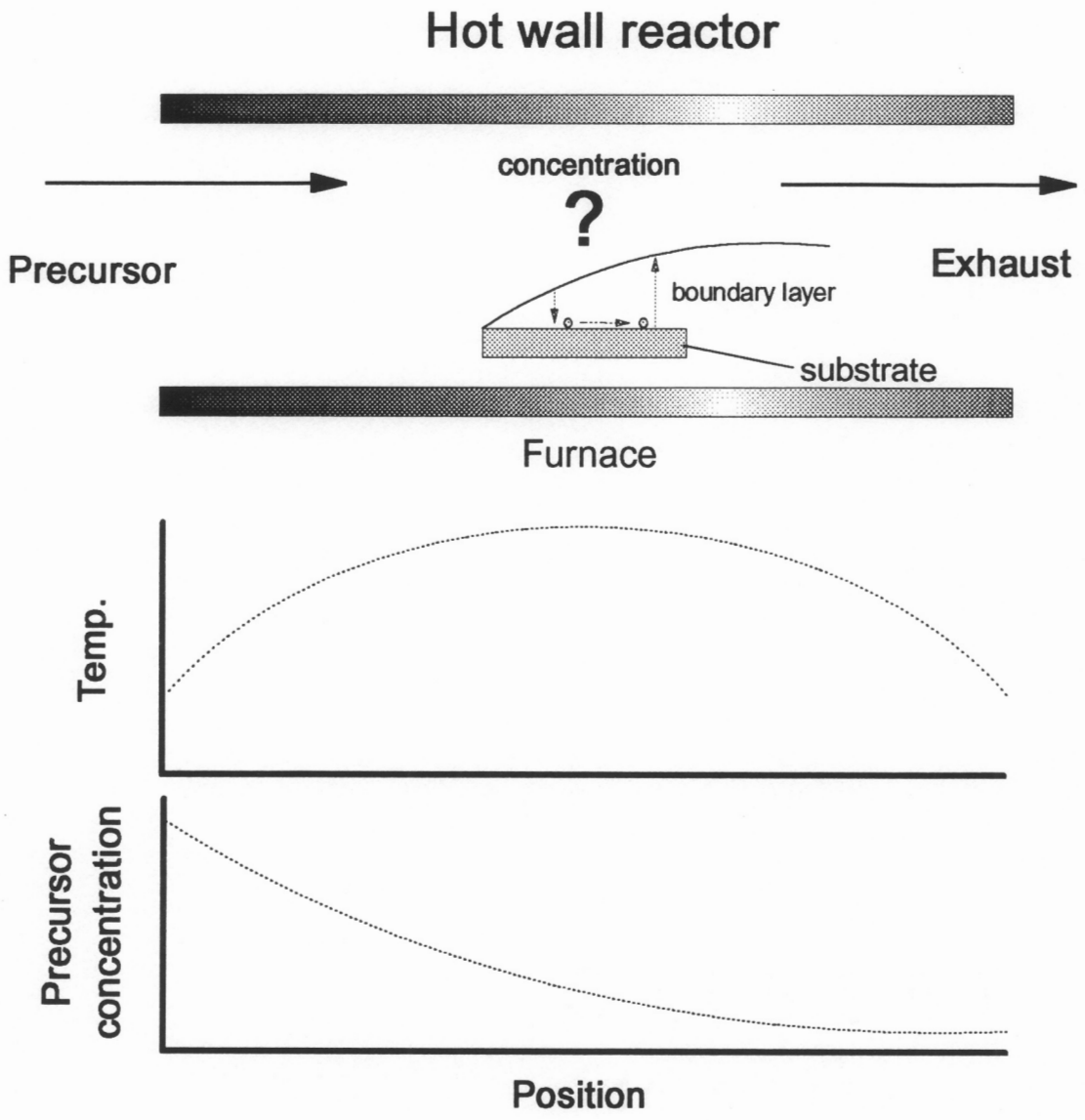

Fig. 1.5: A schematic diagram of the CVD process in a hot wall reactor.

deposition process relatively difficult because the kinetics of the reactive species along the reactor must be considered.

However, since the 1970's, CVD processes in a hot wall reactor with low pressure were rapidly accepted in the semiconductor industry, due to its extremely favorable economics. Studies have shown capital, labor, power and gas cost per wafer to be nearly an order of magnitude below the standard cold wall reactor operating at atmospheric pressure [35]. The major reason for this breakthrough is the very high packing density available with stand–up closely packed wafer loading. The use of a low pressure (0.5 to 1 Torr) results in a reactor condition such that mass transfer limitations (diffusion controlled) at very close wafer spacings are unimportant compared to the rate of the chemical reaction at the wafer surface. With the surface reaction rate controlling the deposition, the uniform temperature inherent in a resistance–heated furnace lead to excellent uniformity of film thickness and composition.

Although LPCVD in a hot wall reactor provides the advantages stated above, the depositions of polycrystalline silicon, silicon nitride, and silicon dioxide have been utilized by the semiconductor industry [35]. The deposition of single crystal material using a hot wall reactor has only been reported for the deposition of Si and Si:Ge under ultrahigh–vacuum (UHV) [36]. So far, SiC deposited in a hot wall reactor has been primary related to the chemical vapor infiltration, which produces bulk SiC [36].

1.3 OBJECTIVE

The objective of the present study is to develop a systematic method to deposit β–SiC on silicon substrates in a hot wall reactor by using the LPCVD process. The procedure first investigated the formation of a SiC buffer layer by reacting the Si(100) substrates with C_2H_2 in a hot wall LPCVD reactor (Chapter 2). Then, β–SiC films were deposited by using methyltrichlorosilane (CH_3SiCl_3 or MTS) and H_2 in the gas system at low pressures (Chapter 3). So far, the easiest way to deposit SiC is by using MTS. With other precursors, the Si/C ratio in the gas phase must be closely monitored for excess carbon or silicon. In the same chapter, the kinetics of the CVD process in a hot wall reactor for MTS–H_2 gas system will be discussed. In Chapter 4, a new approach is presented to deposit single crystal β–SiC on Si(100) substrates. Finally, a set of comprehensive CVD phase diagrams for MTS–H_2 gas system in a hot wall reactor were calculated taking into account the consideration of depletion effects.

1.4 PRESENTATION OF THE PRESENT STUDY

This study is presented in the form of journal publications, which appear as separate chapters (Chapter 2 to 5) following this introduction chapter. Each chapter is complete within itself with its own abstract, introduction, results, discussion, and summary. The overall summary of this work is given Chapter 6.

1.5 REFERENCES

1. H. Jagodzinski and H. Arnold, in *Silicon Carbide, A High–Temperature Semiconductor*, edited by J.R. O'Connor and J. Smiltens (Pergamon Press, New York), p. 136 (1960).
2. N.W. Jepps and T.F. Pagae, Progress in Crystal Growth and Characterization , **7**, p. 259 (1983).
3. J.A. Powell, in *Novel Refractory Semiconductors*, edited D. Emin, T.L. Aselage, C. Wood (Mater. Res. Soc. Symp. Proc., vol **97**, Pittsburgh, PA), pp. 159 (1987)
4. H.P. Philipp and E.A. Taft, in *Silicon Carbide, A High–Temperature Semiconductor*, edited by J.R. O'Connor and J. Smiltens (Pergamon Press, New York), p. 371 (1960).
5. W. van Muench and E. Pettenpaul, J. Appl. Phys., **48**, 4823 (1977).
6. W. van Muench and I. Pfaffender, J. Appl. Phys., **48**, 3831 (1977).
7. R.J. Trew, J–B Yan, and P.M. Mock, Proc. of the IEEE, **79**, 598 (1991).
8. R.W. Brander and R.D. Sutton, J. Phys. D: Appl. Phys., **2**, 309 (1969).
9. S. Yoshida, H. Daimon, M. Yamanaka, E. Sakuma, and K. Endo, J. Appl. Phys., **60**, 2989 (1986).
10. T. Sigii, T. Aoyama, and T. Ito, J. Electrochem. Soc., **136**, 3111 (1989).
11. Cree Research Inc., 2810 Meridian Parkway, Durham, NC 27713.
12. H.S. Hong, T.S. Glass, and R.F. Davis, J. Mater. Res., **4**, 210 (1989).
13. T.T. Cheng, P. Pirouz, and T.A. Powell, in *Chemistry and Defects in Semiconductor Heterostructures*, edited by M. Kawabe (Mater. Res. Soc.

Symp. Proc., vol **148**, Pittsburgh, PA), p. 229 (1989).

14. F. Langlais, F. Hottier, and R. Cadoret, J. Cryst. Growth, **56**, 659 (1982).
15. B.S. Meyerson, IBM J. Res. Develop., **34**, 806 (1990).
16. K.E. Spear, Pure and Appl. Chem., **54**, 1297 (1982).
17. M.M. Faktor and I. Garrett, *Growth of Crystals from the Vapor*, (Chapman and Hall, London), (1974).
18. J. Schlichting, Powder Metallurgy Intern., **12**, 141 (1980).
19. S. Nishino, J.A. Powell, and H.A. Will, Appl. Phys. Lett., **42**, 460 (1983).
20. R.F. Davis, G. Kelner, M. Shur, J.W. Palmour, and J.A. Edmond, Proc. of the IEEE, **79**, 677 (1991).
21. M.L. Locatelli and S. Gamal, J. Phys., III France, **3**, 1101 (1993).
22. H. Matsunami, Physica B, **185**, 65 (1993).
23. R.F. Davis, in *Chemical Vapor Deposition of Refractory Metals and Ceramics*, edited by T.M. Besmann and B.M. Gallois (Mater. Res. Soc. Symp. Proc., vol. **168**, Pittsburgh, PA), pp. 145 (1990).
24. R.F. Davis, in *The Physics and Chemistry of Carbides, Nitrides, and Borides*, edited by R. Freer (Kluwer Academic Publishers, The Netherlands), p. 589 (1990).
25. H.J. Kim, H–S Kong, J.A. Edmond, J.T. Glass, and R.F. Davis, in Ceramic Transactions, 2, Silicon Carbide '87, edited by J.D. Cawley and C.E. Semler, p. 457 (1987).
26. I. Golecki, F. Reidinger, and J. Marti, Appl. Phys. Lett., **60**, 1703 (1992).
27. A.J. Steckl, C. Yuan, and J.P. Li, Appl. Phys. Lett., **63**, 3347 (1993).
28. J.M. Grow, R.A. Levy, M. Bhaskaram, H.J. Boeglin, and R. Shalvoy, J. Electrochem. Soc., **140**, 3001 (1993).

29. B.W. Sheldon, T.M. Besmann, K.L. More, and T.S. Moss, J. Mater. Res., **8**, 1086 (1993).

30. P. Rai–Choudhury and N.P. Formigoni, J. Electrochem. Soc., **116**, 1440 (1969).

31. Y. Furumura, M. Doki, F. Mieno, T. Eshita, T. Suzuki, and Maeda, J. Electrochem. Soc., **135**, 1255 (1988).

32. K. Ikoma, M. Yamanaka, H. Yamaguchi, and Y. Shichi, J. Electrochem. Soc., **138**, 3028 (1991).

33. A. Suzuki, K. Furukawa, Y. Higashigaki, S. Harada, S. Nakajima, and T. Inoguchi, J. Cryst. Growth, **70**, 287 (1984).

34. H. Matsunami, S. Nishino, and T. Tanaka, J. Cryst. Growth, **45**, 138 (1978).

35. R.S. Rosler, Solid State Technol., 63, (Apr. 1977).

36. T.M. Besmann, B.W. Sheldon, R.A. Lowden, and D.P. Stinton, Science, **253**, 1104 (1991).

Chapter 2 was published and entitled

"Conversion of single crystal Si(100) to SiC films by C_2H_2"
in Journal of Materials Research, vol. **8**, No. 3, 535–544 (1993)

and

"SiC thin films by chemical conversion of single crystal Si"
in *Chemical vapor deposition of refractory metals and ceramics II*,
Materials research society symposium proceedings, vol. **250**,
(Materials research society, Pittsburgh, PA, 1992), pp 179–185

Chapter 2: CONVERSION OF SINGLE CRYSTAL Si(100) TO SiC FILM BY C_2H_2

2.1 ABSTRACT:

SiC thin films grown from the reaction between acetylene (C_2H_2) and the Si(100) substrates in a horizontal hot wall CVD reactor by different procedures were studied using the x–ray photoelectron spectroscopy (XPS) and scanning electron microscopy (SEM). The growth of the SiC films was observed from the behavior of Si_{2p} peaks and their plasmons. A SiC thin film with a thickness of 35Å and having a smooth surface morphology was obtained in C_2H_2 diluted by H_2 at 1050^{0}C for a period of 60 minutes. Etch pits and hillocks were observed with increasing reaction time at 1050^{0}C. For the conversion conducted in C_2H_2, but in the absence of H_2, a SiC monolayer with smooth morphology was obtained at 950^{0}C for 7 minutes and defects were observed for longer reaction times at this temperature. Defects were also observed for reaction times as short as 10 seconds at higher reaction temperatures (*e.g.* 1000^{0}C). H_2 seems to play a key role in suppressing the formation of defects and the reaction between C_2H_2 and Si substrate. The formation of defects was correlated to the out–diffusion of Si in the carburization process.

2.2 INTRODUCTION:

The cubic form of silicon carbide (β–SiC) is as a potential candidate for high temperature, high power semiconductor devices because of its excellent thermal

stability, wide band gap, high electron mobility, high electron drift velocity, and high breakdown field. Single crystal β–SiC thin films are conventionally grown on Si(100) substrates by Chemical Vapor Deposition (CVD) in cold wall reactors. However, due to the large mismatch in lattice constants (20%) and the difference in thermal expansion coefficients between the SiC thin film and the underlying Si substrate (8%) problems were encountered when directly growing single crystal SiC thin film on a Si(100) substrate [1]. Thus, the resulting SiC thin films often exhibited poor morphology and peeling of the SiC film from Si substrate was often observed after the deposition. Furthermore, in depositing SiC thin films on Si substrates, etching problems were reported for Cl–based precursor systems (*e.g.* CH_2Cl_2–SiH_4–H_2 and CH_3SiCl_3) due to the formation of Cl radicals [2]. To solve these problems, the growth of a buffer layer prior to the CVD process has been proved to be a necessary step in obtaining good quality SiC thin films on Si substrates [3]. The buffer layer is generally grown at a temperature different from the temperature for the CVD process. Following the growth of a buffer layer, the temperature of Si substrate was changed to the deposition temperatures for carrying out the bulk growth of SiC thin films by the CVD process in a cold wall reactor. For convenience, the buffer layers were also grown in a cold wall reactor by reacting the Si substrate with a hydrocarbon gas, as shown in Table 2.1.

Although the formation of a buffer layer and the subsequent SiC deposition in cold wall reactors is convenient and eliminate the problems of particulate contamination, the throughput is relatively low when compared to that of hot wall reactors. In addition, hot wall reactors may be helpful in lowering the deposition temperature since many of the various reactants decompose endothermically. In fact, single crystal Si thin films were successfully grown on Si substrates at low

Table 2.1: The conversion of Si to SiC

C–source gas	Temperature (°C)	Pressure (Torr)	Reactor type	References
C_2H_2	900–1100	10^{-6}–10^{-4}	cold wall	4
C_2H_2	800–1100	10^{-7}–5×10^{-4}	cold wall	5
C_2H_2	1130–1370	10^{-5}–10^{-2}	cold wall	6
C_2H_2	1225–1380	5×10^{-6}–3×10^{-3}	cold wall	7
C_2H_2	900–1200	2×10^{-6}–3×10^{-6}	cold wall	8
C_2H_2	900	7.6×10^{-6}	cold wall	9
C_2H_2	950	10^{-6}	–	10
*C_2H_2	837–1037	7.5×10^{-10}	cold wall	11
C_2H_4	1280–1330	7.5×10^{-7}	cold wall	12
C_2H_4	1360	7.5×10^{-7}	cold wall	13
C_2H_4	1327	–	–	14
*C_2H_4	667	4×10^{-5}	cold wall	15
*C_2H_4	697	6×10^{-10}	cold wall	16
C_3H_8	1000–1170	–	–	1
C_3H_8	1360	–	cold wall	17

* : molecular beam

temperatures by using an ultrahigh vacuum/low pressure hot wall CVD reactor [18,19]. Therefore, in hot wall reactor, it is possible to perform the homoepitaxial growth of SiC thin films on the Si substrates by making the SiC buffer layers in the same type of reactor. Although the growth of a SiC buffer layer had been reported in hot wall CVD reactors at relatively low pressures by Nagasawa et al [20] and Hattori et al [21], the nature of this buffer layer was not investigated. Thus, in this work the reaction between C_2H_2 and a Si(100) substrate was studied by using x–ray photoelectron spectrometer (XPS) and scanning electron microscope (SEM), and the optimum parameters for growing a SiC buffer layer in a conventional horizontal hot wall CVD reactor were identified.

2.3 EXPERIMENTAL PROCEDURE:

Single–crystal Si(100) substrates were used in this study. Before introducing the substrates into the reaction chamber, the organic contamination on the surface of the Si substrate was washed using acetone and then by dipping the substrate into methanol and deionized water. Following these procedures, the residual surface oxides were etched away using 10 wt% HF for a period of 10 seconds. Finally the substrates were cleaned by distilled water. Prior to transferring these Si substrates into the reactor, the surfaces were dried using dry nitrogen.

The reactor was initially evacuated to the base pressure of 10^{-3} Torr. Two procedures were employed after this base pressure was achieved. For Procedure I, as shown in Fig. 2.1(a), the wafers were heated to the reaction temperature, ranging from 900 to 1000° C, in a flowing H_2 atmosphere at a pressure of 1.8 Torr. The heating rate was maintained at 30° C/min. As soon as the temperature

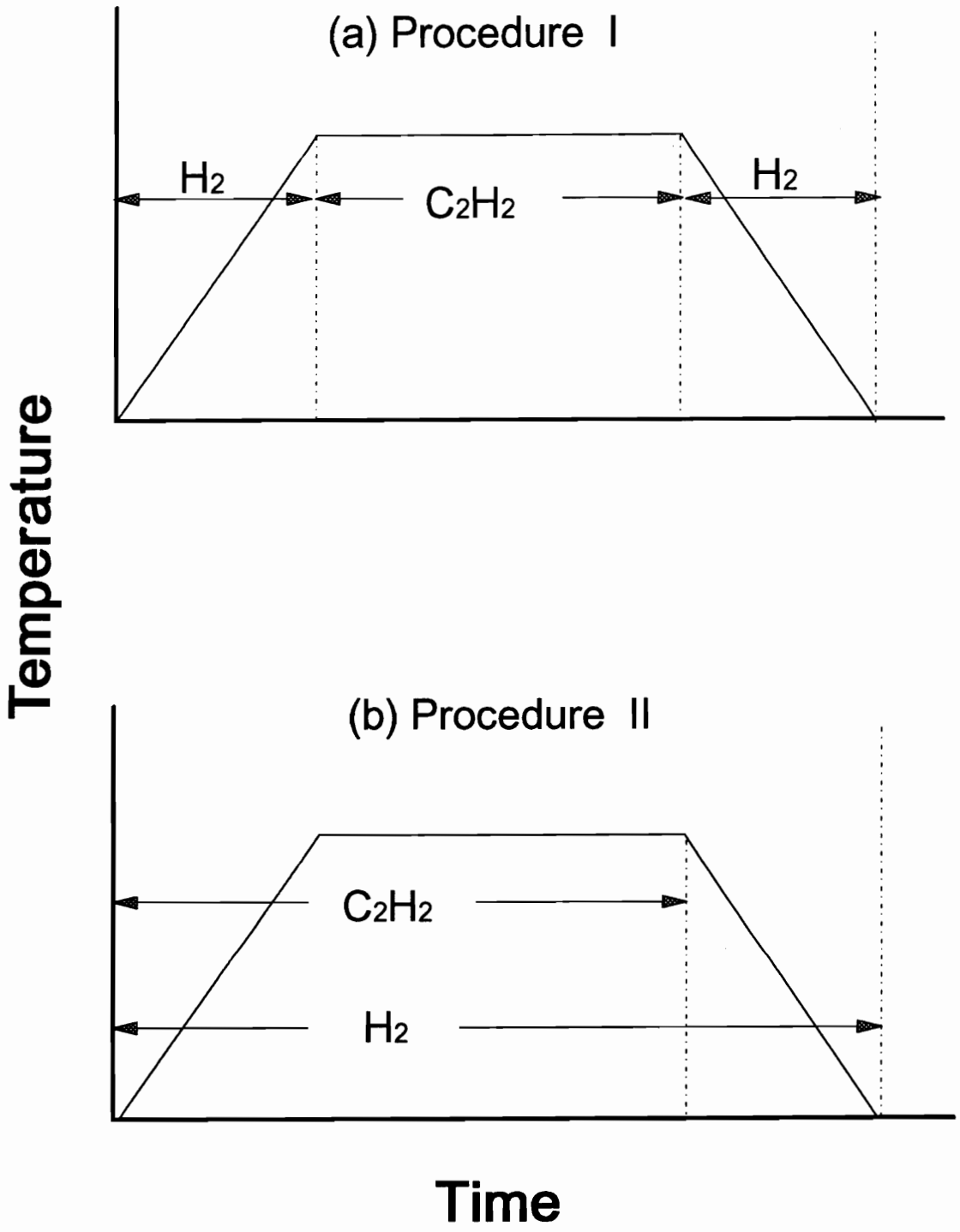

Figure 2.1: The reaction procedures for (a) Procedure I and (b) Procedure II.

equilibriation was achieved the flow of H_2 was stopped and purified C_2H_2 (99.6%) was introduced at a pressure of 0.1 Torr for a predetermined reaction time. The substrates were furnace cooled in H_2 at a pressure of 1.8 Torr after the reaction was completed. For Procedure II, as shown in Fig. 2.1(b), H_2 and the purified C_2H_2 were introduced into the reactor simultaneously at a total pressure of 1.8 Torr from room temperature to 1050° C. The partial pressure of purified C_2H_2 was kept at 10 mTorr. The cooling step was the same as that in Procedure I. The characterization of the reacted Si surfaces was carried out by using a Kratos x–ray photoelectron spectrometer (XPS) with a MgKα x–ray source. Au_{4f} peaks were used to calibrate the binding energies. Scanning electron microscopy (SEM) was used to observe the surface morphology of the reacted Si substrates.

2.4 RESULTS AND DISCUSSION:

2.4.1 Reaction products

Reactions between Si and C_2H_2 were monitored by following the changes in Si_{2p} and C_{1s} XPS peaks and the plasmon loss features of Si_{2p}. Figure 2.2 depicts the Si_{2p} spectral regions from the Si(100) surface before and after Procedure I. The temperature varied from 950 to 1000° C at various reaction times. The Si_{2p} spectrum for a clean Si(100) substrate is shown in Fig. 2.2(a). In Fig. 2.2(a), the major peak observed is the Si_{2p} peak and the less intense feature, which has the energy loss of 17 eV, is the bulk plasmon loss feature from the Si substrate. As the reaction temperature was increased from 950° C to 1000° C, the intensity of the initial Si plasmon feature decreased, while intensity of a second plasmon loss feature at about 22.5 eV increased (Figs. 2.2(b) ~ 2.2(d)). This latter feature corresponds

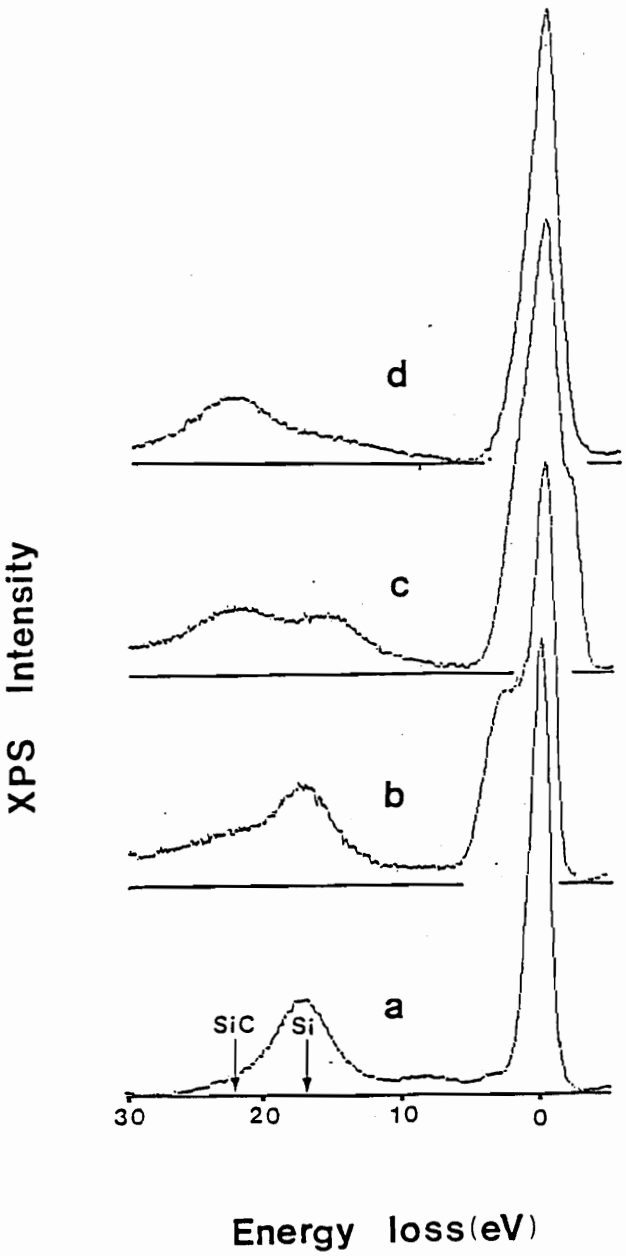

Figure 2.2: Si_{2p} XPS peaks and associated plasmon loss features for (a) clean Si substrate and Si substrates reacted by Procedure I at (b) 950° C for 11 min., (c) 1000° C for 20 sec., and (d) 1000° C for 40 sec.

to the bulk SiC plasmon as discussed by Bozso et al [15,22] and Katayama et al [23]. As shown in Fig. 2.3, the small shoulder in Fig. 2.2(b), which exhibits a higher binding energy than the major Si_{2p} peak, is believed to be from SiC and SiO_2 on the surface of the substrate. These two Si compounds were from the reaction between the Si substrate and C_2H_2 and the contamination from the atmosphere. Likewise, the shoulder with lower binding energy in Fig. 2.2(c) was from the Si substrate.

The Si_{2p} plasmon loss feature at about 22.5 eV provides the evidence for the formation of SiC. Additional information can be obtained by deconvoluting the peaks in Fig. 2.2, assuming Gaussian line shapes (Fig. 2.3). The Si_{2p} peak, with the binding energy of 99.1 eV, from clean Si substrate is shown in Fig. 2.3(a) for comparison with those from the reacted Si substrates. As depicted in Fig. 2.3, the relative intensities of Si_{2p} from the Si substrate decreased as the reaction temperature increased from 950° C to 1000° C (Figs. 2.3(b) ~ 2.3(d)). Furthermore, for samples reacted at 1000° C, the Si_{2p} peak from Si substrate disappeared when the reaction times were longer than 40 seconds. The Si_{2p} spectra of the samples with reaction times longer than 40 seconds at 1000° C were essentially similar to the one depicted in Fig. 2.3(d) . The SiC/Si ratio of the samples obtained at 900° C (for 5~15 min) and 950° C (for 1~11 min) were smaller than those prepared at 1000° C (for less than 5 min) and the Si_{2p} spectra were similar to Fig. 2.3(b). This result indicated that the SiC films obtained at 1000° C were thicker than those prepared at 900° C and 950° C.

The Si_{2p} spectral regions and the associated plasmon loss features for Procedure II are shown in Fig. 2.4. The intensity of the plasmon loss feature from SiC increased with increasing time. This result corresponds to the deconvoluted Si_{2p} peaks shown in Fig. 2.5. The SiC/Si ratio increased with increasing time. For

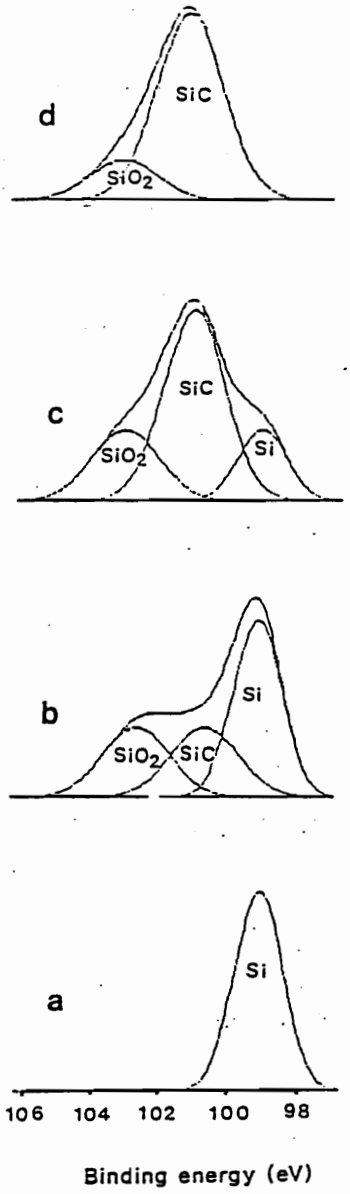

Figure 2.3: The deconvolution of Si_{2p} XPS peaks for (a) clean Si substrate and Si substrates reacted by Procedure I at (b) 950° C for 11 min., (c) 1000° C for 20 sec., and (d) 1000° C for 40 sec.

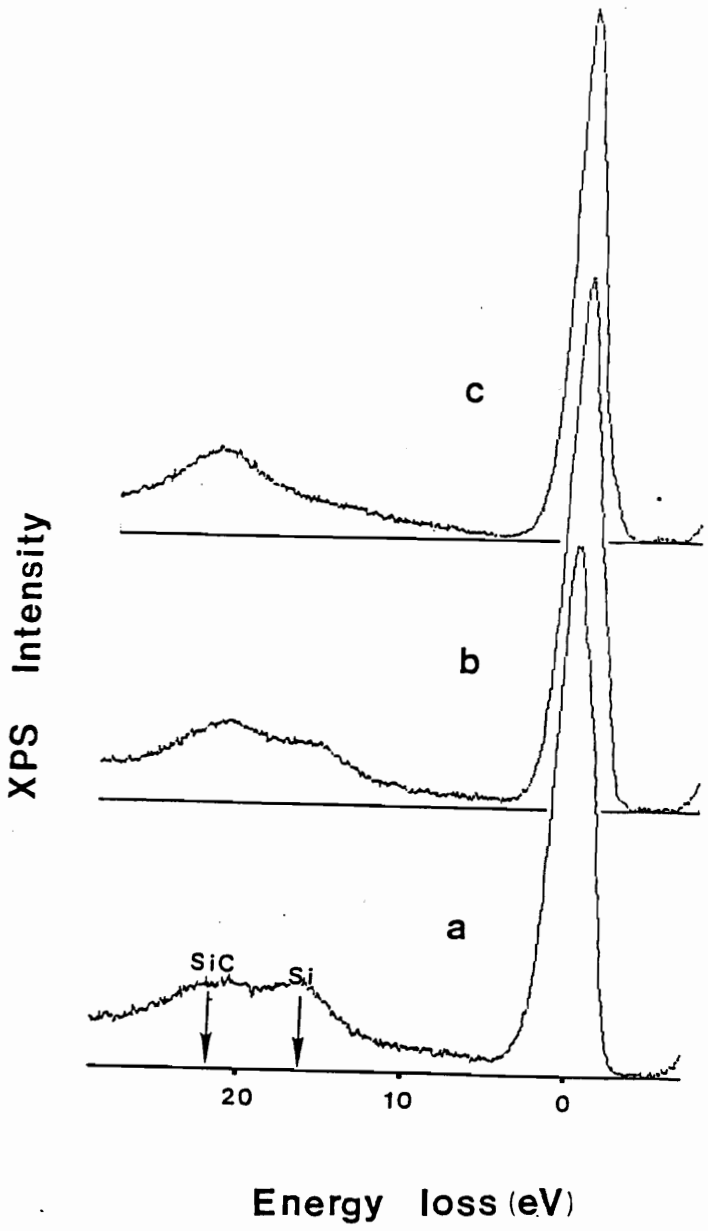

Figure 2.4: Si_{2p} XPS peaks and associated plasmon loss features of Si substrates reacted by Procedure II for (a) 30 min., (b) 60 min., and (c) 75 min.

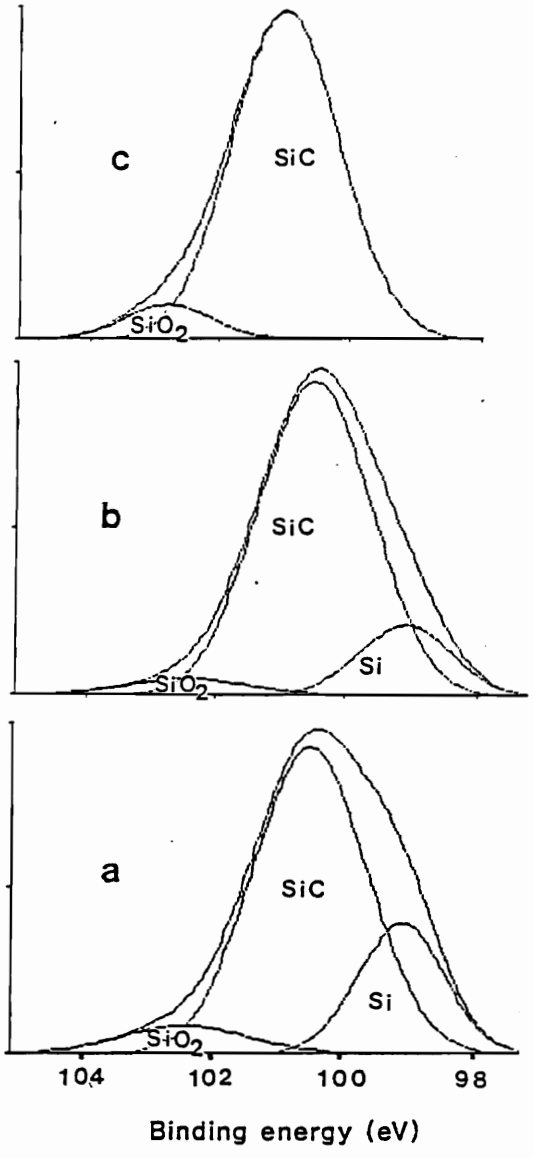

Figure 2.5: The deconvolution of Si_{2p} XPS peaks for Si substrates reacted by Procedure II for (a) 30 min., (b) 60 min., and (c) 75 min.

Procedure II, the presence of H_2 from the beginning of the heating cycle seems to play a key role in initializing the reaction between C_2H_2 and the Si substrate. As shown in Fig. 2.6, only carbon atoms from the dissociated C_2H_2 formed on the surface of the Si substrate when the reaction was performed at 1050° C without using H_2 initially. Again the O_{1s} and O_{KLL} peaks were from the atmospheric oxygen.

By deconvoluting the Si_{2p} spectra, and assuming that the mean free paths of the photoelectron in Si and SiC are the same (λ_{si} = 2.25nm), the thickness of the reaction product can be estimated by using the following equation [9]:

$$R = \frac{(\rho_{si}/\rho_{sic})\times\{\exp(-d/\lambda_{si}\mathrm{Cos}\theta)\}}{1-\exp(-d/\lambda_{si}\mathrm{Cos}\theta)} \qquad (2.1)$$

where R is the intensity ratio of Si_{2p} from Si substrate to that from SiC layer; d is the thickness of the SiC layer; ρ_{si} and ρ_{sic} are the densities of Si atoms in Si substrate and in the SiC layers, respectively; and θ is the angle between the normal direction to the sample surface and the photoelectron detector. It was found that the thickness obtained at 900° C (for 5 to 15 min) and 950° C (for 1 to 11 min) was limited to about 0.5 to 1 monolayer of SiC during Procedure I. The thickness of the converted SiC films formed at 1000° C (form 10 to 20 sec) for Procedure I and at 1050° C (for 60 minutes) for Procedure II are around 30Å and 35Å, which correspond to several monolayers. The inability to observe the Si_{2p} from Si substrate for both procedures can be attributed to thicker SiC films in comparison with the nominal XPS sampling depth.

The binding energies of Si_{2p} from the SiC films showed little shift for Procedure I, as shown in Fig. 2.7. Table 2.2 lists the average binding energies of

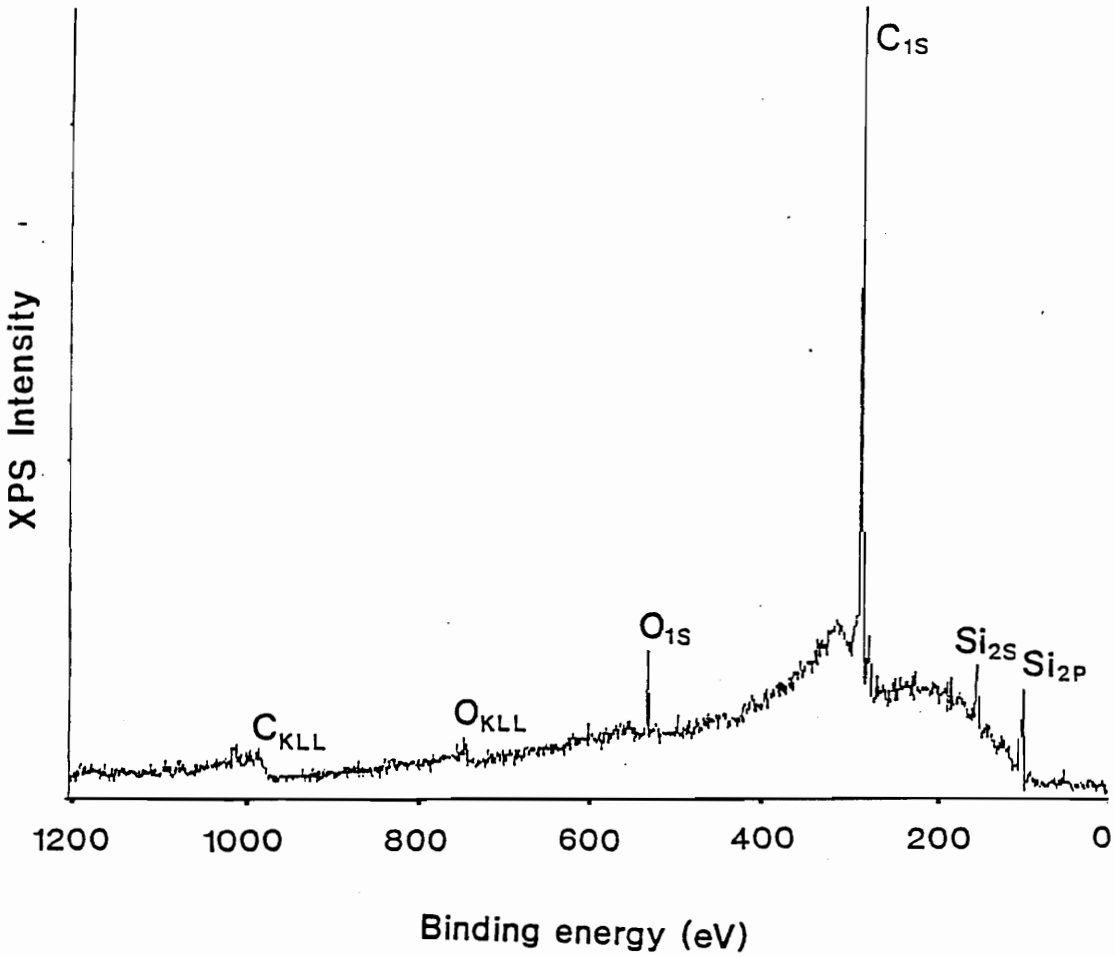

Figure 2.6: The wide scan XPS of Si surface reacted with C_2H_2 at 1050°C for 60 min. without using H_2 as a dilute gas. The pressure of C_2H_2 was 0.1 Torr.

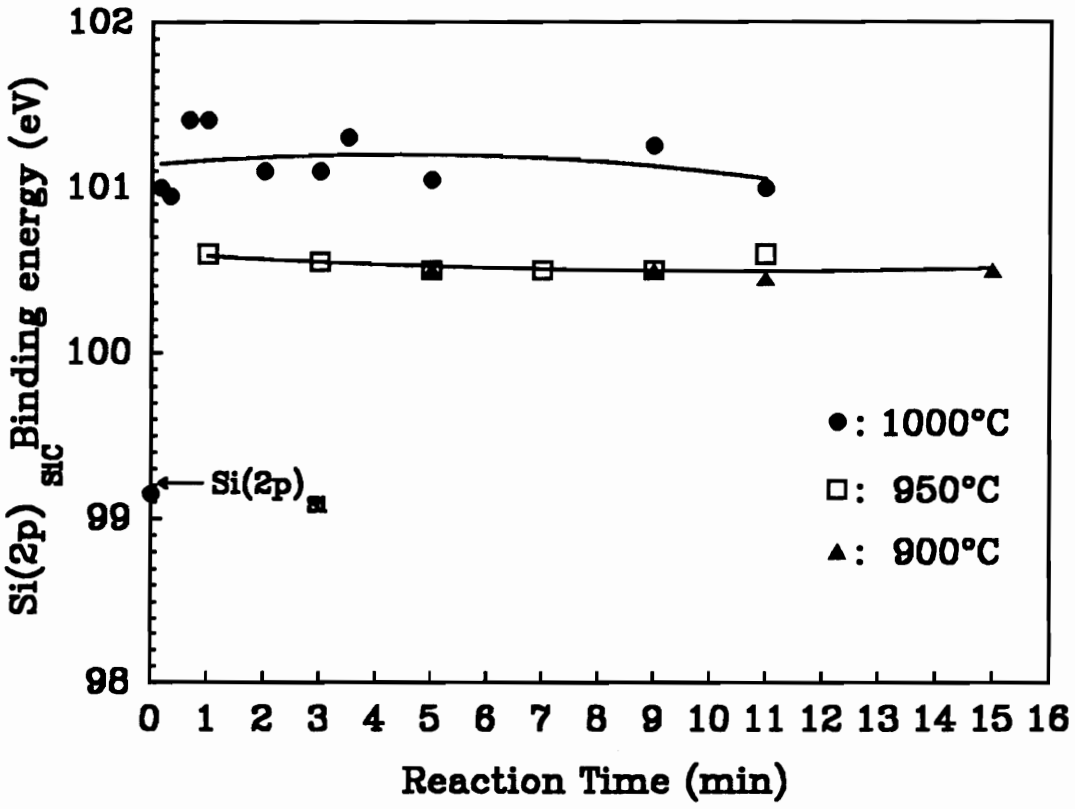

Figure 2.7: The binding energies of Si_{2p} for the SiC layers from Procedure I for various time.

Table 2.2: Average binding energy (BE) of Si_{2p}

T(°C)	Time	Si_{2p} (eV) Si	SiC	SiO_2	ΔBE (SiC–Si)
		Procedure I			
900	5~15min	99.1	100.5	102.5	1.4 eV
950	1~11min	99.1	100.5	102.6	1.4 eV
1000	10~20 sec	99.1	101	103	1.9 eV
1000	40 sec~11min	–	101.2	103.1	–
		Procedure II			
1050	30~60 min	99.1	100.5	102.5	1.4 eV
1050	75~90 min	–	101	102.9	–

Si_{2p} peaks form different reaction conditions for Procedures I and II. For specimens reacted at 900° C and 950° C in Procedure I and those reacted for 30 and 60 minutes in Procedure II, the binding energies and the energy difference between Si substrate and SiC layer agreed very well with the reported values [9,16,24]. However, for the samples prepared at 1000° C in Procedure I and those obtained with the reaction times of 75 and 90 minutes in Procedure II, the Si_{2p} peaks from SiC and SiO_2 were slightly shifted to higher binding energies (0.5 eV). The shift to higher binding energies was also confirmed by careful measurement of the plasmon loss features and the Au_{4f} peaks. The shift to the higher binding energies can be attributed to the differential charging of SiC and SiO_2 in comparison with Si.

The stoichiometry of the SiC product layers was determined from the deconvoluted Si_{2p} and C_{1s} peaks. Figure 2.8 shows the stoichiometry of the converted SiC layers as a function of reaction time for both Procedures I and II. In general, the SiC layers obtained were Si–rich for both procedures. This can be attributed to the rapid supply of Si atoms to the substrate–gas interface as compared to C atoms [11]. The Si–rich SiC layers were also reported for the reaction between Si and other hydrocarbon gases [9]. As shown in Fig. 2.8, the SiC films obtained from Procedure II were less rich in Si and were very close to the stoichiometric SiC. It was reported that, for Si_xC_{1-x}:H amorphous films grown by reactive sputtering, the plasmon loss feature exhibited a monotonic 5.5 eV shift between values of X=1 (17.2 eV) and X=0.45 (22.7 eV) [23]. The X values for the samples in Fig. 2.8 ranged only from 0.5 to 0.66, which agree well with the plasmon loss features for these samples (Figs. 2.2 and 2.4). This small range of the X values can also be demonstrated by the little shift in binding energy during the reaction (Fig. 2.7) since the binding energy of Si_{2p} from Si_xC_{1-x} decreases monotonically as

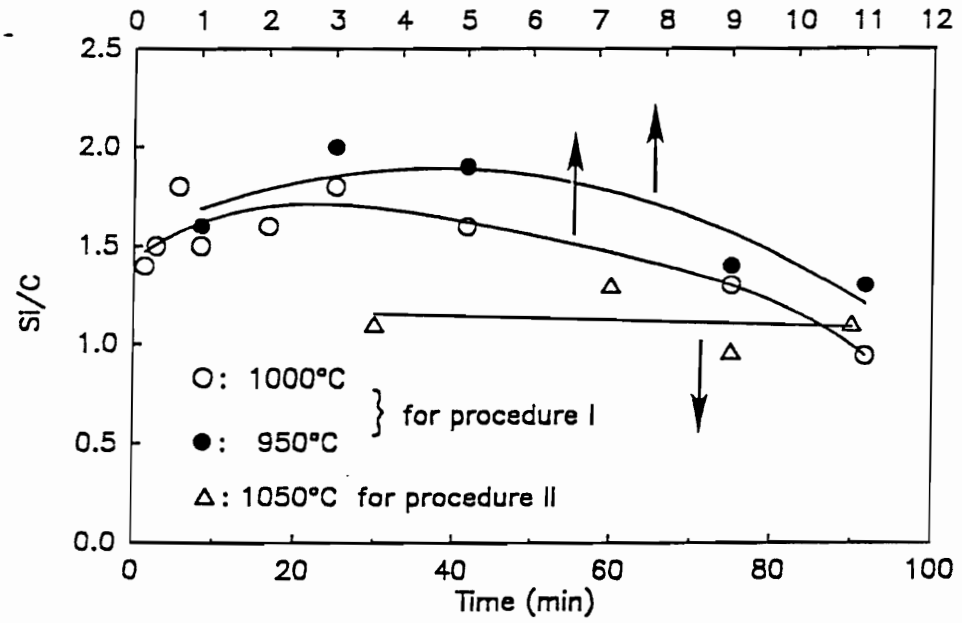

Figure 2.8: The stiochiometry of the converted SiC layers from Procedures I and II for various times.

the content of carbon decreases [25].

From Fig. 2.8, it is also evident that the Si/C ratios decreased with increasing reaction time and temperature. According to the model proposed by Smith [6], C–containing molecules must be absorbed and dissociated to yield carbon atoms on the Si surface before the formation of SiC. The surface flux of the adsorbed carbon from dissociated carbon containing species (*e.g.* CH ,CH_2 ,and C_2H_2), J_{BS}, can be expressed as:

$$J_{BS} = C \exp(-E_{BSD}/kT) \qquad (2.2)$$

where C is a constant depending on the surface density of carbon atoms, surface lattice, and the atomic frequency; and E_{BSD} is the activation energy for the dissociation of carbon containing species to yield carbon atoms on the surface. As expected from Equ. 2.2, the Si/C ratios of the SiC layers obtained at higher temperatures should be smaller than those obtained at lower temperatures due to the larger surface flux of C atoms.

2.4.2 SEM morphology

For Procedure I, the morphology of the Si(100) surface reacted at 950°C is shown in Fig. 2.9. No defects were observed for the samples reacted for 7 minutes, as shown in Fig. 2.9(a). The presence of defects was initially observed only when the reaction time was increased to 9 minutes (Fig. 2.9(b)). Figure 2.10 shows the morphology of the reacted (100) Si surfaces at 1000°C. In contrast to the samples reacted at 950°C, defects can be seen for reaction times as short as 10 seconds. Initially the defects were nondescriptive, as shown in Fig. 2.10(a). With increasing

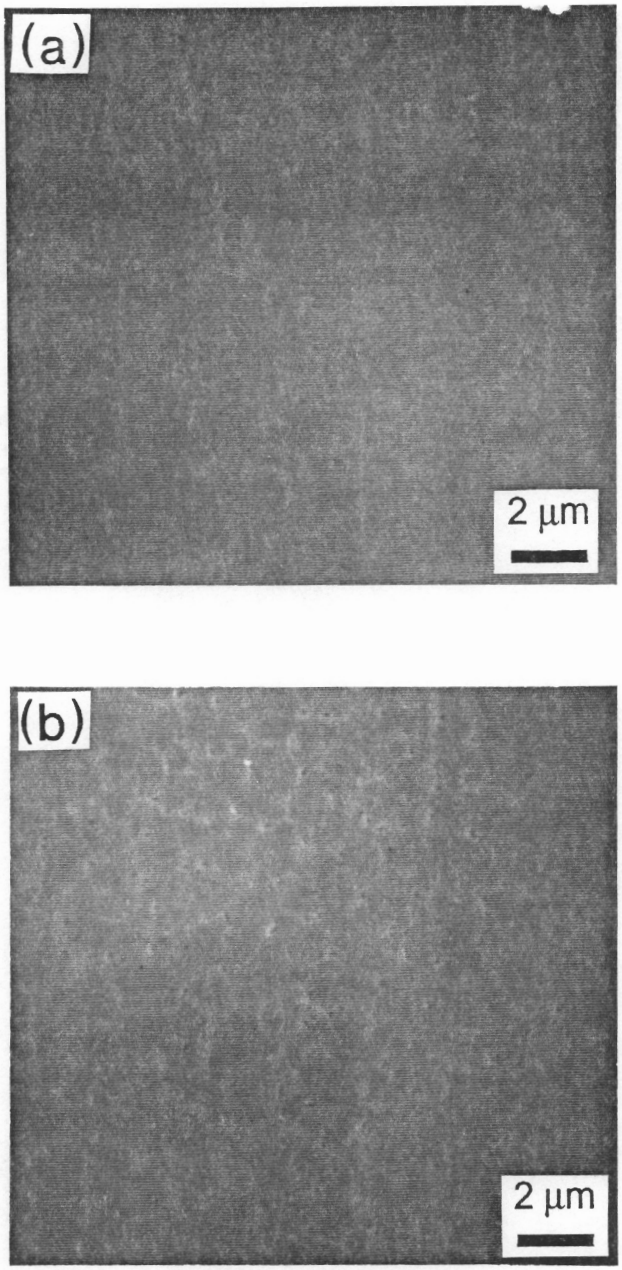

Figure 2.9: Surface morphology of Si substrates reacted at 950° C for (a) 7 min., and (b) 9 min. from Procedure I.

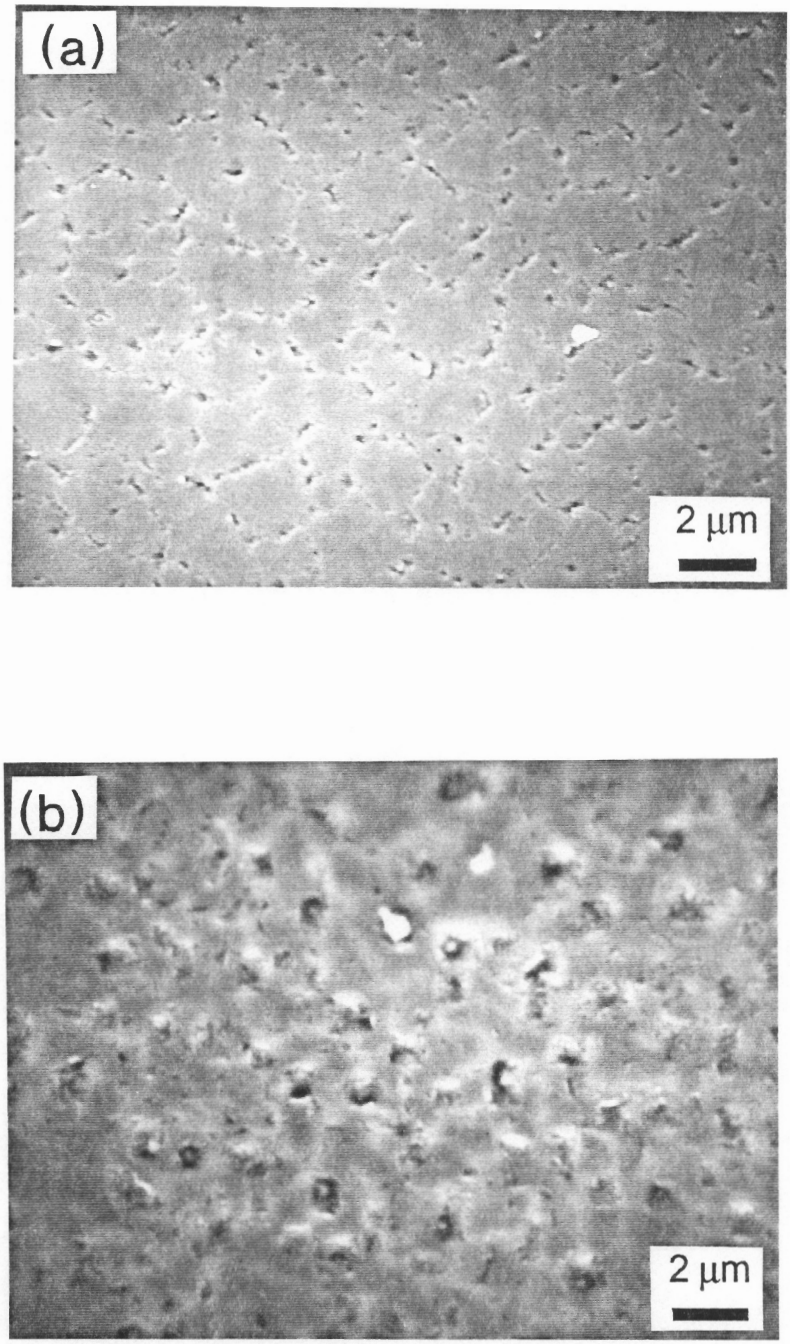

Figure 2.10: Surface morphology of Si substrates reacted 1000° C for (a) 10 sec., and (b) 5 min. from Procedure I.

reaction time, the defects increased in size and depth (Fig. 2.10(b)). It was also observed (Fig. 2.10) that the defects began to acquire regular edges with increasing time.

The high magnification micrographs of defects, for the reaction times of 10 seconds and 3 minutes at 1000° C, are shown in Fig. 2.11. The edges of defects were more defined for reaction time of 3 minutes than those reacted for 10 seconds. According to Newman et al. [26], these edges of the defects were believed to be lying parallel to silicon <110> directions. The formation of these defects is related to the etching of the Si(100) substrate which exposes the {111} planes of Si due to the slowest out–diffusion rate of Si from these planes. The resulting pyramidal shape defects can be seen (Fig. 2.11(b)) in accordance with this model.

In contrast to Procedure I, the pyramidal shape defects were not observed for Procedure II even with higher temperature and longer reaction times, as shown in Fig. 2.12. The reacted Si surfaces were smooth under SEM for reaction time up to 60 minutes. Hillock types of topography were obtained for longer reaction time (Figs. 2.12(c) and 2.12(d)). Figure 2.13 shows cross sections of the reacted Si substrates with and without the formation of hillocks. Some etch pits were shown under the hillocks in the Si substrate while no etch pits were observed for those with smooth topography. Mogab et al. [5] and Nagasawa et al. [20] reported that higher C_2H_2 pressures result in the formation of hillocks on porous defects to seal off the Si migration in the growth process. In our case, the formation of hillocks and etch pits were also shown to be a function of time.

Although the magnitude of reaction temperature and time for Procedure I were smaller than those for Procedure II, it is evident that the formation of defects was suppressed during Procedure II in comparison with Procedure I. The presence

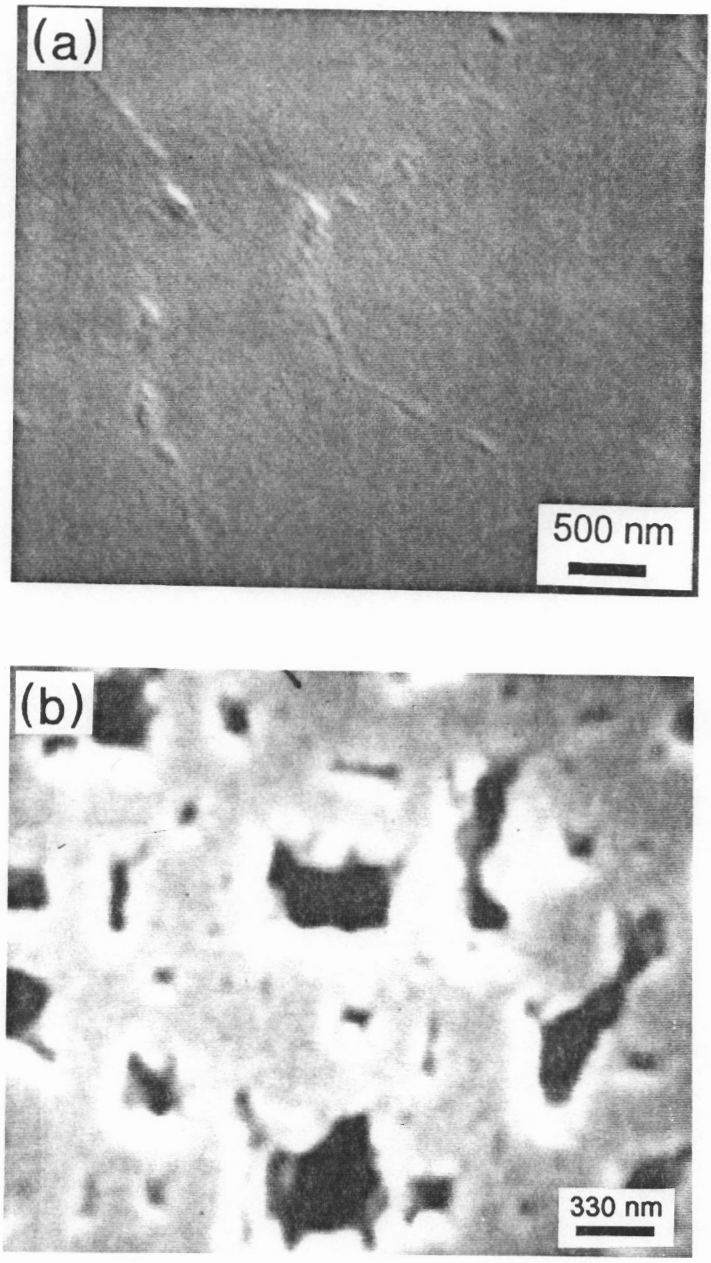

Figure 2.11: Surface morphology with high magnification of Si substrates reacted at 1000° C for (a) 10 sec., and (b) 3 min. from Procedure I.

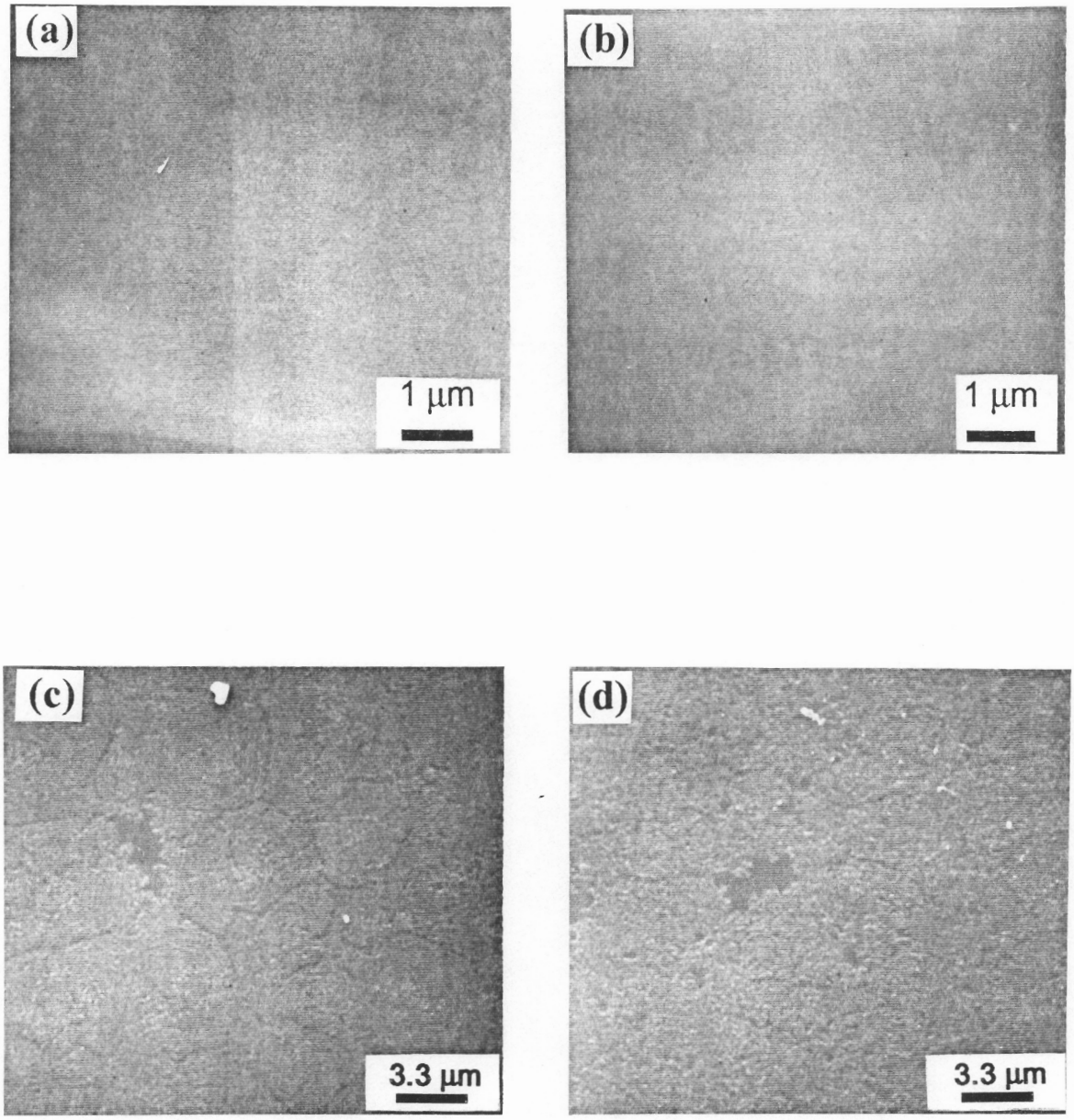

Figure 2.12: Surface morphology of Si substrates reacted for (a) 30 min., (b) 60 min., (c) 75 min., and (d) 90 min. from Procedure II.

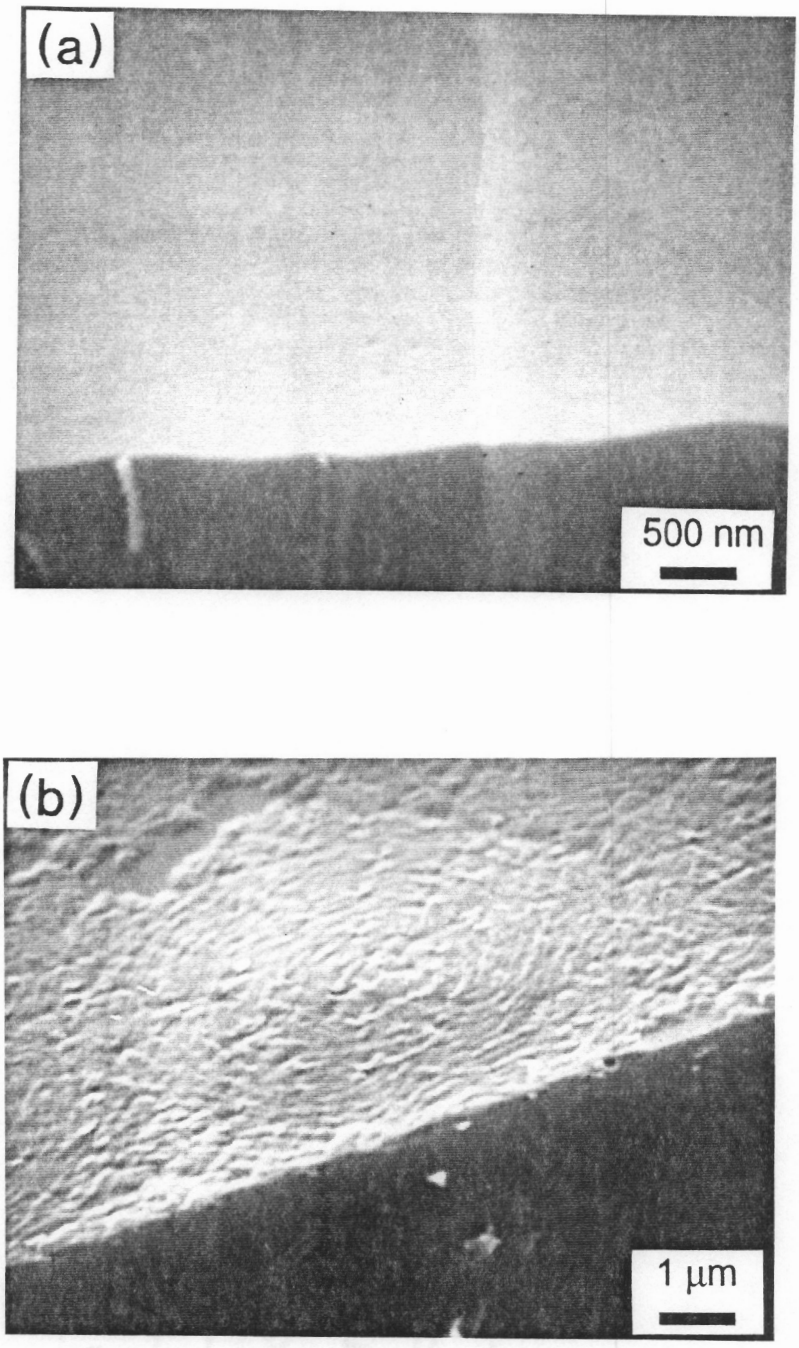

Figure 2.13: Cross–sectional SEM micrographs of Si substrates reacted for (a) 60 min., and (b) 75 min. from Procedure II.

of H_2 seems to play a key role in suppressing the formation of defects. For Procedure I, it is believed that the defects were formed by considerable Si diffusion from the bulk of Si substrate to surface because of the lack of initial carbonized SiC layer due to no C_2H_2 gas supply in the heating process [20]. In order to obtain a smooth and thick SiC layer, C_2H_2 and H_2 must be added simultaneously to the reaction reactor during the heating and reaction processes.

2.4.3 Defect formation process

The defect formation is closely related to the out–diffusion of Si during the reaction. Strinespring et al. [24] argued that the Si atoms must be supplied by out–diffusion if the SiC layer exceeded a monolayer thickness because of the nonreactivity of the hydrocarbon gases with SiC, especially for the SiC surface terminated with C–H bonds. Since the diffusivities of the Si and C atoms through the SiC layer are extremely small [27–29], the formation of defects may provide a higher rate of Si diffusion from the bulk of Si substrate to the surface. Thus, the defects are expected to be present with increasing thickness of SiC layer for both Procedures I and II.

During Procedure I, one of the possible processes for the formation of defects on (100) Si substrates is described in Fig. 2.14. A monolayer of SiC layer was first obtained without the formation of defects as shown in Fig. 2.14(a). As the the reaction proceeds, defects were formed and the sizes of these defects increase with increasing reaction time and temperature [5]. Meanwhile the thickness of the SiC layer increased because of the reaction between the out–diffused Si atoms and C_2H_2 gas. This step is believed to expose the unreacted Si substrate underneath the converted SiC layer (Fig. 2.14(b)). At this point, the unreacted Si substrate reacted

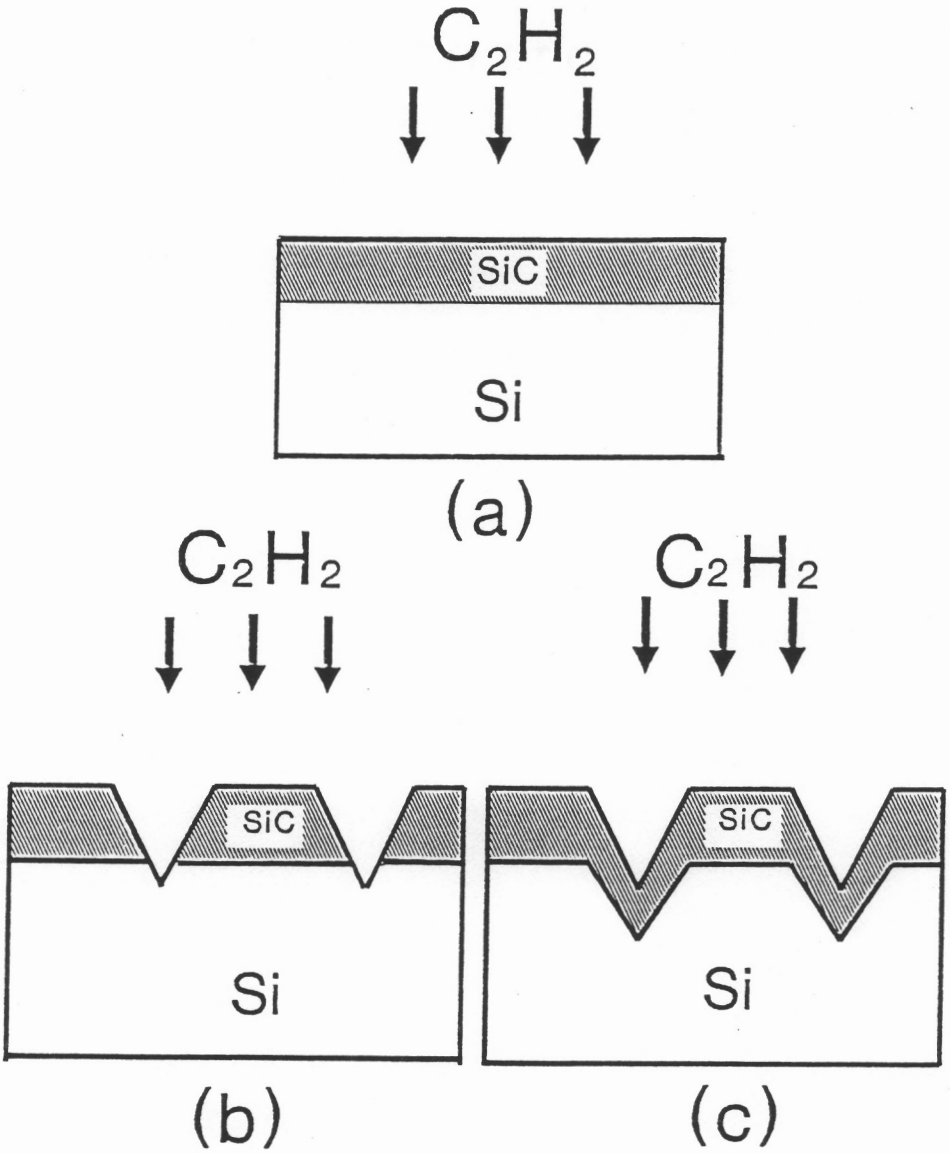

Figure 2.14: Illustration of the proposed process for the formation of defect.

with C–containing species in the gas phase to form the SiC film on the surface of the defects. Since the newly formed SiC could act again to reduce the out–diffusion of Si atoms from the bulk of substrate to surface, defects were created again in the SiC layer as shown in Fig. 2.14(c). By repeating the procedure mentioned above, the sizes of the defect could be increased to provide more conduits for the out–diffusion of Si atoms from the bulk of the substrate. In other words, the size and the depth of the defects increased with increasing time at a given temperature.

2.5 SUMMARY:

In a horizontal, hot wall CVD reactor, SiC buffer layer was obtained by the chemical conversion of Si(100) surface at 1050° C and at low pressures using H_2 and C_2H_2 as the carrier gas and carbon source, respectively. A good quality SiC layer with a thickness of 35Å and smooth morphology was obtained at 1050° C for 60 minutes. In the absence of H_2, the reaction is highly active and results in the formation of defects at lower temperature and shorter time. Since the Si atoms were supplied faster to the interface between C_2H_2 and the converted SiC film than the C atoms, the converted SiC layers were Si–rich. It is suggested that the presence of defects provide effective paths for the Si out–diffusion in the carbonization process. A possible process for the formation of defects was proposed.

2.6 REFERENCES:

1. T.T. Cheng, P. Pirouz, and T.A. Powell in *Chemistry and Defects in Semiconductor Heterostructures*, edited by M. Kawabe (Mater. Res. Soc. Symp. Proc., vol **148**, Pittsburgh, PA) p 229 (1989).
2. K. Ikoma, M. Yamanaka, H. Yamaguchi, and Y. Schichi, J. Electrochem. Soc. **138**, 3208 (1991).
3. A. Addamiano and J.A. Sprague, Appl. Phys. Lett., **44**, 525 (1984).
4. A.J. Learn and I.H. Khan, Thin Solid Films. **5**, 145 (1970).
5. C.J. Mogab and H.J. Leamy, J. Appl. Phys., **45**, 1075 (1974).
6. F.W. Smith, Surf. Sci., **80**, 388 (1979).
7. F.W Smith and B. Meyerson, Thin Solid Films, **60**, 227 (1979).
8. I.H. Khan and A.J. Learn, Appl. Phys. Lett., **15**, 410 (1969).
9. T. Sugii, T Aoyama, and T. Ito, J. Electrochem. Soc., **137**, 989 (1990).
10. K.E. Haq and I.H. Khan, J. Vac. Sci. Technol., **7**, 490 (1970).
11. I. Kusunoki, M. Hiroi, T. Sato, Y. Igari, and S. Tomoda, Appl. Surf. Sci., **45**, 171 (1990).
12. H.J. Kim, R.F. Davis, X.B. Cox, and R.W. Linton, J. Electrochem. Soc., **134**, 2269 (1987).
13. H.J. Kim, H–S Kong, J.A. Edmond, J.T. Glass, and R.F. Davis, in *Ceramic Transactions Vol 2, Silicon Carbide '87*, edited by J.D. Cawley and C.E. Samler.
14. P. Liaw and R.F. Davis, J. Electrochem. Soc., **132**, 642 (1985).
15. F. Bozso and J.T. Yates, Jr., J. Appl. Phys., **57**, 2771 (1985).

16. P.A. Taylor, M. Bozack, W.J. Choyke, and J.T. Taylor, Jr., J. Appl. Phys., **65**, 1099 (1989).

17. M. Iwami, M. Hirai, M. Kusaka, Y. Yakota, and H. Matsunami, Jpn. J. Appl. Phys., **28**, L293 (1989).

18. B.S. Meyerson, Appl. Phys. Lett., **48**, 797 (1986).

19. B.S. Meyerson, E. Ganin, D.A. Smith, and T.N. Nguyen, J. Electrochem. Soc., **133**, 1232 (1986).

20. H. Nagasawa and Y–I Yamaguchi, J. Crystal Growth, **115**, 612 (1991).

21. Y. Hattori, T. Suzuki, T. Murata, T. Yabumi, K. Yasuda, and M. Saji, J. Crystal Growth, **115**, 607 (1991).

22. F. Bozso, L. Muehlhoff, M. Trenary, W.J. Choyke, and J.T. Yates, Jr., J. Vac. Sci. Technol., **A2**(3), 1271 (1984).

23. Y. Katayama, T. Shimada, and K. Usami, Phys. Rev. Lett., **46**, 1146 (1981).

24. C.D. Stinespring and J.C. Wormhoudt, J. Appl. Phys., **65**, 1733 (1989).

25. Y. Katayama, K. Usami, and T. Shimada, Philos. Mag., **B43**, 283 (1981).

26. R.C. Newman and J. Wakefield, in *Solid State Physics in Electronics and Telecommunication*, edited by M. Desirant and J.L. Michels, p. 318.

27. C.D. Stinespring and W.F. Lawson, Surf. Sci., **150**, 209 (1985).

28. J.D. Hong and R.F. Davis, J. Am. Ceram. Soc., **63**, 546 (1980).

29. J.D. Hong, R.F. Davis, and D.E. Newbury, J. Mater. Sci., **16**, 2485 (1981).

Chapter 3 was published and entitled

"Low pressure chemical vapor deposition (LPCVD) of β–SiC on Si(100) using MTS in a hot wall reactor"

in Journal of Materials Research, vol. **8**, No. 10, 2617–2626 (1993)

Chapter 3: LOW PRESSURE CHEMICAL VAPOR DEPOSITION (LPCVD) OF β–SiC ON Si(100) USING MTS in A HOT WALL REACTOR

3.1 ABSTRACT:

Stoichiometric β–SiC thin films with a high preferred orientation of (111) planes were successfully deposited on Si(100) substrates at a relatively low temperature of 1050° C from the mixture of methyltrichlorosilane (CH_3SiCl_3 or MTS) and H_2 in a hot wall LPCVD reactor. No etching of the Si substrate and smooth topography of the deposit were observed at high H_2/MTS ratios and/or low deposition pressures. The presences of excess silicon, excess carbon, or incorporated hydrogen atoms in the films were not detected. Poor topography, degradation in preferred orientation, and etching of the Si substrate were observed at high values of deposition pressure, MTS concentration, and temperature. The etching on Si substrate was due to the out–diffusion of Si atoms from the substrate and the presence of Cl–containing radicals resulting from the decomposition of MTS molecules while transporting to the Si substrates. A deposition mechanism was proposed to model the deposition of SiC in a hot wall reactor by using (1): gas phase decomposition of MTS molecules; (2): adsorption of the intermediates on the surface; (3): reaction of the adsorbed intermediates to form SiC. The deposition rates were predicted very well for various deposition conditions in a hot wall LPCVD reactor.

3.2 INTRODUCTION:

β–SiC has been considered as a promising semiconductor for high temperature, high frequency, and high power electronic devices because of its superior properties, such as wide band gap, high saturated electron velocity, and high breakdown electric field [1–3]. Moreover, its resistance to intrinsic oxidation, corrosion, and creep at high temperatures also makes it a desirable protective coating for the devices operating at elevated temperatures [4,5]. In general, β–SiC is grown on α–SiC or single crystal Si for electronic applications. However, for the growth of β–SiC on α–SiC, the size is limited because of the difficulty in obtaining large area of α–SiC. Furthermore, the cost is high for using α–SiC substrates. Single crystal Si has been used widely as substrates for the growth of β–SiC due to the easy availability of high purity, high quality Si wafer. Unfortunately, growing β–SiC on Si substrates has known to be difficult due to the large mismatch (20 %) in lattice constants, and the differences in thermal expansion coefficients between the SiC film and the underlying Si substrate (8 %) [6]. Therefore, the growth of a SiC buffer layer by carbonizing the Si substrate with a hydrocarbon gas has been shown to be a necessary procedure in obtaining good quality SiC films on Si substrates [7]. Nevertheless, the processes mentioned above were performed at high temperatures and cold wall reactors.

In the present research, SiC thin films were grown on Si(100) substrates with a buffer layer by using the MTS–H_2 mixture in a hot wall LPCVD reactor at a lower temperature of 1050° C. MTS is a well known SiC precursor in CVD process because of its 1:1 molar ratio of silicon to carbon [8]. Therefore it is expected to result in a dense and stoichiometric SiC deposit from thermodynamic studies [9].

However, for the deposition of β–SiC thin films from this Cl–based precursor system, etching problems on Si substrates were reported because of the formation of Cl–containing radicals during the CVD process [10,11]. Although β–SiC thin films were reported to be deposited on Si substrates using MTS as the precursor, the Si substrates were etched before performing the CVD process [12]. So far, no attempt has been made to deposit SiC on smooth Si substrates by using MTS in a hot wall reactor. The use a hot wall reactor is based on the following reasons: (a) ability to deposit β–SiC thin films simultaneously upon many silicon wafers; (b) elimination of contamination from the susceptor by using very low deposition pressures [13].

In addition to the experiment conducted at 1050° C, the effects of experimental parameters (*e.g.* temperature, pressure, and MTS concentration) on the etching of Si substrates and on the growth rates of the SiC films were also studied in this research. A deposition mechanism, including both gas phase and surface reactions, was proposed for the SiC LPCVD process using MTS–H_2 precursor. Kinetic data were obtained by analyzing the deposition rates with a finite element (FEM) model.

3.3 EXPERIMENTAL PROCEDURE:

The schematic CVD hot wall reactor used in this research is shown in Fig. 3.1. The CVD reactor was a quartz tube with inner and outer diameters of 5.08 cm and 5.43 cm, respectively. An uniform temperature (± 5° C) zone of 6 cm was located around the center of the reactor. In order to maintain a constant and sufficient equilibrium vaporizing pressure of MTS, the bubbler was maintained at a constant temperature of 33° C. Furthermore, the needle valves and the tubing

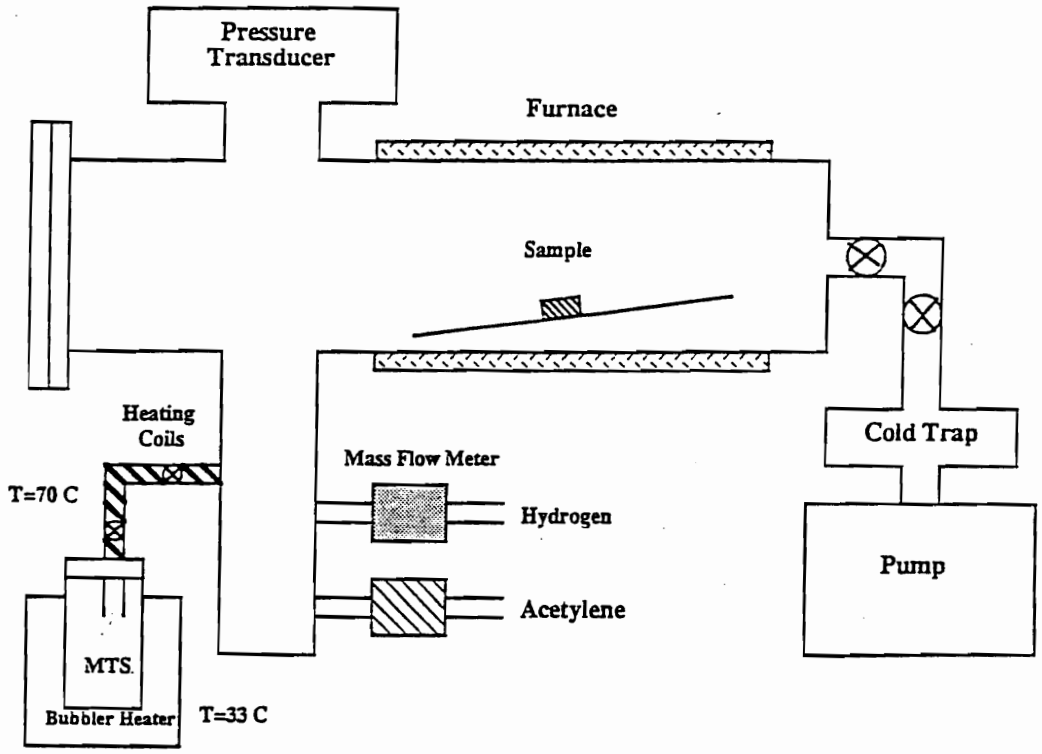

Figure 3.1: The schematic diagram of the hot wall LPCVD reactor.

between bubbler and reactor were held at 70° C to prevent the condensation of MTS (b.p. of MTS is 66° C) inside the tubing. Thermal profiles during the experiment are shown in Fig. 3.2.

Single crystal Si(100) substrates were used in this study. Before the deposition of SiC thin films from the mixture of MTS and H_2, a thin SiC buffer layer was grown by reacting the Si(100) substrate with acetylene (C_2H_2) which was diluted in flowing hydrogen (H_2) to a total pressure of 1.8 Torr. The growth process for this SiC buffer layer was carried out at 1050° C for a period of 60 min. Details of the growing procedure of the SiC buffer layer has been described elsewhere [14].

For each run of the SiC deposition, the substrate was placed at the center of the hot wall CVD reactor. The flow rate of H_2 was 300 sccm. H_2 to MTS ratio was calibrated at the predetermined values for each run. The CVD of SiC was started immediately after the SiC buffer layer. The deposition process was carried out at the temperature of 1050° C. The run time of each experiment was about 3 to 5 hours depending on the deposition parameters and the H_2/MTS ratio. Three deposition pressures of 1.8 Torr, 5 Torr, and 8 Torr were employed and the H_2/MTS ratio was adjusted to be 10, 50, or 100. The substrates were furnace cooled to room temperature in flowing H_2 after the deposition was completed. The phase–analysis of the deposited films were performed by x–ray diffraction (XRD) with a CuKα radiation and the transmission electron microscopy (TEM). Scanning electron microscopy (SEM) was used to observed the film morphology. The chemical bonding in the deposited films were examined by Fourier transform infrared spectroscopy (FTIR). To investigate the kinetics and reaction mechanism for depositing SiC thin films by using MTS, the deposition temperatures were varied from 1000° C to 1150° C. The thickness of the films were from cross sectional SEM

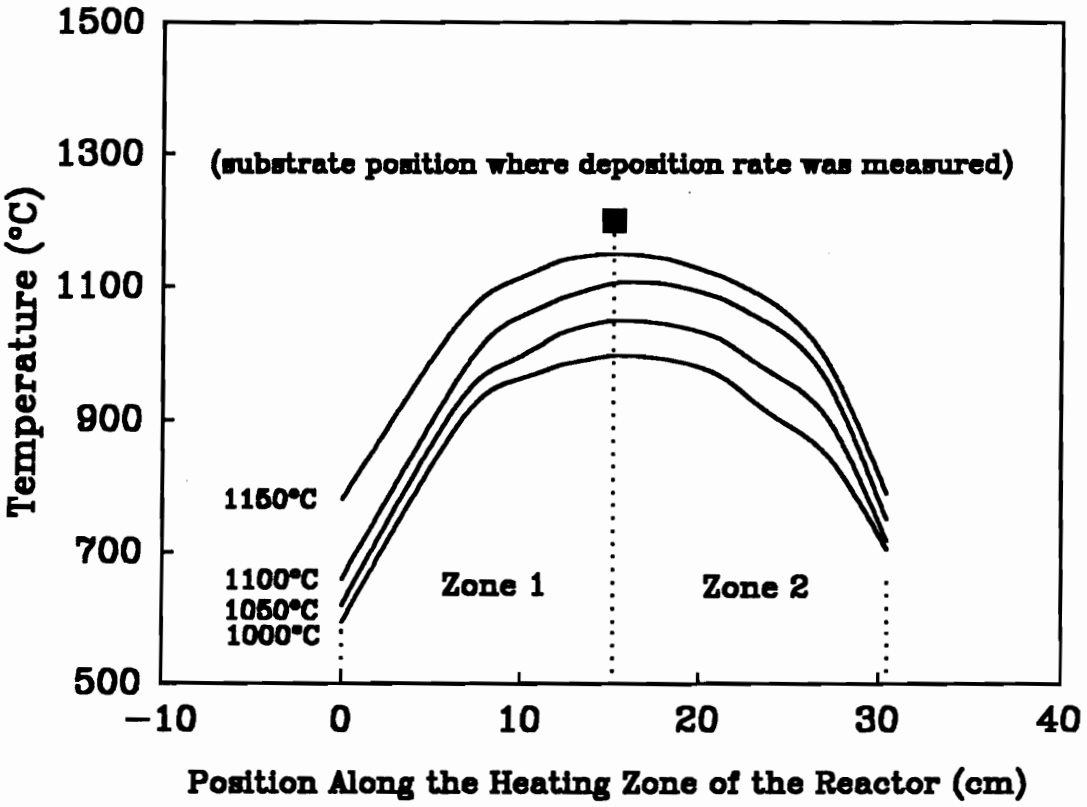

Figure 3.2: The thermal profiles of the CVD reactor. Temperature indicates the measured values at the center of the reactor.

to obtain the deposition rate and confirmed by weight increase of the substrate located at the center of the reactor.

3.4 RESULTS AND DISCUSSION:

3.4.1 Chemical vapor deposition of SiC films on Si(100) at 1050° C.

Figures 3.3(a), 3.3(b), and 3.3(c) show the cross sectional SEM of SiC thin films deposited on Si(100) substrates at 1050° C and a H_2/MTS = 100 for various deposition pressures of 1.8 Torr (Fig. 3.3(a)), 5 Torr (Fig. 3.3(b)), and 8 Torr (Fig. 3(c)). As can be seen from Figs. 3.3(a) and 3.3(b), there is no evidence of etching of the Si(100) substrates during deposition. Also, topography of SiC thin films at 1.8 and 5 Torr is smooth. The defect free Si(100) substrates after the CVD procedure indicated that the formation of the SiC buffer layers was effective in preventing from the etching of Si(100) substrates by the Cl–containing species during deposition.

However, defects on Si substrate were observed at a high deposition pressure (*i.e.* 8 Torr). In addition, a relatively rough topography of the deposited SiC thin films were observed at a higher deposition pressure of 8 Torr, as shown in Fig. 3.3(c). When the H_2/MTS ratios were further decreased to 50 and 10, changes in the etching of Si(100) substrates and topography of the deposited SiC thin films were observed as the deposition pressure was increased from 1.8 Torr to 5 Torr, as seen in Fig. 3.4 and Fig. 3.5, respectively. When comparing Figs. 3.4 and 3.5 to Fig. 3.3, the etching on the Si(100) substrates and a relatively rough topography were observed even at a lower pressure of 5 Torr for higher MTS concentrations (H_2/MTS = 50 and 10). Figure 3.6 shows the effects of MTS concentration at a

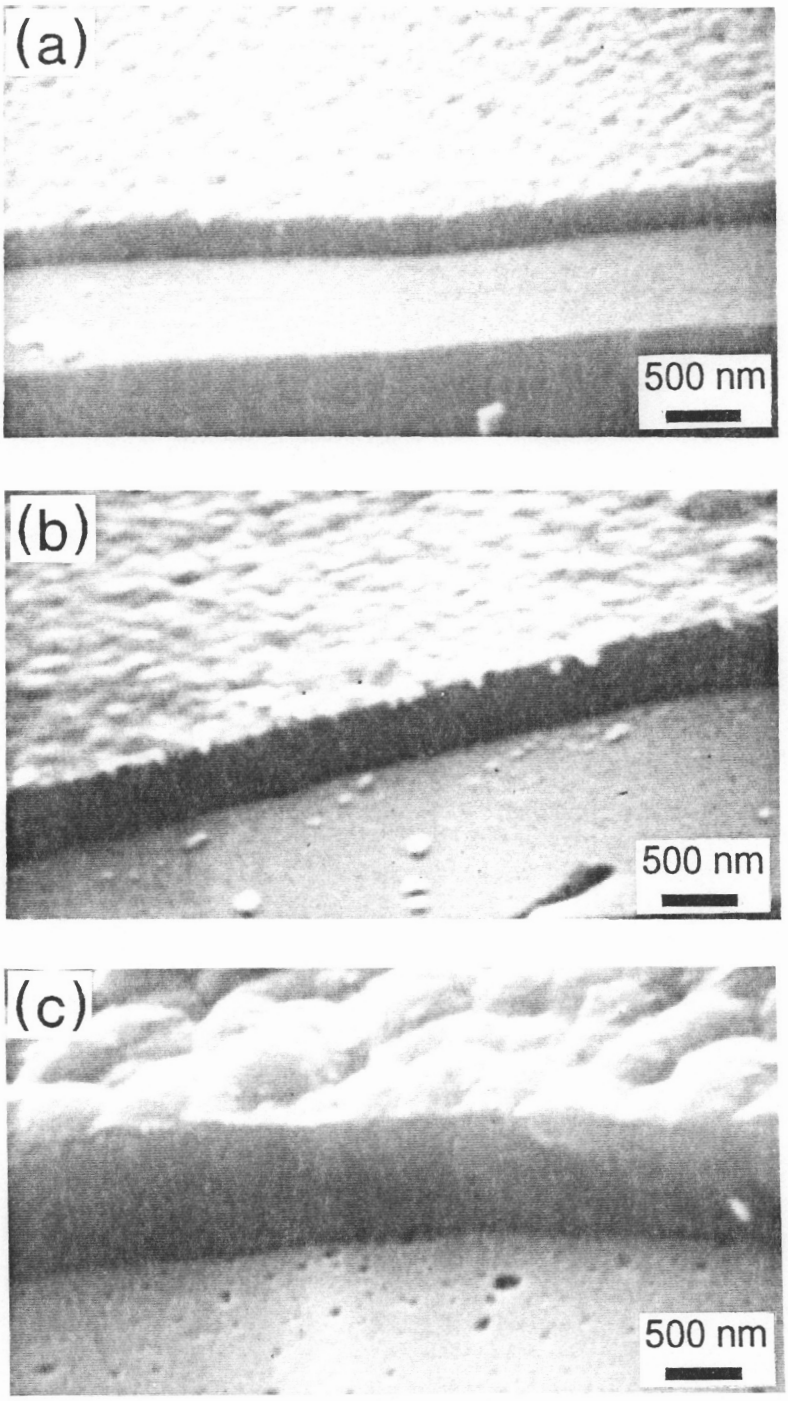

Figure 3.3: SEM micrographs of the SiC thin films on Si(100) substrates grown at 1050° C and H_2/MTS = 100 for (a) 1.8 Torr, (b) 5 Torr, and (c) 8 Torr.

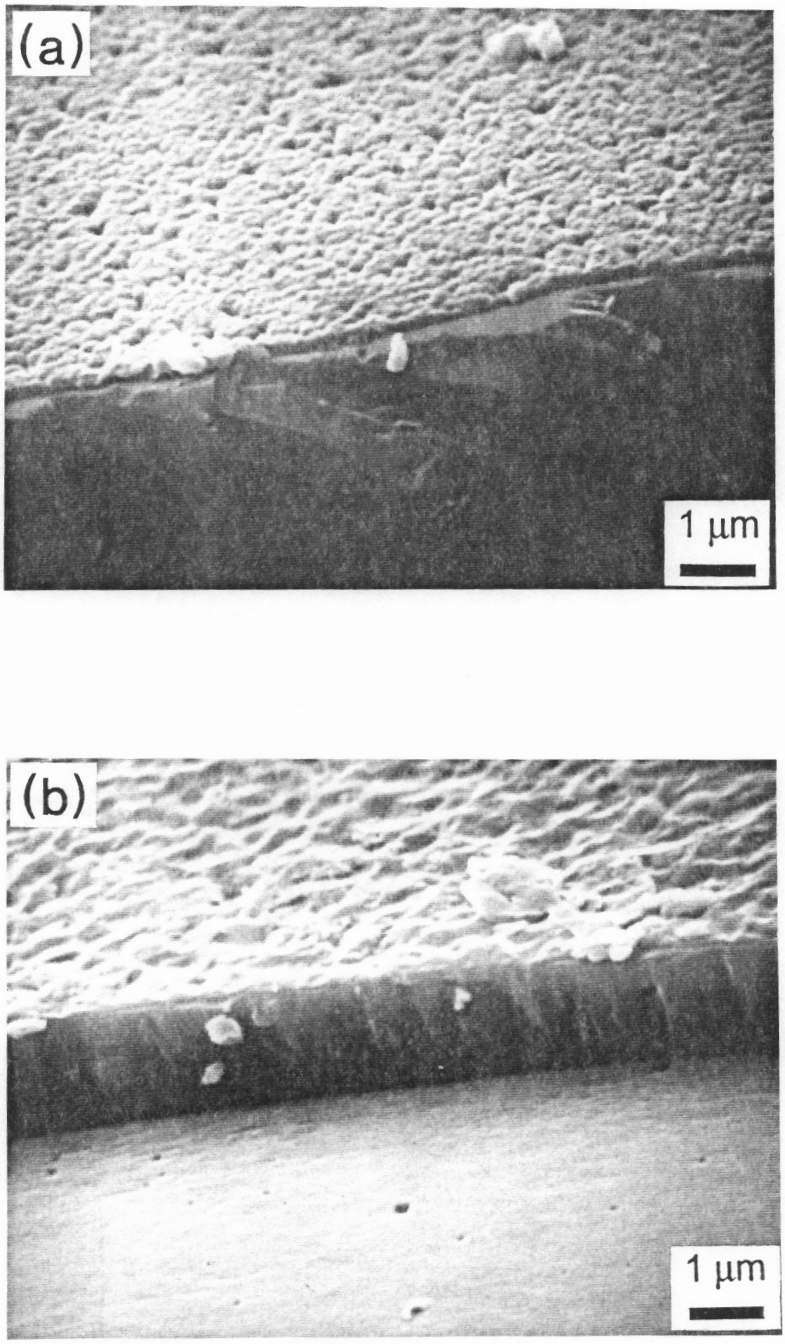

Figure 3.4: SEM micrographs of the SiC thin films on Si(100) substrates grown at 1050° C and H_2/MTS = 50, for (a) 1.8 Torr and (b) 5 Torr.

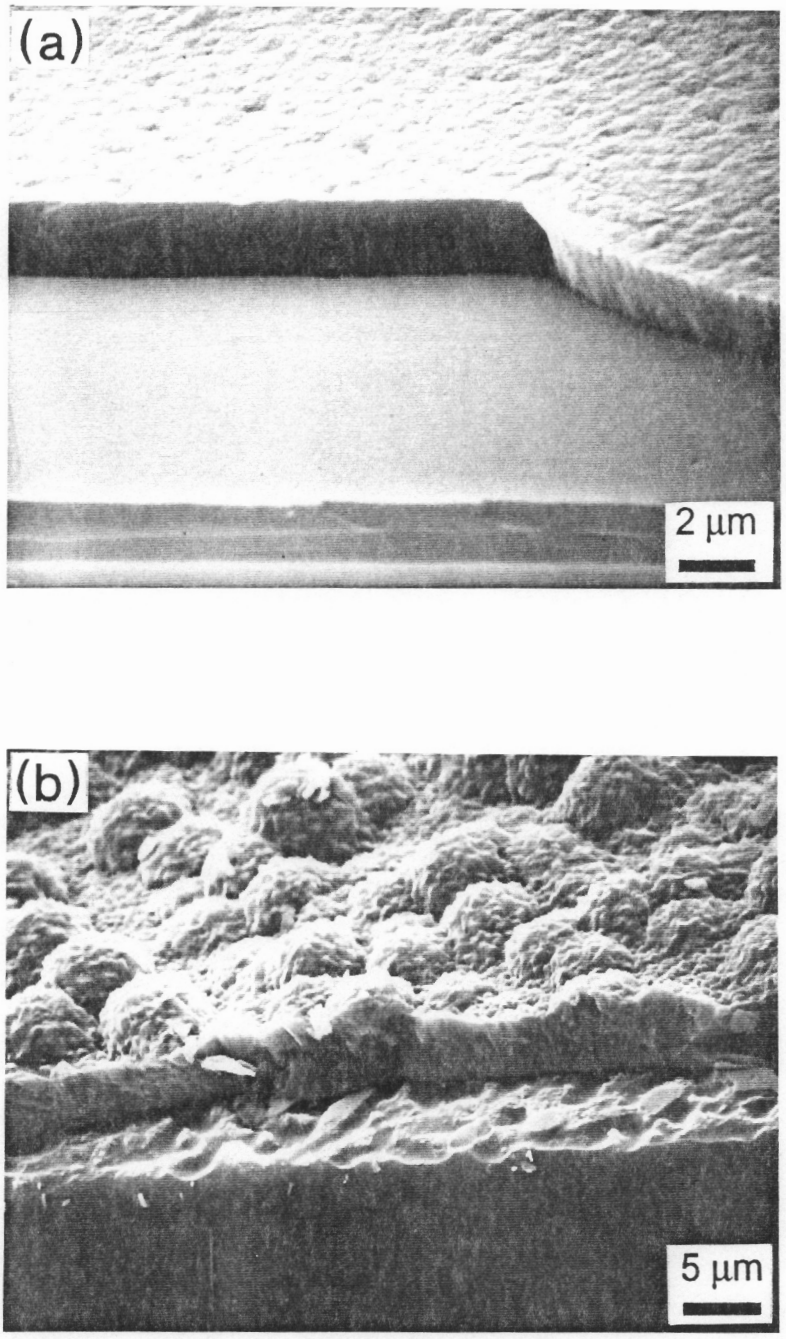

Figure 3.5: SEM micrographs of the SiC thin films on Si(100) substrates grown at 1050° C and H_2/MTS = 10 for (a) 1.8 Torr and (b) 5 Torr.

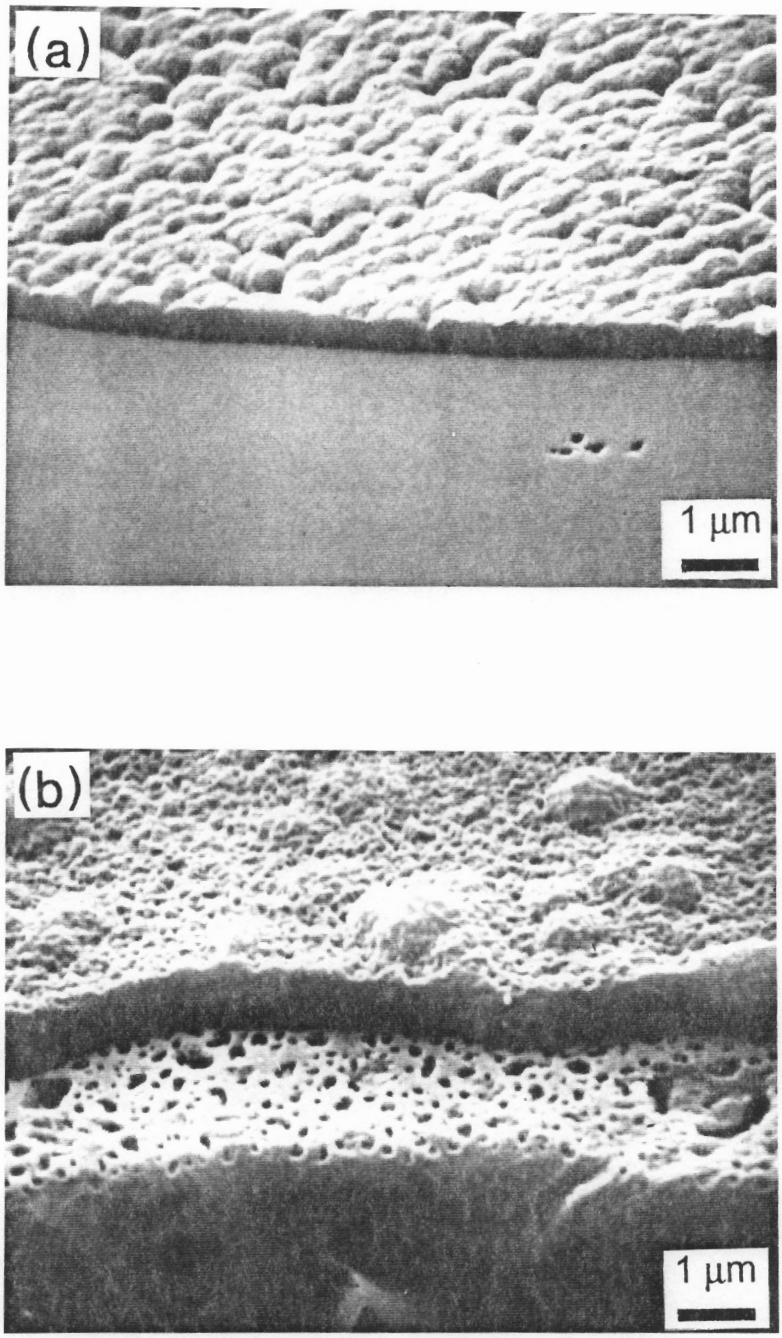

Figure 3.6: SEM micrographs of the SiC thin films on Si(100) substrates grown at 950° C, H_2/MTS = 10, and (a) 5 Torr and (b) 8 Torr.

lower deposition temperature of 950° C. The etching of the Si(100) substrates was also observed. Thus, it is evident from Figs. 3.3 to 3.6 that the formation of the etched Si substrates is due to high MTS concentrations and deposition pressures.

The typical XRD pattern for SiC thin films corresponding to Figs. 3.3 to 3.5 is shown in Fig. 3.7. It is to be noted that the films showed a preferred orientation of (111) of β–SiC, which indicated the films were highly oriented. Free Si, which is frequently obtained during the deposition of SiC thin films from the mixture of MTS/H_2 below 1400° C [15–20], was not detected. This observation was also confirmed by a clean electron diffraction pattern of β–SiC with very fine grains, as shown in Fig. 3.8. Figure 3.9 shows the FTIR spectrum which indicates the presence of only Si–C bonds [21–23]. No evidences of free silicon, carbon, and incorporated hydrogen atoms from the MTS–H_2 mixture were observed [19]. This indicated that the SiC thin films deposited at 1050° C were stoichiometric in this study.

In comparison to other studies [15,19], the defect free Si substrates and the stoichiometric β–SiC thin films obtained at this relatively lower deposition temperature were resulted from the lower deposition pressures [24]. According to Langlais et al [25], under low pressures and high H_2/MTS ratios, the MTS molecules dissociate into intermediate species containing Si (IP_{si}), C (IP_c), and gaseous by–products (BP_1), while transporting to Si substrates. The reactions of formation of Si and C from the adsorbed IP_{si} and IP_c, respectively, were similar to each other on the surface sites resulting in the stoichiometric SiC deposition despite of the polarity of IP_{si} in Si–C–H–Cl gas systems [26]. This deposition mechanism was also confirmed by comparing the calculated apparent activation energies to those for the deposition of stoichiometric SiC from MTS shown in the later section [17,25]. In

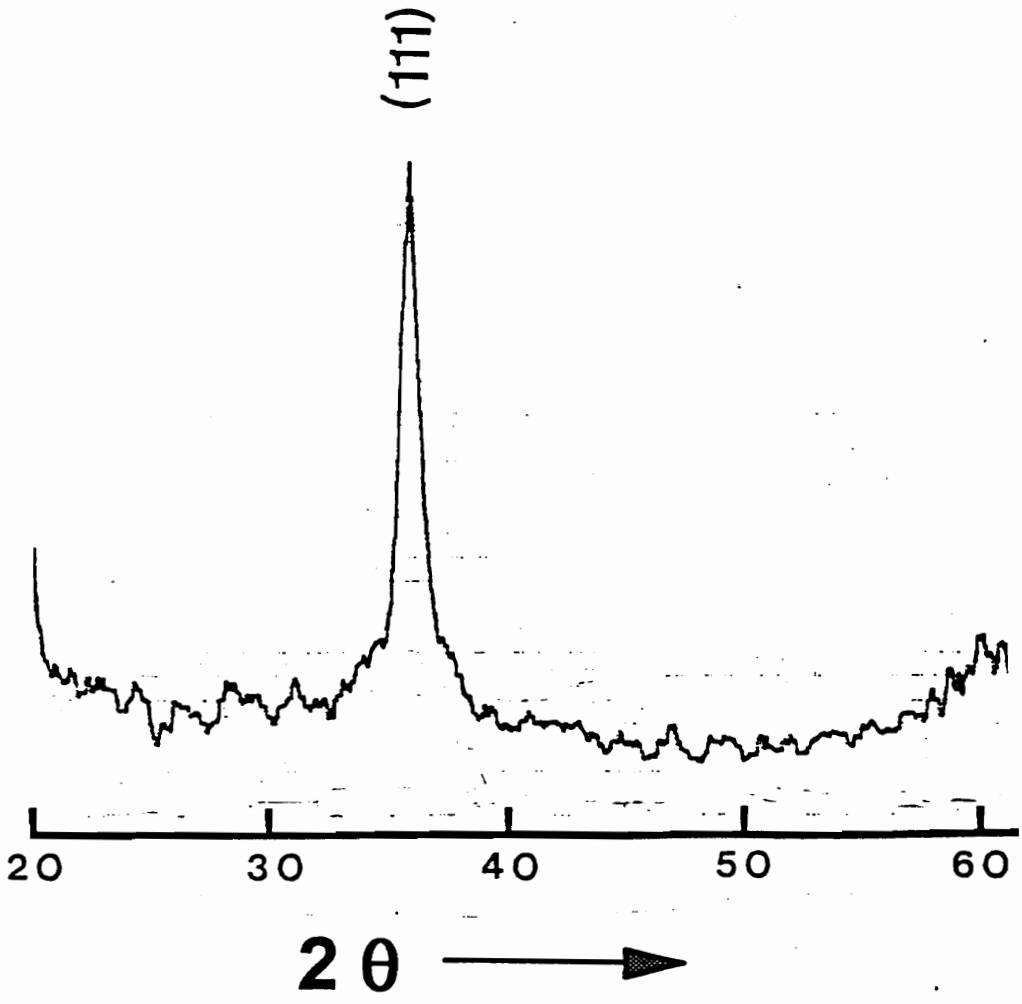

Figure 3.7: The XRD of CVD SiC thin films grown at 1050° C, H_2/MTS=100, and 1.8 Torr, which shows a highly preferred orientation of (111) planes of β–SiC.

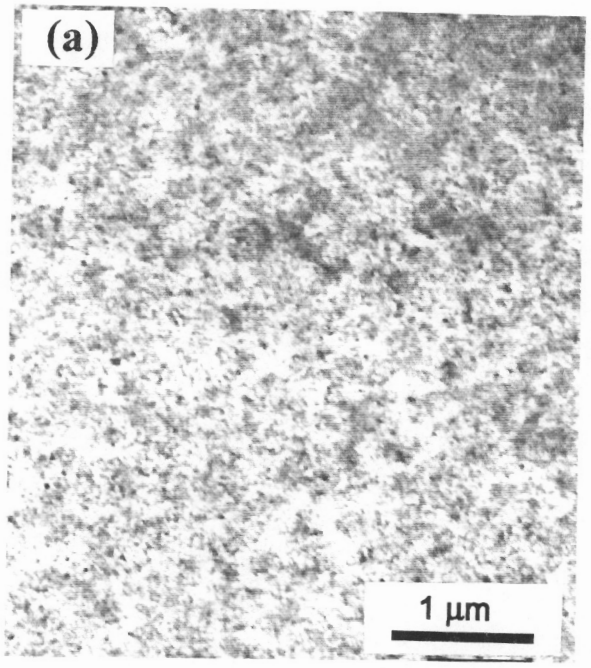

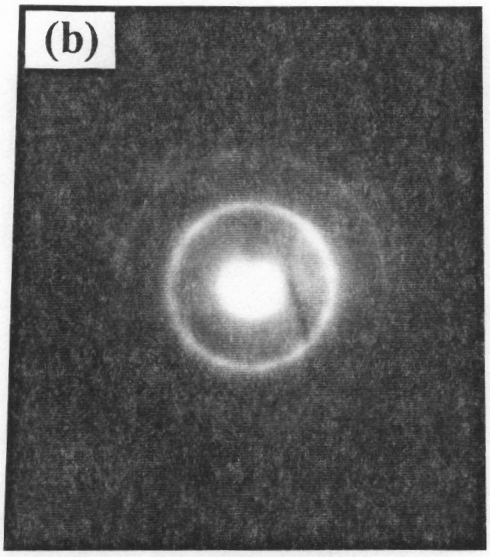

Figure 3.8: Plane view TEM micrograph (a) and the diffraction pattern (b) of a β–SiC thin film deposited at 1050° C, 1.8 Torr, and H_2/MTS=100, shownig very fine grains and the polycrystalline nature of β–SiC.

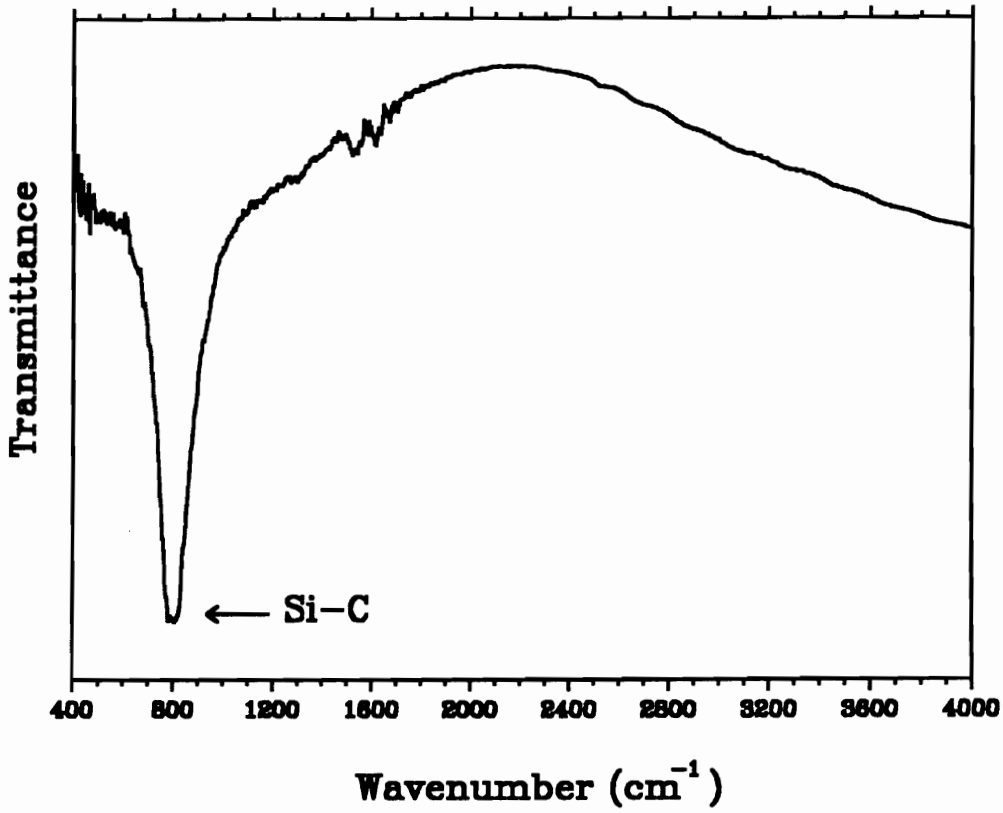

Figure 3.9: The FTIR transmission spectrum of CVD β–SiC deposited at 1050° C, 1.8 Torr, and H_2/MTS = 100.

addition, the amounts of Cl–containing radicals on the surfaces of Si substrates could have also been reduced because of the high desorption rates at low pressures. The Si substrates could thus be prevented from being etched under these conditions. Under higher pressures and MTS concentrations, the residence time of the MTS molecules (in zone 1 of Fig. 3.2), was increased. It is believed that the increase in residence time resulted in a larger amount of Cl–containing radicals through the decomposition of MTS when compared to those under low pressures and small MTS concentrations. Thus the etching on the Si substrates were observed for these conditions.

Furthermore, the disappearance of the incorporated hydrogen atoms are also believed to be caused by the high desorption rate of the absorbed species, which can cause a reduction in the concentration of the absorbed hydrogen atoms (H_{ad}) by suppression the following reaction [19]:

$$H_{2(g)} \Longleftrightarrow 2H_{(ad)} \tag{3.1}$$

where $H_{(ad)}$ is the absorbed hydrogen atom on the surface of the Si(100) substrate. Thus the absorbed hydrogen atoms (H_{ad}) can be transported into the gaseous flow before they can be absorbed onto the surface of the Si substrates.

3.4.2 Chemical vapor deposition of SiC thin films on Si(100) above 1050° C

Figure 3.10 shows the SEM micrographs of the SiC thin films deposited at 1100° C and 1.8 Torr under various H_2/MTS ratios. When compared to the SiC thin films deposited at 1050° C and 1.8 Torr, it is obvious that the temperature is also an important factor in causing etching on Si(100) substrates. Considering the nature of the hot wall reactor, the concentrations of the gaseous by–products, which contain Cl–containing radicals (Si etchants), on the surface of the Si(100) substrate

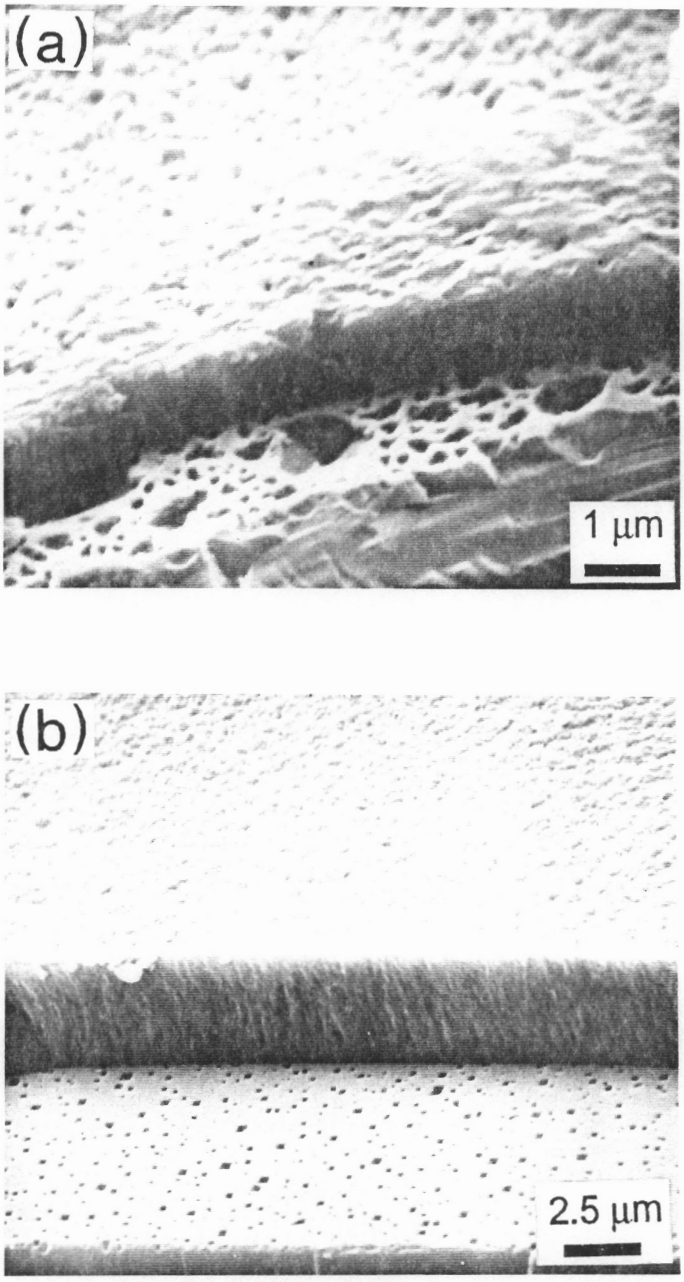

Figure 3.10: SEM micrographs of the β–SiC thin films on Si(100) substrates grown at 1100° C and 1.8 Torr for (a) H_2/MTS = 100 and (b) H_2/MTS = 10.

are expected to increase with increasing temperature. Thus, the Si(100) substrates are likely to be etched due to the higher concentrations of Cl radicals. It is also believed that these defects are formed by the out–diffusion of the Si atoms from the Si(100) substrates when the substrate temperatures are increased to those values that are higher than that required for the formation of the SiC buffer layer (*i.e.* 1050° C). The same defect formation process was also reported by Yoshinobu et al. for the Gas Source Molecular Beam Epitaxial of SiC thin films on Si substrates [27]. Therefore, the deposition temperatures not higher than the temperature for the buffer formation procedure are also desirable to obtain defect free Si(100) substrates when MTS is used as the source of SiC.

In contrast to the SiC thin films deposited at 1050° C, (200), (220), and (311) planes of β–SiC were observed at higher deposition temperatures. Furthermore, the (220) peak of β–SiC was more prominent than (111) peak at higher deposition temperatures, pressures, and MTS concentrations, as shown in Fig. 3.11. This tendency in the change of preferred orientation agrees with other reports for the deposition of SiC films by using MTS/H_2 [28,29]. The appearance of the (220) peak of β–SiC resulted from the changes on substrate surface during the early growth stage of SiC thin films and it affected the random orientation during the period [28]. These changes could be surface roughness and structural properties of the Si substrates. Additionally, with the increase in the growth rate, the influence of the substrate surface will be tenuous in the early stage of the SiC growth process.

3.4.3 Deposition mechanism and kinetics of SiC thin films deposited on Si(100)

The effect of temperature on the deposition rate of SiC films at H_2/MTS = 100 for various pressures is shown in Fig. 3.12. In general, the deposition rates

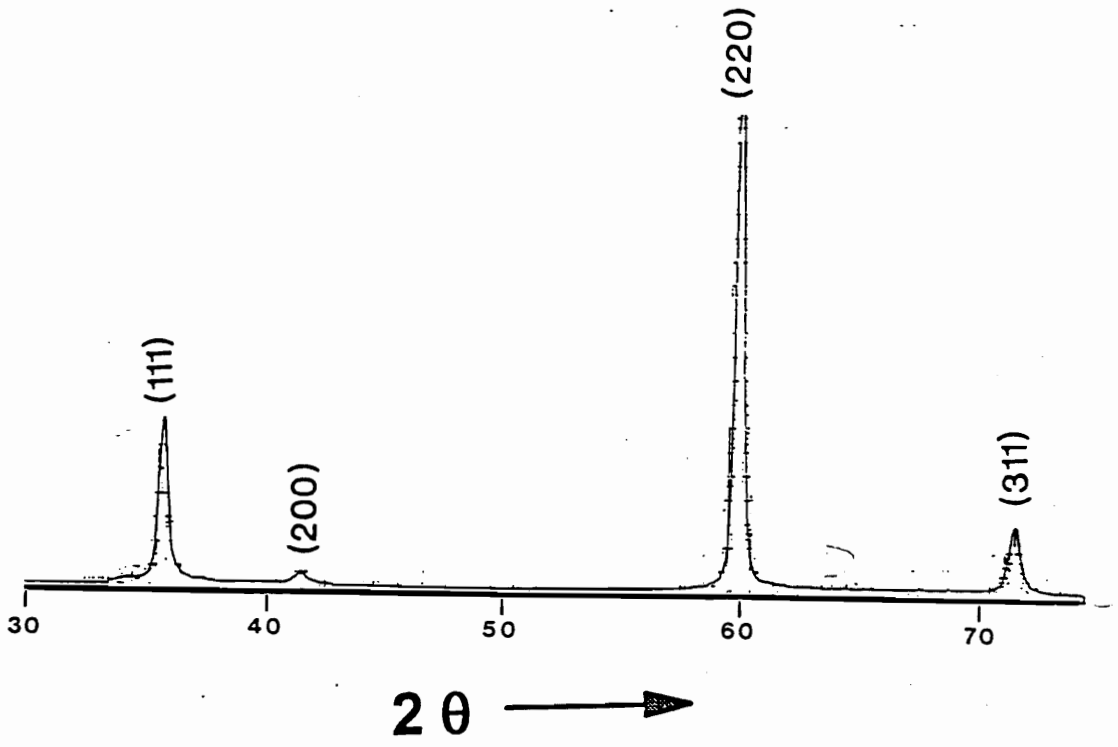

Figure 3.11: XRD of the CVD SiC thin films grown at 1150° C, H_2/MTS = 10, and 8 Torr.

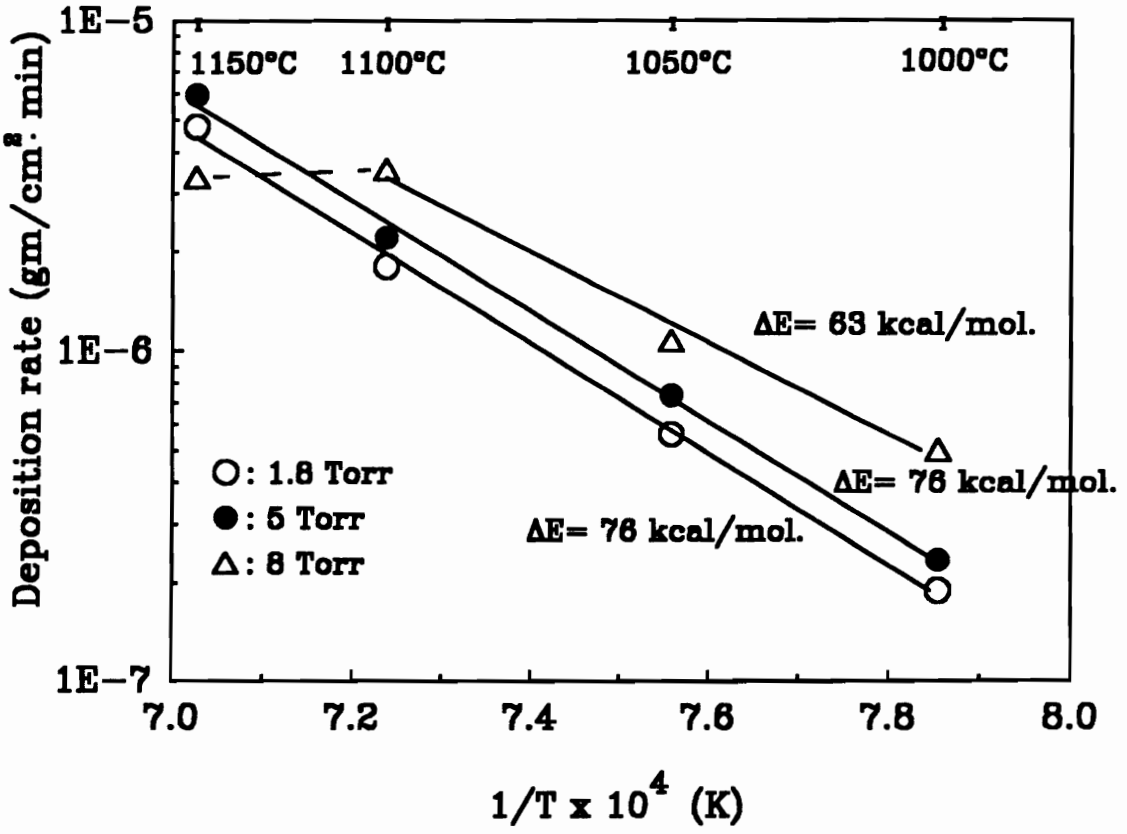

Figure 3.12: The effect of temperature on the SiC deposition rate from MTS in a hot wall LPCVD reactor for H_2/MTS = 100 and for various total system pressures.

increased with increasing temperature and pressure (the exception being the sample deposited at the highest temperature and pressure). As can be seen from Fig. 3.12, the deposition rate obtained at 8 Torr was even smaller than those obtained at 1.8 Torr and 5 Torr at 1150° C. When the H_2/MTS ratio was reduced to 50 (*i.e.* higher MTS concentration), the same phenomenon was observed at 5 Torr and the deposition rates for 5 and 8 Torr were almost the same as that for 1.8 Torr at 1150° C (Fig. 3.13). The decrease in deposition rates at high temperature and pressure, as shown in Figs. 3.12 and 3.13, is due to the hot wall nature of the reactor. It is possible that MTS is depleted by reacting on the walls of the reactor while transporting to Si substrates (zone 1 in Fig. 3.2). Thus, when the residence time of the MTS is increased by increasing the pressure and concentration, more gas species are depleted on the walls of the reactor before they can reach the substrate. The deposition temperature has a similar effect on the deposition rate of SiC thin films because the depletion effect will be more prominent with increasing temperature. The depletion effect decreases the local concentrations of MTS and of intermediate species at the Si substrate which is located at the center of the reactor. Therefore, the depletion effect could significantly change the deposition rates on the Si substrate depending on the experimental conditions. The depletion phenomena can also be used to explain the changes in the effective order of the reaction, as shown in Fig. 3.14. At 1150° C, the increase in concentration of the intermediates due to the increase in pressure is offset by the depletion effect. As a result, effective order of the reaction is deteriorated to zero.

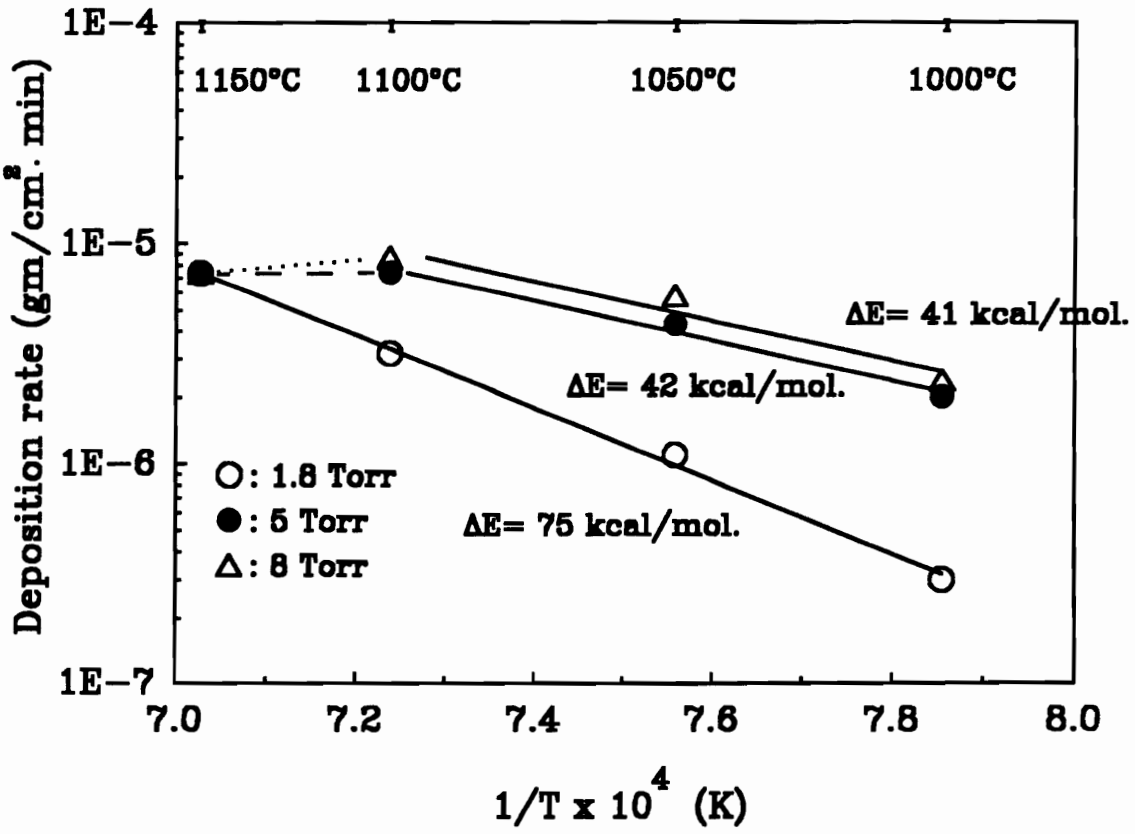

Figure 3.13: The effect of temperature on the SiC deposition rate from MTS in a hot wall LPCVD reactor for H_2/MTS = 50 and for various total system pressures.

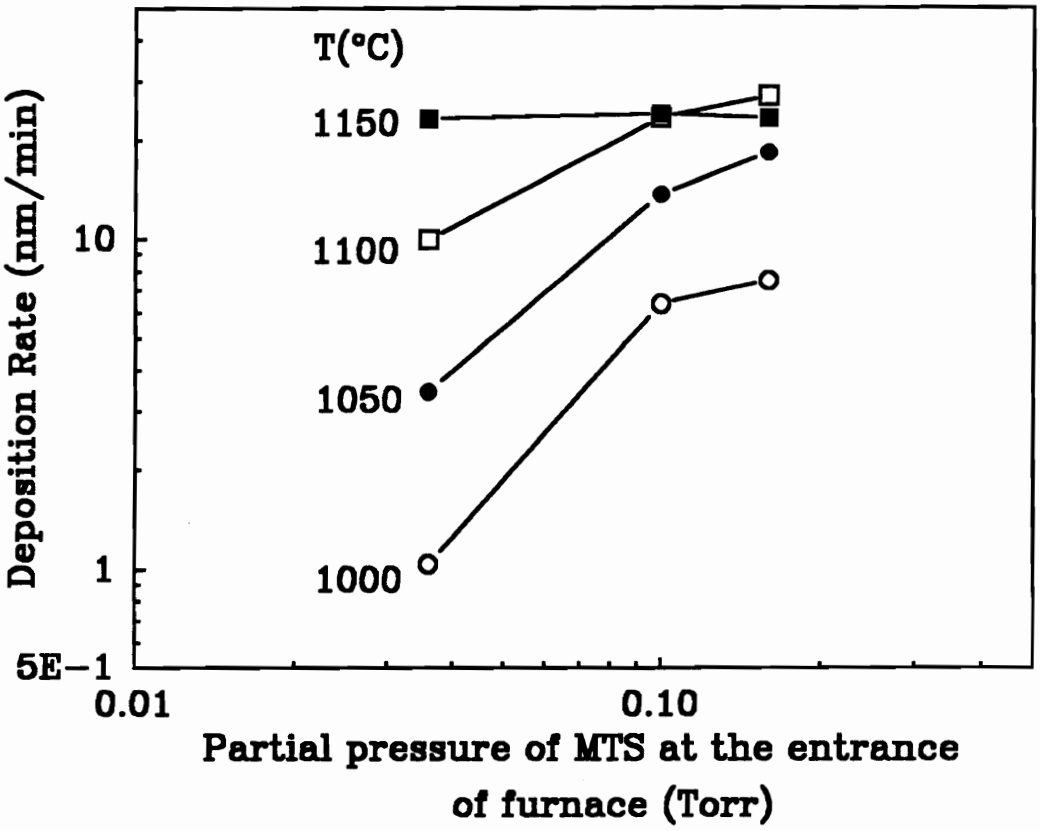

Figure 3.14: The deposition rates as a function of partial pressure of MTS at H_2/MTS = 50 for various temperatures.

The apparent activation energies were calculated by using the following Arrenhius equation:

$$G = G_0 \exp\left(-\frac{\Delta E}{kT}\right) \tag{3.2}$$

where G_0 is a pre–exponential factor, ΔE the apparent activation energy, k the Boltzmann constant and T the deposition temperature. As shown in Figs. 3.12 and 3.13, it is clear that the apparent activation energies vary in a large range. Similar variations in activation energy have been reported previously for the deposition of SiC thin films from MTS in a hot wall arrangement [30]. For H_2/MTS = 100, the apparent activation energies were 76 kcal/mole for both 1.8 Torr and 5 Torr. When the deposition pressure was raised to 8 Torr, the apparent activation energy decreased to 63 kcal/mole (Fig. 3.12). This decrease in apparent activation energy is also believed to be caused by the depletion effect mentioned above. Thus the concentrations of MTS, IP_{si}, and IP_c are smaller at higher deposition pressures. Similar tendencies were also observed for H_2/MTS = 50. However, in this case, the depletion effect occurred at a lower pressure of 5 Torr when compared to the 8 Torr for H_2/MTS = 100. In general, as shown in Figs. 3.12 and 3.13, the apparent activation energy decreased with increasing deposition pressure and MTS concentration.

In order to analyze the deposition rates in a hot wall CVD process a finite element model (FEM) was developed. A deposition mechanism which includes gas phase reaction and surface reaction were considered to correlate with the FEM model. The steps involved in the deposition mechanism of SiC from MTS/H_2 precursor are as follows:

(I). Gas phase decomposition of the MTS molecules

This reaction produces two kinds of intermediate species, one bearing silicon

(IP_{si}) and the other bearing carbon (IP_c), and gaseous by–products (BP_1).

$$CH_3SiCl_{3(g)} \underset{k_{-1}}{\overset{k_1}{\Longleftrightarrow}} IP_{si(g)} + IP_{c(g)} + BP_{1(g)} \tag{3.3}$$

where k_1 and k_{-1} represent the rate constants of the forward and backward reaction, respectively.

(II). Absorption of the intermediate species

$$IP_{si(g)} + * \overset{K_{a1}}{\Longleftrightarrow} IP_{si}* \tag{3.4}$$

$$IP_{c(g)} + * \overset{K_{a2}}{\Longleftrightarrow} IP_{c}* \tag{3.5}$$

where K_{a1} and K_{a2} are the equilibrium constants of the absorption processes associated with the species IP_{si} and IP_c, the symbol * represents the vacant surface sites, and IP_{si}* and IP_c* represent the absorbed species on the surface of Si substrate.

(III). Reaction of the absorbed intermediates

This reaction results in $Si_{(s)}$, $C_{(s)}$, and $SiC_{(s)}$, and other by–products.

$$IP_{si}* + IP_c* \overset{k_t}{\Longrightarrow} SiC_{(s)} + BP_{2(g)} \tag{3.6}$$

$$IP_{si}* \overset{k_{si}}{\Longrightarrow} Si_{(s)} + BP_{3(g)} \tag{3.7}$$

$$IP_c* \overset{k_c}{\Longrightarrow} C_{(s)} + BP_{4\,(g)} \tag{3.8}$$

Since the SiC films of this study are stoichiometric, the surface reactions (3.7) and (3.8) were neglected.

According to Langmuir isothermal expression [31], based on the above proposed model, the deposition rate of the SiC films can be expressed as:

$$\text{Deposition Rate of SiC (mol/cm}^2\text{–sec)} = k_t[IP_{si}*][IP_c*]$$

$$= k_tK_{a1}K_{a2}[IP_{si}][IP_c]/(1+K_{a1}[IP_{si}]+K_{a2}[IP_c])^2 \tag{3.9}$$

The equation of continuity for gas species i of the SiC CVD process can expressed as [32]:

$$\nabla \cdot N_i = \Sigma \rho_{ij} R_j \tag{3.10}$$

where the values of index i ranged from 1 to 5, that is, values of the pressure of MTS, H_2, IP_{si}, IP_c, and BP_i; N_i is the molar flux of species i, including both convective and diffusive flux. The right hand side of Eq. 3.10 represents the summation of chemical reactions, including both gas phase and surface reaction, associated with the gas species i.

Based on the above model and the calculations shown elsewhere [33], the comparison between the modeling predictions and the experimental results for H_2/MTS=50 are shown in Fig. 3.15. The agreement between the modeling calculations and experimental results is good except for the case of 1150° C and 8 Torr, at which the modeling calculation predicted a higher deposition rate. The estimated values of the kinetic constants for Eq. 3.3 to 3.6 are:

$$k_1\ (cm^3/mol\text{–}sec) = 0.2E{+}26\ EXP[(-448.2\ kJ/mol)/RT] \tag{3.11}$$

$$k_{-1}\ (cm^6/mol^2\text{–}sec) = 1.1E{+}32\ EXP[(-416.2\ kJ/mol)/RT] \tag{3.12}$$

$$K_{a1}\ (cm^3/mol) = 0.5E{+}11\ EXP[(-21.6\ kJ/mol)/RT] \tag{3.13}$$

$$K_{a2}\ (cm^3/mol) = 7.1E{+}09\ EXP[(-33.1\ kJ/mol)/RT] \tag{3.14}$$

$$k_t\ (mol/cm^2\text{–}sec) = 4.6E{+}05\ EXP[(-265.1\ kJ/mol)/RT] \tag{3.15}$$

The obtained kinetic constants were further used to estimate the deposition rates of SiC with the H_2/MTS ratios at 10 and 100, and the pressure of 1.8 Torr. The correlation between the modeling results and experimental data is good, as shown in Fig. 3.16.

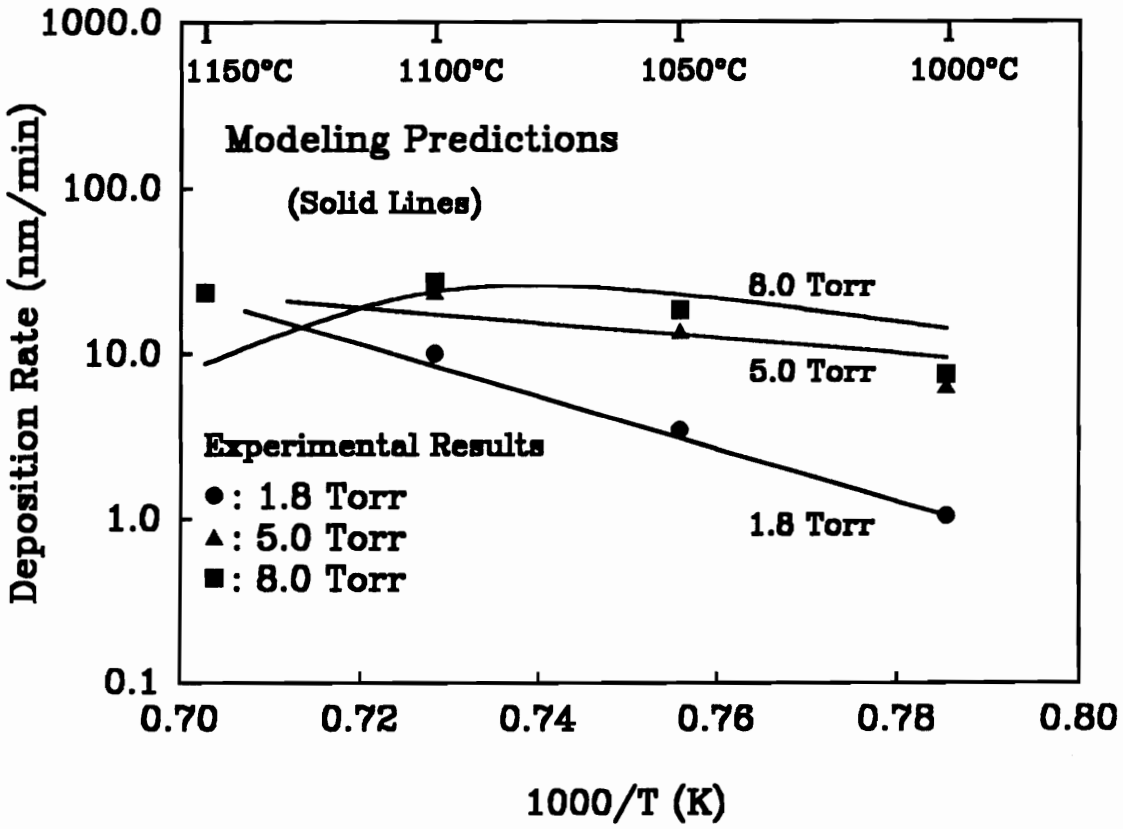

Figure 3.15: Comparison of the modeling predictions and the experimental results for H_2/MTS = 50.

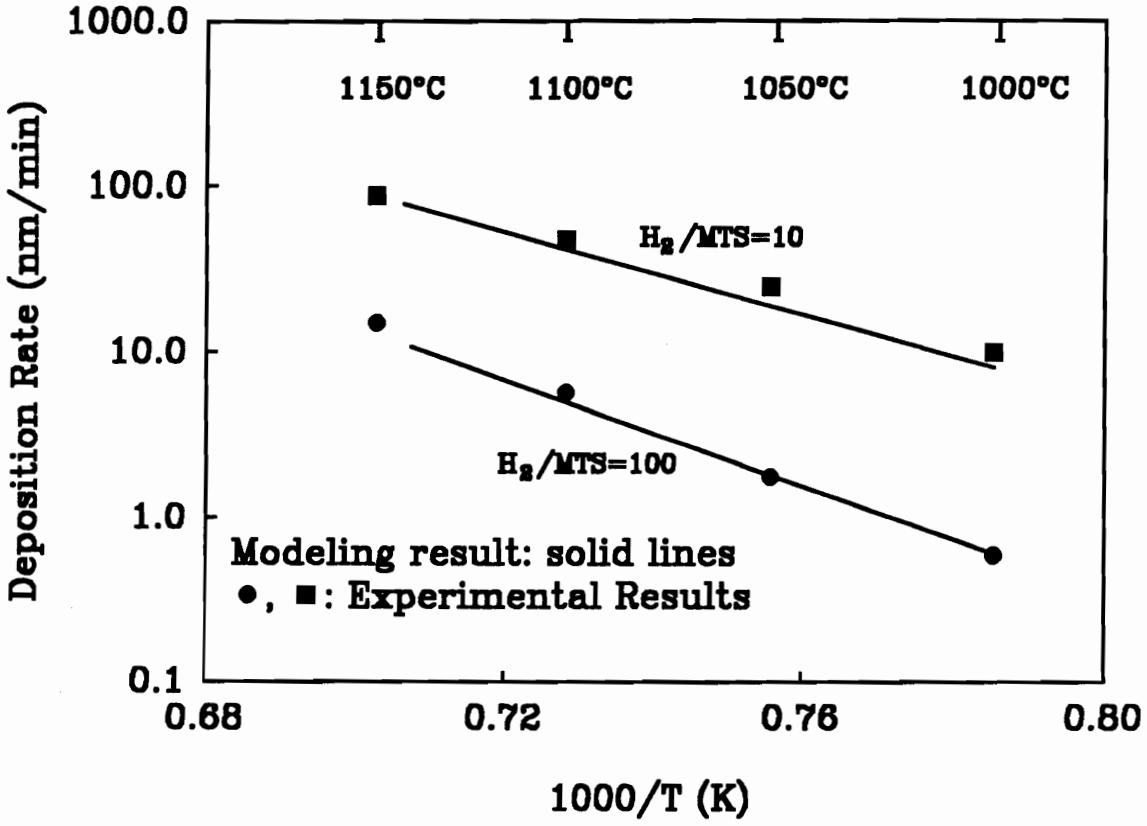

Figure 3.16: Comparison of the modeling predictions and the experimental results at 1.8 Torr for H_2/MTS = 10 and 100.

3.5 SUMMARY:

Stoichiometric, and polycrystalline β–SiC thin films with smooth surfaces have been successfully grown on Si(100) substrates with SiC buffer layers at 1050° C by using a mixture of MTS and H_2 in a hot wall LPCVD reactor. The deposited SiC thin films were stoichiometric and showed a preferred orientation of β–SiC (111). Defect free Si substrates and smooth topography was obtained at lower MTS concentrations and/or low deposition pressures. No existence of free silicon, carbon, and hydrogen atoms were observed. This has been attributed to the lower deposition pressures which suppresses the formation of gaseous intermediate species and Cl radicals. The etching on the surfaces of Si(100) substrates observed at higher MTS concentrations and deposition pressures is likely to occur due to the presence of Cl radicals from the decomposition of MTS occurring in zone 1, as shown in Fig. 3.2. Etching on the Si(100) substrates was also observed when the deposition temperatures were higher than that for buffer layer procedure (*i.e.* 1050° C). This could be the result of out–diffusion of Si atoms and the presence of Cl radicals.

Kinetic data of the proposed deposition model were derived by analyzing the deposition rates of the hot wall CVD process using the FEM method. This model agreed very well with the experimental data. Forward and backward rate constants of the gas phase reaction and rate constant of the surface constants were obtained.

3.6 REFERENCES:

1. H.P. Philipp and E.A. Taft, in *Silicon Carbide, A High Temperature Semiconductor*, edited by J.R. O'Connor and J. Smiltens (Pergamon, New York), p. 371 (1960).
2. W. von Muench and E. Pettenpaul, J. Appl. Phys., **48**, 4823 (1977).
3. W. von Muench and I. Pfaffender, J. Appl. Phys., **48**, 4831 (1977).
4. R.J. Price, Neucl. Technol., **35**, 320 (1977).
5. K. Sasaki, E. Samkuma, S. Misawa, S. Yoshida, and S. Gonda, Appl. Phys. Lett., **45**, 72 (1984).
6. T.T. Cheng, P. Pirouz, and T.A.Powell, in *Chemistry and Defects in Semiconductor Heterostructures*, edited by M. Kawabe (Mater. Res. Soc. Symp. Proc., vol. **148**, Pittsburgh, PA), p 229 (1989).
7. A. Addamiano and J.A. Sprague, Appl. Phys. Lett., **42**, 525 (1984).
8. M.J. Chappell and R.S. Millman, J. Mater. Sci., **9**, 1933 (1974).
9. A.I. Kingon, L.J. Lutz, and R.F. Davis, J. Am. Ceram. Soc., **66**, 558 (1983).
10. K. Ikoma, M. Yamanaka, H. Yamaguchi, and Y. Schichi, J. Electrochem. oc., Soc., **138**, 3028 (1991).
11. M.E. Weber and P.B. Armentrout, J. Phys. Chem., **93**, 1596 (1989).
12. S. Nishino and J. Saraie, in *Amorphous and Crystalline Silicon Carbide*, edited by G.L. Harris and C.Y.–W. Yang (Springe–Verlag Berlin, Heidelberg, 1989), p. 45.
13. F. Langlais, F. Hottier, and R. Cadoret, J. of Crystal Growth, **56**, 659 (1982).
14. C.C. Chiu and S.B. Desu, J. Mater. Res., **8**, 535 (1993).

15. J. Chin, P.K. Gantzel, and R.G. Hudson, Thin Solid Films, **40**, 57 (1977).

16. D.H. Kuo, D.J. Cheng, W.J. Shyy, and M.H. Hon, J. Electrochem. Soc., **137**, 3688 (1990).

17. D. Neuschütz and F. Salehomoum, in *Chemical Vapor Deposition of Metal and Ceramics II*, edited by T.M. Besmann, B.M. Gallois, and J.W. Warren (Mater. Res. Soc. Symp. Proc., **250**, Pittsburgh, PA) p. 41 (1992).

18. B.J. Choi, S.H. Jeun, and D.R. Kim, J. Eur. Ceram. Soc., **9**, 357 (1992).

19. C–H Chu, Y–M Lu, M.H. Hon, J. Mater. Sci., **27**, 3883 (1992).

20. K. Minato and K. Fukuda, J. Neucl. Mater., **149**, 233 (1987).

21. E. Gat, M.A. El Khakani, M. Chaker, A. Jean, S. Boily, H. Pépin, J.C. Kieffer, J. Durand, B. Cros, F. Rousseaux, S. Gujrathi, J. Mater. Res., **7**, 2478 (1992).

22. W.G. Spitzer, D.A. Kleinmann, and D. Walsh, Phy. Rew., **113**, 127 (1959).

23. W.G. Spitzer, D.A. Kleinmann, and C.J. Frosch, Phy. Rew., **113**, 133 (1959).

24. S. Motojima and M. Hasegawa, J. Vac. Sci. Technol. A, **8**, 3763 (1990).

25. F. Langlais and C. Prebende, in *Proceedings of the 11th International Conference on Chemical Vapor Deposition*, edited by K.E. Spear and G.W. Cullen, p. 686 (1990).

26. G.S. Fischman and W.T. Petuskey, J. Am. Ceram. Soc., **68**, 185 (1985).

27. T. Yoshinobu, H. Mitsui, Y. Tarui, T. Fuyuki, and H. Matsunami, J. Appl. Phys., **72**, 2006 (1992).

28. D.J. Cheng, W.J. Shyy, D.H. Kuo, and M.H. Hon, J. Electrochem. Soc., **134**, 3145 (1987).

29. M.G. So and J.S. Chun, J. Vac. Sci. Technol., **A6**, 5 (1988).

30. J. Schlichting, Powder Metall. Inter., **12**, 141 (1980).

31. S.B. Desu, J. Am. Ceram. Soc., **72**, 1615 (1989).

32. R.B. Bird, W.E. Steward, and E.N. Lifgtfoot, in *Transport Phenomena*, (John Wiley & Sons, New York, 1960).

33. C.Y. Tsai, S.B. Desu, and C.C. Chiu, J. Mater. Res., **9**, 104 (1994).

Chapter 4 was entitled

"Deposition of epitaxial β–SiC films on modified Si(100)
from MTS in a hot wall LPCVD reactor"
submitted to Journal of Materials Research

"Epitaxial growth of β–SiC on Si(100) using MTS
in a hot wall LPCVD reactor"
accepted by Philosophical Magazine Letters

"Growth of epitaxial β–SiC films on porous Si(100) substrates
from MTS in a hot wall LPCVD reactor"
in *Metal–organic chemical vapor deposition of electronic ceramics*
Materials research society symposium proceedings, vol. **335**
(Materisls research scoiety, Pittsburgh, PA, 1994)
(in press)

Chapter 4: DEPOSITION OF EPITAXIAL β–SiC FILMS ON MODIFIED Si(100) FROM MTS IN A HOT WALL LPCVD REACTOR

4.1 ABSTRACT:

Epitaxial β–SiC thin films were grown on modified Si(100) substrates from methyltrichlorosilane (CH_3SiCl_3 or MTS) in a hot wall reactor by using low pressure chemical vapor deposition (LPCVD). At 1150° C, the growth rate of the β–SiC films was 120 Å/min. Epitaxial β–SiC(100) thin films were deposited after the deposition time of 12.5 min. However, the crystallinity of the deposited films was influenced by the deposition time. For example, the occurrence of rotational β–SiC(100) crystals and polycrystalline β–SiC with a highly preferred orientation of (100) planes were obtained for the deposition time of 50 min. XRD and TEM showed the appearance of polycrystalline β–SiC films with a preferred orientation of β–SiC(111) after further increasing the deposition times (time $\geq$ 75 min). At 1100° C, polycrystalline β–SiC films with poor surface morphology were observed even though the film had a preferred orientation of β–SiC(100) for short deposition time (*e.g.* 12.5 min). Polycrystalline β–SiC(111) film was obtained for the deposition time of 200 min at this temperature.

4.2 INTRODUCTION:

β–SiC is a promising semiconductor for high temperature, high frequency, and high power electronic devices because of its large band gap, high saturated

electron velocity, and high breakdown electric field. In addition, its intrinsic resistance to oxidation, corrosion, and creep at high temperatures also makes it a desirable protective coating for the devices operating at elevated temperatures.

The growth of β–SiC on Si substrates by chemical vapor deposition (CVD) is an attractive process in fabricating β–SiC films. Recently there has been significant progress in depositing single crystal β–SiC films on Si substrates. However, all of these efforts have been conducted by using a cold wall reactor, and at higher temperatures (T>1300° C). Below 1300° C, stoichiometric β–SiC films were grown on smooth Si substrates in a hot wall LPCVD reactor by using MTS precursor; however, the deposited β–SiC films were polycrystalline with a preferred orientation of (111) of β–SiC [1]. Furthermore, a large number of defects were produced by depositing β–SiC on smooth Si(100) substrates because of a large lattice constant mismatch (20%) between β–SiC deposit and the underlying Si substrate. Therefore, by using modified Si substrates, it is expected that (i) the number of defects will be reduced due to the release of strain between the β–SiC deposit and Si substrates, and (ii) the formation of the preferred orientation of β–SiC(111) will be depressed and the β–SiC(100) will be promoted since the sites to nucleate β–SiC(111) might be eliminated [2]. Until now, no attempt has been made to deposit single crystal β–SiC on Si(100) in a hot wall LPCVD reactor. Advantages in using hot wall LPCVD reactors are (i) the ability to deposit single crystal β–SiC thin films simultaneously upon many Si wafers and (ii) elimination of contamination from the susceptor by using very low deposition pressure [3].

The purpose of this study is to present a novel procedure to grow single crystal β–SiC films with the orientation of (100) on modified Si(100) substrates by using a hot wall LPCVD reactor and MTS/H_2 mixture. The effect of deposition

time on the orientation of the films was also reported.

4.3 EXPERIMENTAL PROCEDURE:

The hot wall LPCVD reactor was a quartz tube with inner and outer diameters of 5.08 cm and 5.43 cm, respectively, as shown in Fig. 3.1. The uniform temperature (± 5° C) zone of 6 cm was located around the center of the reactor. To obtain a constant and sufficient equilibrium vaporizing pressure of MTS, the bubbler was maintained at a constant temperature of 33° C. Furthermore, the needle valves and the tubing between bubbler and reactor were held at 70° C to prevent the condensation of MTS inside the valves and the tubing.

Single crystal Si(100) substrates were used in this study. The reaction chamber was evacuated and purged with H_2. Then the Si substrates were heated in flowing H_2 in order to remove any residue of the native oxide on the surface. Before the deposition of SiC films from the mixture of MTS and H_2, a modified surface with a porous nature and a thin layer of converted SiC on the Si substrate was obtained by reacting the Si(100) substrate with purified acetylene (99.6%) without flowing H_2, as shown in Fig. 4.1. The total pressure for this process was 0.1 Torr. This process was performed at 1000° C for 5 min. Details of the process for obtaining modified Si substrates has been described elsewhere [4,5].

After the modified Si substrate was obtained at 1000° C, the temperature of the furnace was increased to 1100° C or 1150° C to carry out the CVD process at a total pressure of 1.8 Torr. During the CVD process, the flow rate of H_2 was kept at 300 sccm, and the H_2 to MTS ratio was calibrated to be 100. The samples were furnace cooled to room temperatures in flowing H_2 after the depositions were

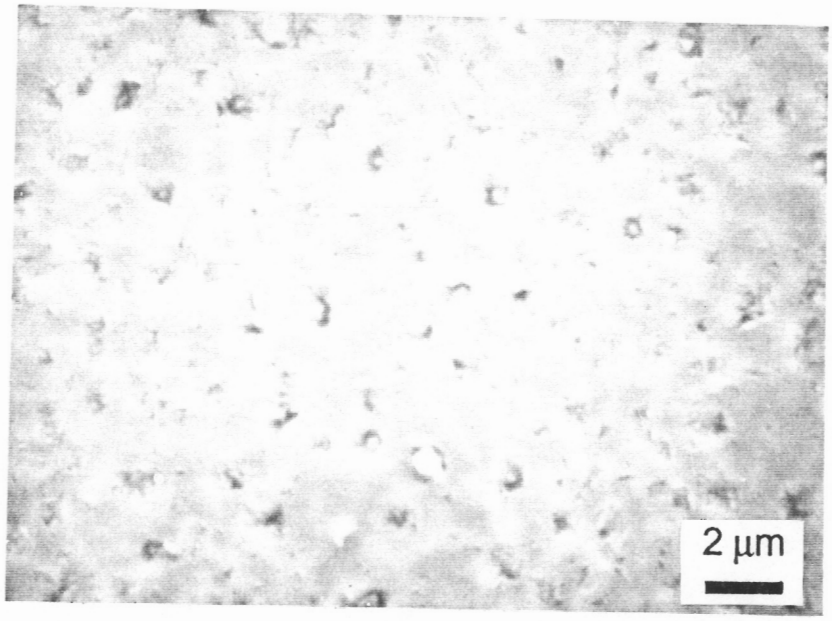

Figure 4.1: Topography of a modified Si(100) substrate from the reaction between smooth Si(100) surface with C_2H_2 at 1000° C.

completed. The overall experimental procedure is shown in Fig. 4.2. The phase–analysis of the deposited β–SiC films was examined by XRD with a CuKα radiation and transmission electron microscopy (TEM). Scanning electron microscopy (SEM) was used to observe the thickness and morphology of the deposited β–SiC films.

4.4 RESULTS AND DISCUSSION:

4.4.1 Epitaxial Growth of β–SiC at 1150° C on modified Si(100).

The β–SiC films obtained at this temperature (1150° C) were shiny and mirror–like. A typical cross section SEM micrograph showing the surface morphology and thickness of the film is presented in Fig. 4.3. The film was deposited for 12.5 min. In general, the growth rate of the SiC thin films is 120Å/min at this temperature. It is interesting to note that no SiC deposit was observed on the facets inside the pore (Fig. 4.3) although the surface reaction is expected to be the controlling reaction under these deposition conditions [1]. We do not have an explanation for this at this point.

Figure 4.4 shows the XRD pattern of sample deposited for 12.5 min ,whose cross section SEM is given in Fig. 4.3. The peaks for single crystal Si(100) substrates underneath the β–SiC film are at 69° and 62° for Si Kα(400) and Si Kβ(400), respectively. As shown in Fig. 4.4, the (200) and (400) planes were the only diffraction planes from the deposited β–SiC thin films from the XRD pattern. This indicated that these films have a highly preferred orientation of β–SiC(100). In order to further examine the preferred orientation of the films by using TEM, the electron beam was normal to the surfaces of the samples under TEM. For this short

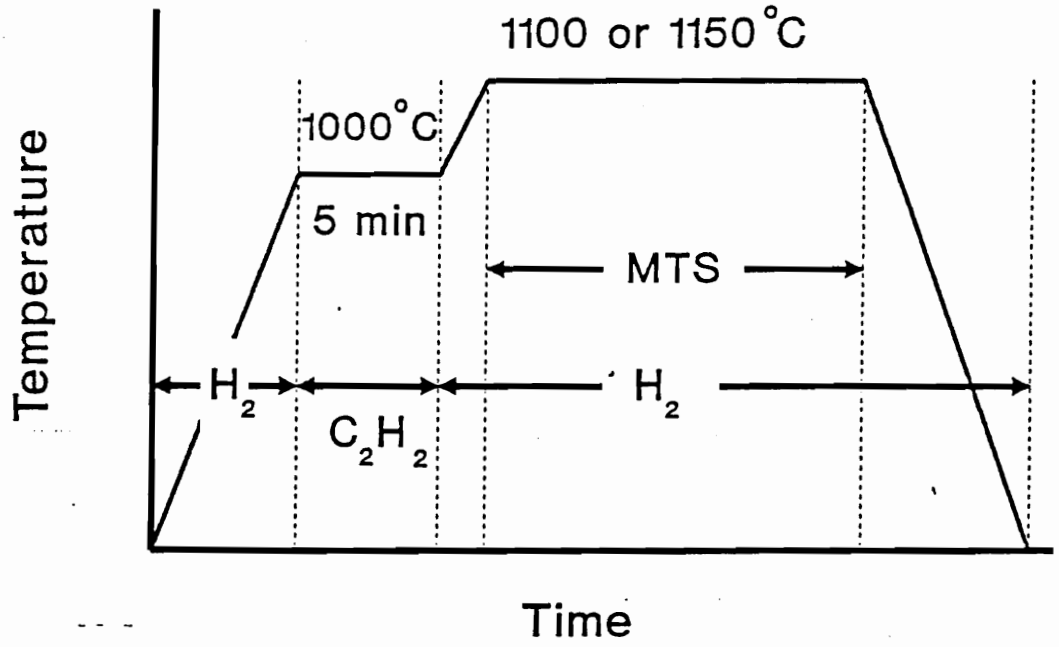

Figure 4.2: The overall schematic experimental procedure for forming the modified Si(100) substrate and growing β–SiC films from the MTS/H_2 gas system.

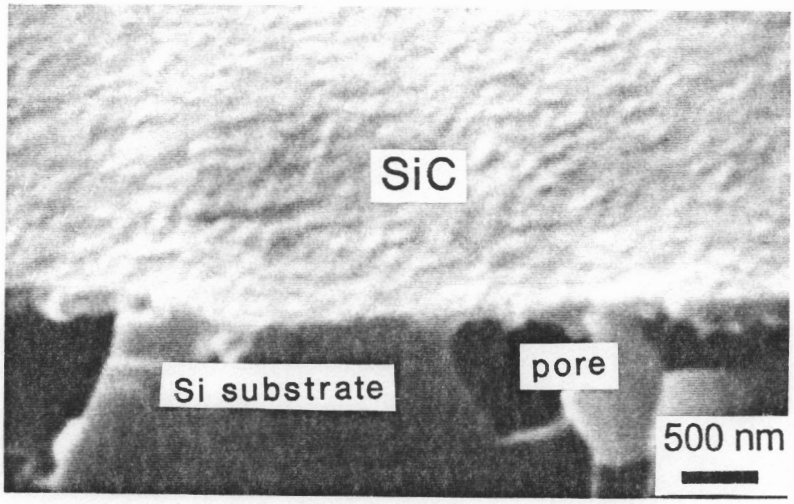

Figure 4.3: A typical cross section scanning electron micrograph of the β–SiC thin films deposited at 1150° C. The film was deposited for 12.5 min. This image was taken at an angle of 60° with the vertical axis of the surface.

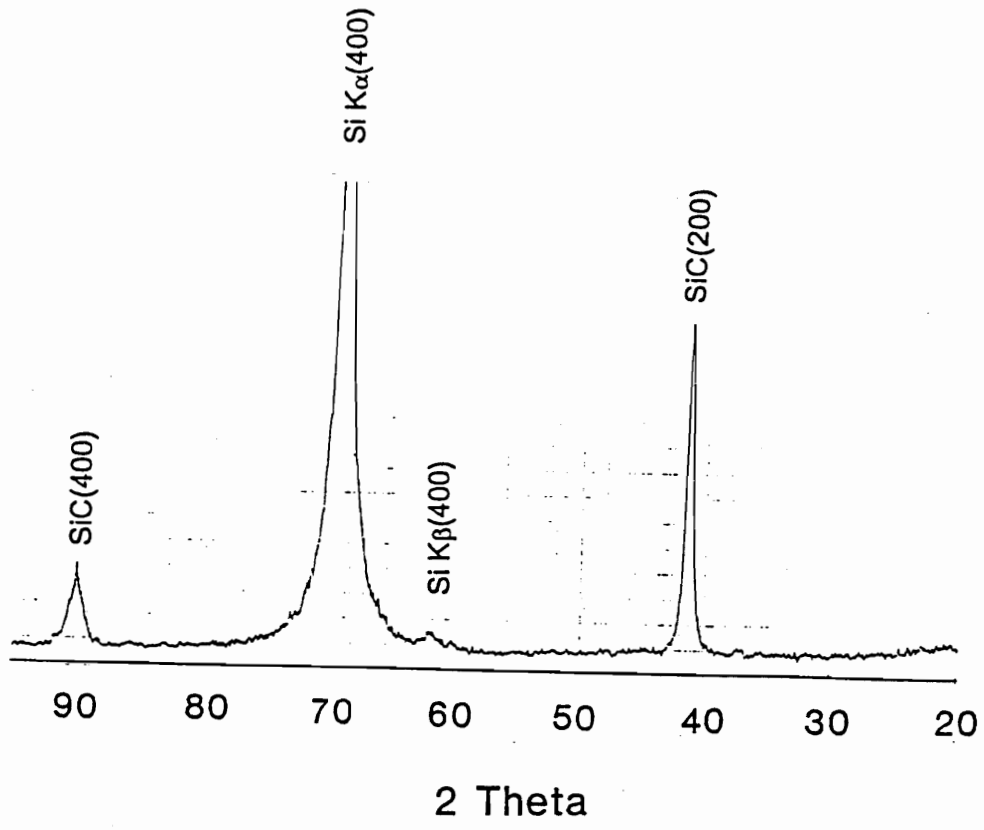

Figure 4.4: The XRD pattern of the β–SiC thin film deposited at 1150° C for 12.5 min.

deposition time (12.5 min), since the thicknesses of the β–SiC films were thin enough to be penetrated by the electron beam in the TEM, the specimens were prepared by back–etching the Si substrates with a solution of $HF+HNO_3+CH_3COOH$ (3:5:3). The Si etch rate of this solution is 34.8 μm/min [6]. The resultant bright field plane–view TEM micrograph with the associated selected area diffraction (SAD) pattern is depicted in Fig. 4.5. As shown in Fig. 4.5, the SAD pattern ,which shows a transmission electron diffraction pattern with a zone axis of <001> for β–SiC, also confirmed the preferred orientation from the XRD pattern (Fig. 4.4). The dot pattern and the ring pattern obtained from these samples (the SAD pattern in Fig. 4.5) indicated that β–SiC single crystal coexisted with polycrystalline β–SiC during the epitaxial growth of the thin film.

To determine the distribution of single crystal and polycrystalline β–SiC of the film, dark field TEM micrographs were taken. Figures 4.6(a) and 4.6(b) show the dark field images from the single crystal dot pattern and the polycrystalline ring pattern, respectively. As can be seen from Fig. 4.6, the film shows a strong nature of single crystal β–SiC. The polycrystalline β–SiC only consists a small portion of the film. Thus the film is believed to be a mixture of single crystal β–SiC with the polycrystalline β–SiC embedded inside.

It is also interesting to to note that a rectangular feature structure was observed (Fig. 4.6). This structure was probably caused by the nucleation process at the beginning of the CVD process. During this period, the β–SiC film was predominantly nucleated at the edges of the porous defects, which were perpendicular to each other and lying parallel to the silicon <110> direction [7]. Thus, the formation of a rectangular feature was favored. In addition to the small portion of polycrystalline β–SiC, planar defects such as stacking faults were also

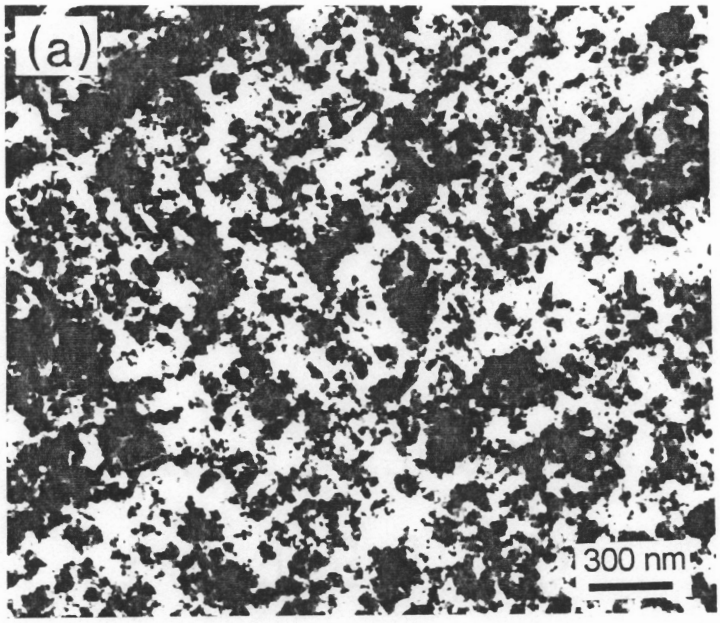

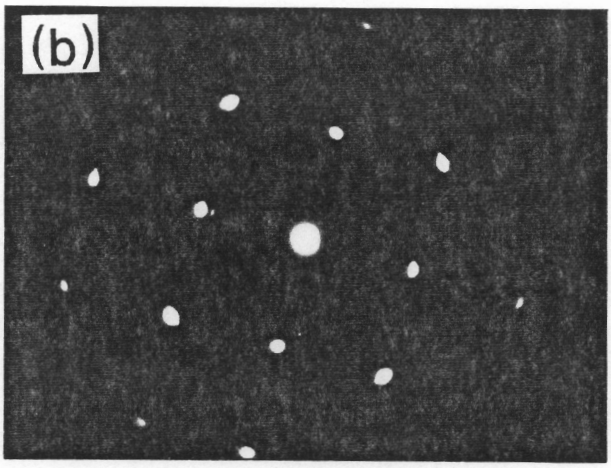

Figure 4.5: (a) Bright field TEM micrograph of the β–SiC thin film and (b) the corresponding electron diffraction pattern of the β–SiC with a <001> zone axis. The sample was ontained at 1150° C for 12.5 min.

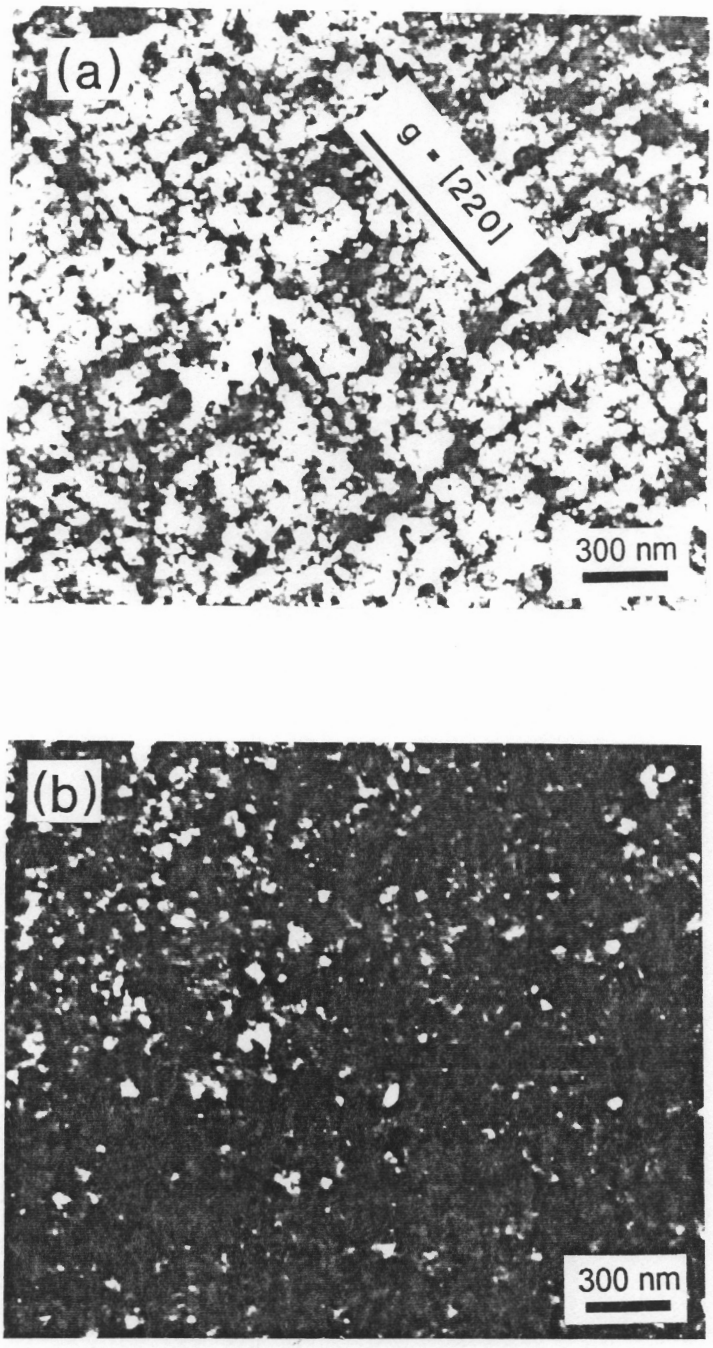

Figure 4.6: Dark field TEM micrographs from (a) single crystal β–SiC and (b) polycrystalline β–SiC.

observed in matrix of single crystal β–SiC thin films from Fig. 4.5 and a dark field TEM image with a higher magnification, as indicated in Fig. 4.7.

Figure 4.8 shows the SAD pattern from the top layers and the XRD pattern of the β–SiC thin films with the deposition time of 50 min. In order to observe the crystal structure at the top surfaces of these samples, the samples were prepared by ion milling from the Si side at an angle of 15° to the surface. Again the electron beam was normal to the surfaces to examine the preferred orientation obtained in these samples. It is clear from both the SAD pattern and the XRD pattern given in Fig. 4.8 that the β–SiC films show partial epitaxy with β–SiC(100) $\not\parallel$ Si(100) at the top surfaces of the samples. When compared to the sample shown in Fig. 4.5, the polycrystalline ring pattern is more prominent in the SAD pattern (Fig. 4.8). However, more than one dot patterns for single crystal β–SiC from electron diffraction with the <001> zone axis was observed. This indicated that nonepitaxial deposition was occurring in the matrix of these samples. The matrix on the top layers of the deposited β–SiC film consists of the crystals which are rotated perpendicularly to the <001> zone axis of β–SiC. The reason for this is likely due to the increasing surface roughness with deposition time, as shown later.

The same sample preparation procedure was employed to make the TEM samples for the films deposited for 100 min. The SAD pattern and the XRD pattern of these samples are shown in Fig. 4.9. In contrast to the films deposited for 12.5 min (Figs. 4.4 and 4.5) and 50 min (Fig. 4.8), only the polycrystalline ring pattern of β–SiC was observed. Furthermore, the (111) plane from β–SiC also appeared in the XRD pattern (Fig. 4.8(a)). This indicates that the preferred orientation was (111) for the polycrystalline β–SiC on the top surfaces of these samples.

From the XRD and TEM results shown above, it is obvious that the

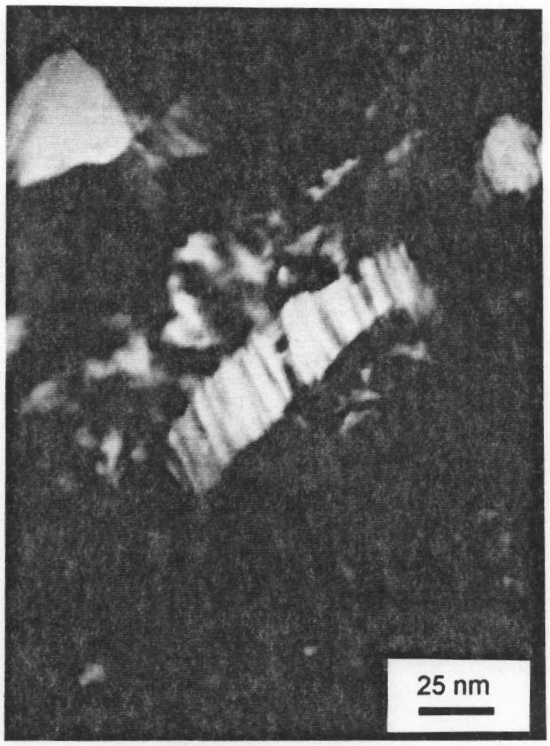

Figure 4.7: Dark field TEM micrograph showing the stacking fault in the β–SiC thin film.

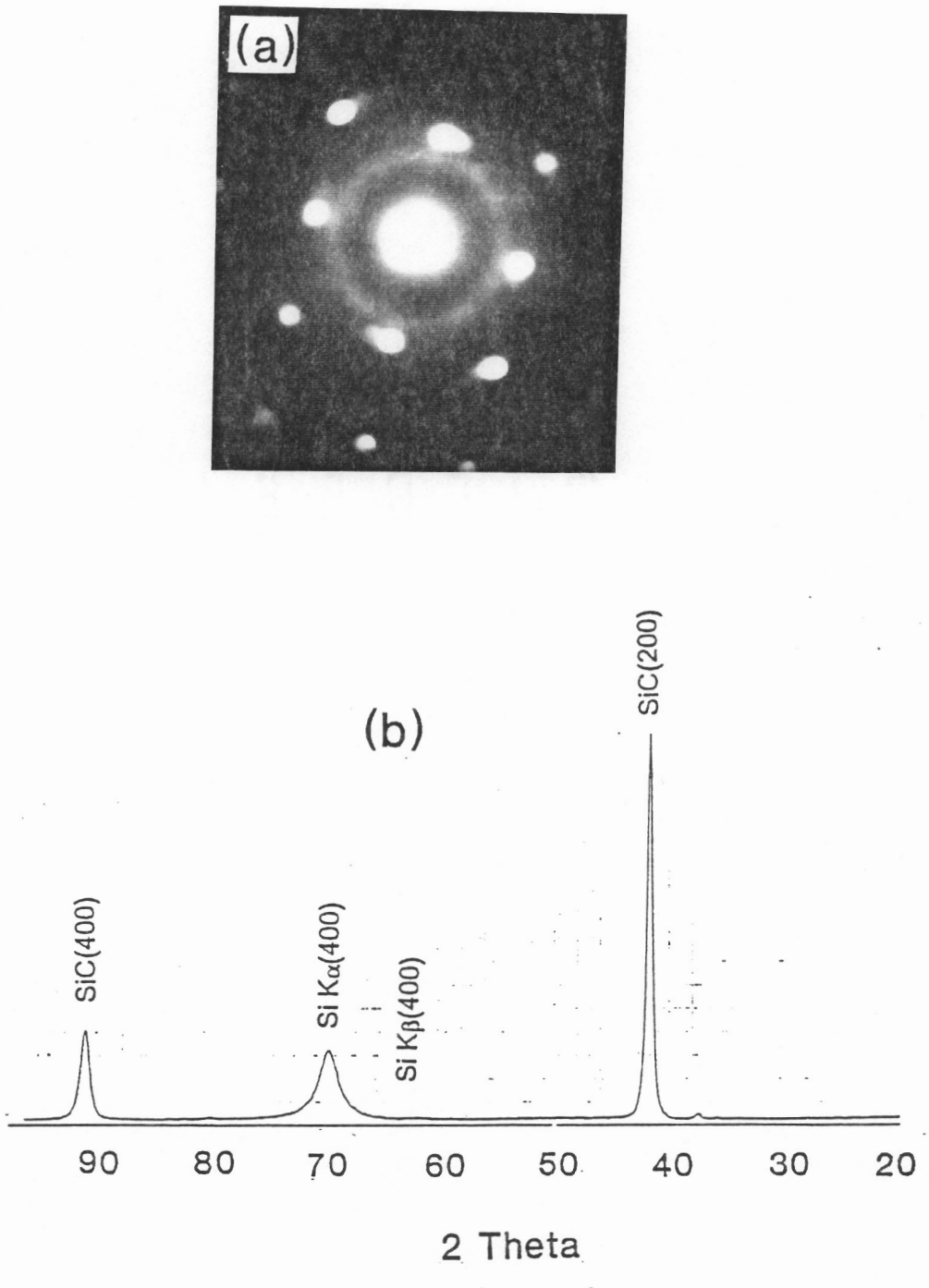

Figure 4.8: (a) The SAD pattern from the top surface of the β–SiC film and (b) the XRD pattern of the β–SiC films deposited at 1150° C for 50 min.

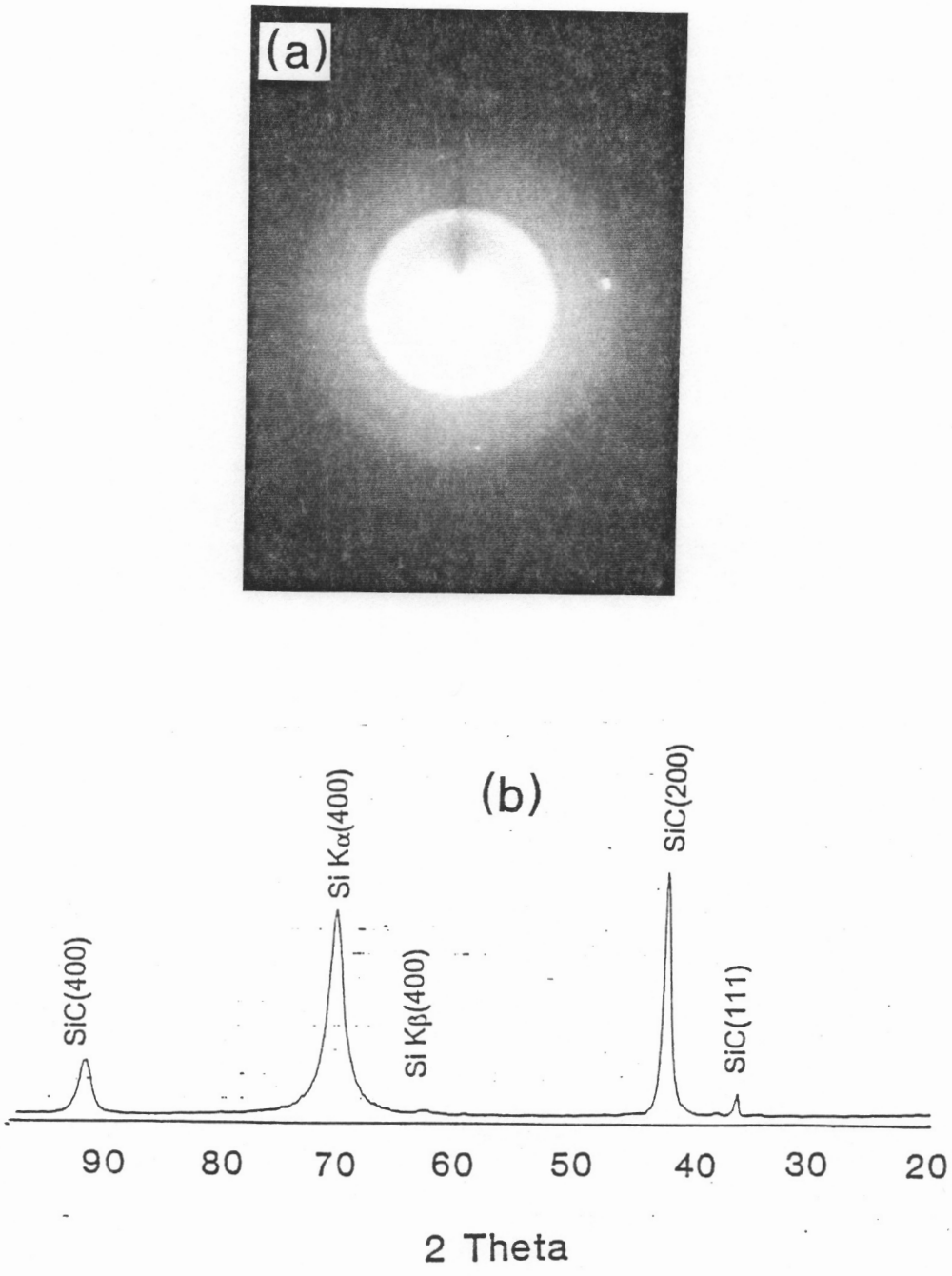

Figure 4.9: (a) The SAD pattern from the top surface of the β–SiC film and (b) the XRD pattern of the β–SiC films deposited at 1150° C for 100 min.

crystallinity of the deposited β–SiC from the mixture of MTS and H_2 was influenced by the deposition time. For short deposition time (*i.e.* 12.5 min), the matrix of the films was single crystalline in nature (β–SiC) with a preferred orientation of (100) planes. As the deposition time increased (50 min), the rotational crystals of β–SiC with the preferred orientation of (100) grew on the top surface of single crystal β–SiC(100) matrix. However, the preferred orientation of β–SiC(100) was preserved (Fig. 4.8). Further increasing the deposition time (100 min), polycrystalline β–SiC with the preferred orientation of (111) was obtained on the top surfaces of the previously deposited polycrystalline β–SiC(100) grains, as shown in Fig. 4.9. In fact, it was found that the polycrystalline β–SiC with a preferred orientation of (111) was started to be deposited at the deposition time of 75 min at this temperature. Jacobson reported a similar phenomenon by using $(CH_3)_2SiCl_2$ as the precursor to deposit β–SiC films on Si(100) substrates [8]. However, in contrast to our results, the preferred orientations are two of the {110} planes from β–SiC after the polycrystalline β–SiC(100) grains were observed. Therefore, the precursors used may play a role in obtaining the preferred orientation on the top surfaces of the films because of the differences in kinetic processes in the CVD procedure, such as surface adsorption, surface diffusion and various surface chemical reactions.

In addition to the effects from the precursors, according to Sheldon et al. [2] and Cheng et al [9], it is believed that the surface roughness, which became prominent with increasing deposition time, can create a large number of nucleation sites by using the MTS/H_2 gas system to deposit β–SiC films. As shown in Fig. 4.10, it is clear that the topography of the SiC films deposited at this temperature was observed to be rougher with increasing deposition time, a typical phenomenon for CVD processes. Therefore after a certain deposition time, the growth of the

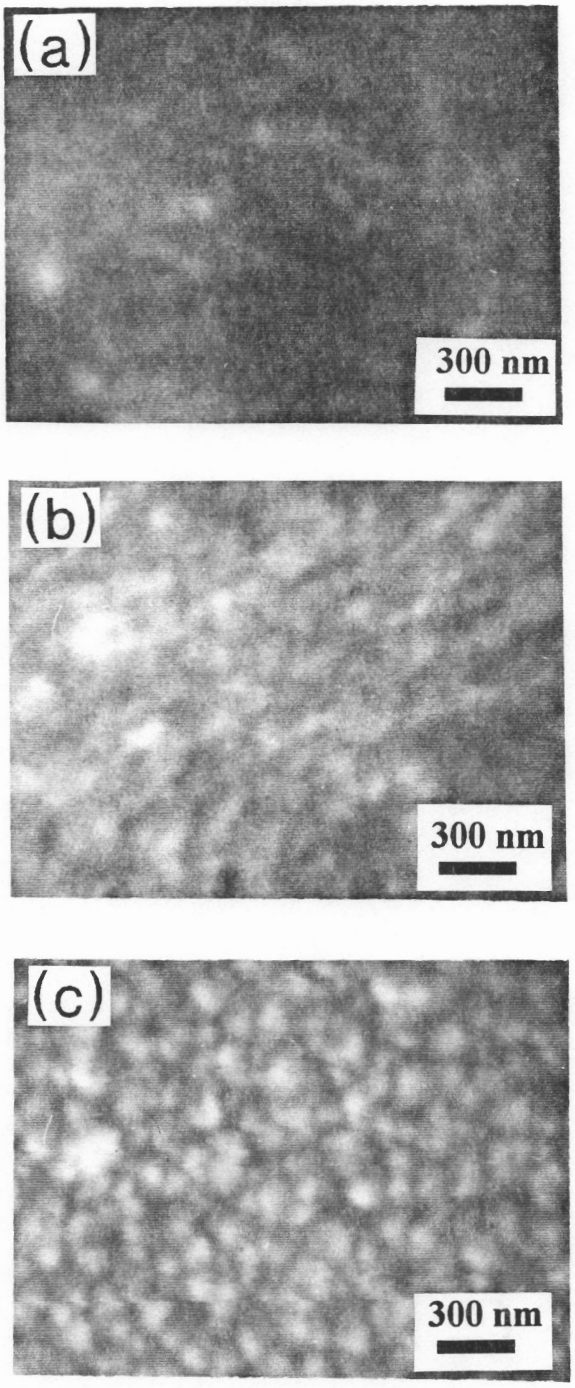

Figure 4.10: The topography of the β–SiC thin films deposited at 1150° C for (a) 12.5 min, (b) 50 min, and (c) 100 min.

preferred orientation of β–SiC(111) was favored and thus controlled the nucleation and the microstructure of the deposited materials. Additionally, with increase in film thickness, the influence from the modified Si(100) substrates, which was believed to cause the formation of β–SiC(100) at the early stage of deposition, will be tenuous in the growing front of the deposited β–SiC films. Thus, the (111) preferred orientation, which is the most commonly observed preferred orientation from MTS/H_2 gas system, occurred after a certain deposited thickness [1,2,9,10].

4.4.2 Epitaxial growth of β–SiC at 1100° C on modified Si(100).

The XRD patterns for the films obtained at this temperature for various deposition times are shown in Fig. 4.11. In contrast to the β–SiC thin films deposited at 1150° C, the β–SiC(111) planes were not observed until the deposition time was increased to 200 min. And the highly preferred orientation of (100) from β–SiC was preserved up to the deposition times as long as 150 min. Figure 4.12 shows the bright field TEM micrograph and the corresponding SAD pattern for the samples deposited for 12.5 min at this temperature, whose XRD pattern is given in Fig. 4.11(a). The sample preparation procedure was the same as that for the sample shown in Fig. 4.5. It is to be noted that, from the transmission electron diffraction pattern shown in Fig. 4.12, the film also showed a strong preferred orientation from the {100} planes and the polycrystalline ring pattern for β–SiC. However, the dot pattern for single crystal with the <001> zone axis was much diffused when compared to that obtained at 1150° C (Fig. 4.5). This indicates that the nature of polycrystalline nature was more dominant than that for single crystal β–SiC. In comparison with the films deposited at 1150° C, it is evident that the growth temperature was a very important factor in the attainment of β–SiC matrix with

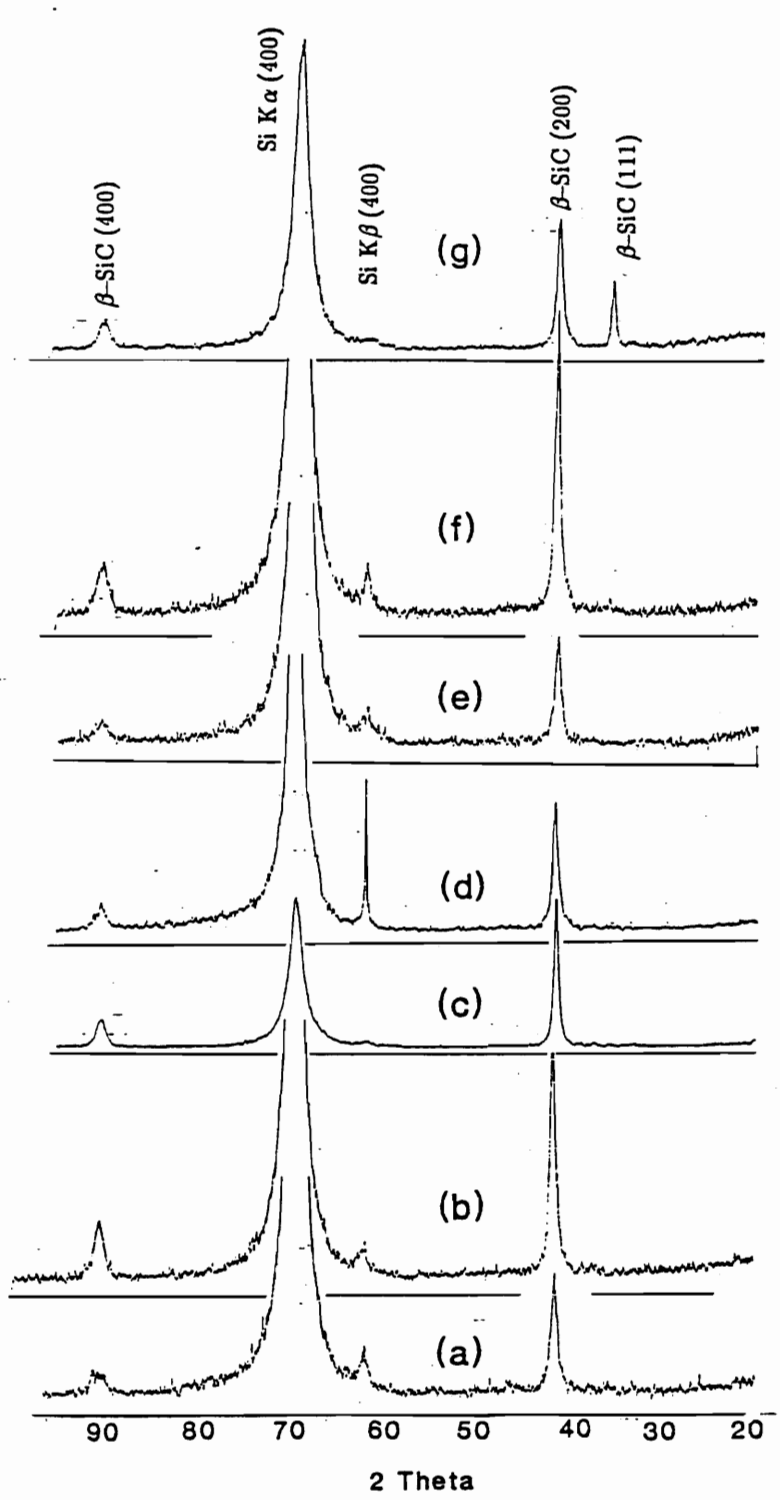

Figure 4.11: The XRD patterns of the β–SiC films deposited at 1100° C for (a) 12.5 min, (b) 25 min, (c) 50 min, (d) 75 min, (e) 100 min, (f) 150 min, and (g) 200 min.

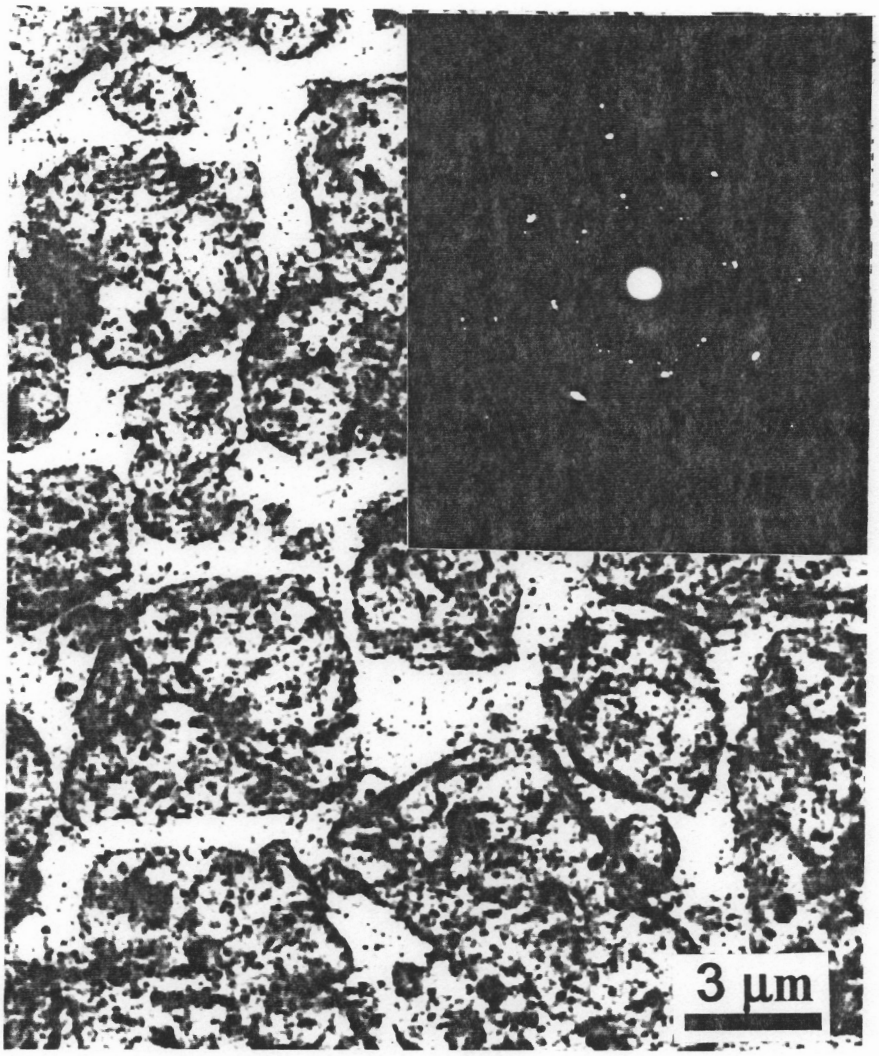

Figure 4.12: Bright field TEM micrograph of the β–SiC film and the corresponding electron diffraction pattern of the polycrystalline β–SiC. The sample was obtained at 1100° C for 12.5 min.

the nature of single crystallinity. This matrix can only be deposited on modified Si(100) substrates at temperatures as low as 1150° C. At lower temperatures (*e.g.* 1100° C), polycrystalline β–SiC was more evident even for the deposition times as short as 12.5 min. However, the films still showed a highly preferred orientation of β–SiC(100). The difference in the crystal structures of the deposited β–SiC films obtained at 1100° C from those obtained at 1150° C was believed to be due to the relatively lower surface mobilities and the slower chemical reactions. At the lower temperatures (*i.e.* 1100° C), chemisorption and other chemical reactions are slower, thus these processes may only be possible at relatively high–energy sites such as the {100} surface sites in this study. Furthermore, slower surface diffusion could limit the migration of the adsorbed species along the surface and resulted in deposition occurring inside the pores of the modified Si substrate and a poor surface morphology, as shown in Fig. 4.13, when comparing to the films deposited at a higher temperature (Fig. 4.3). Therefore isolated features of β–SiC were formed and facilitated the formation of polycrystalline β–SiC with the preferred orientation from the {100} planes.

4.4.3 Comparison to the β–SiC films deposited on smooth Si substrates.

When comparing the results of this study to the β–SiC thin films deposited on smooth and carburized Si(100) substrates by using MTS as the precursor, it is interesting to note that, at the early stage of the CVD process, (100) direction is the only preferred orientation from the β–SiC thin films deposited on the modified Si(100) substrates instead of the preferred orientation from the (111) planes of β–SiC observed on smooth and carburized Si(100) substrates [1,2]. According to Sheldon et al. [2], the β–SiC(111) surfaces occurred because of the appearance of

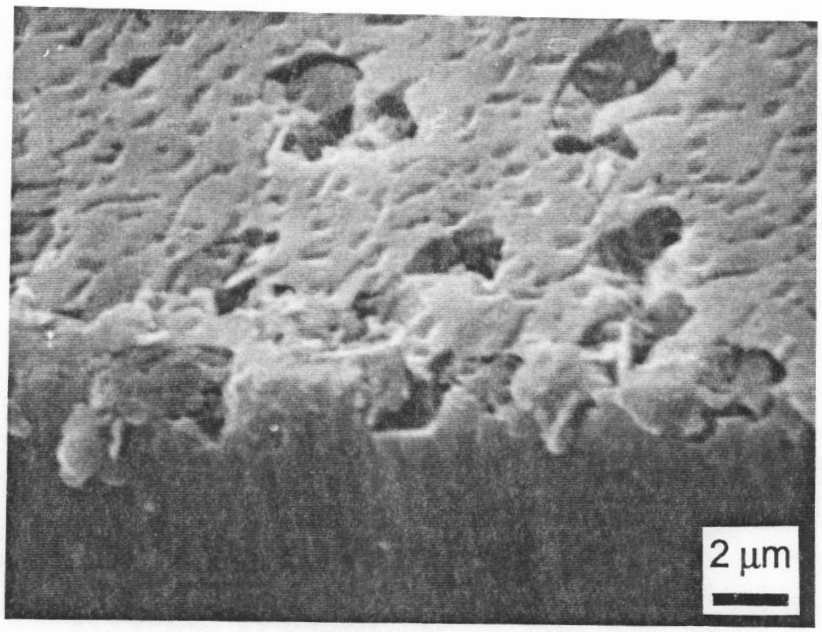

Figure 4.13: A typical cross section scanning electron micrograph of the β–SiC thin film deposited on a porous Si(100) substrate at 1100° C. The film was deposited for 12.5 min. This image was taken at an angle of 60° with the vertical axis of the surface.

some orientated microtwins. These microtwins occurred in a {111} plane on the surface of smooth Si(100) substrate at the early stage of the CVD process, whose surface was converted into a SiC buffer layer by reacting the Si(100) surface with a hydrocarbon gas before the CVD process. Thus the subsequent new {111} surfaces of the deposited β–SiC thin films were nucleated at the intersection of the SiC buffer layer with a twin occurring on a {111} plane on the surfaces. Also the surface roughness on the carburized Si surface, which is caused by the high density of defects due to the lattice mismatch between the Si(100) substrate and the β–SiC buffer layer [11,12,13], was believed to play a role in obtaining the the β–SiC(111) deposit at the early stage of the CVD procedure [2]. For the β–SiC films deposited on the mofidied Si(100) substrates, it was believed that the growth of β–SiC film from MTS at the early stage of nucleation and the subsequent microstructure of the deposited materials were not controlled by the surface roughness of the modified Si(100) substrates. This is because, in the present study, the surfaces of the Si(100) substrates after reacting with C_2H_2 were expected to be much rougher than those showing a smooth SiC buffer layer [1]. Similar types of defects were also believed to be presented on the top surfaces of our samples since the surfaces were also converted to SiC by using a hydrocarbon gas (C_2H_2). Thus the absence of the preferred orientation of (111) from the β–SiC films deposited on the modified Si(100) substrates could be due to the elimination of the microtwins which occurr in a {111} plane on the top surfaces of the Si(100) substrates. In fact, according to Schigeta et al [14], the porous nature of Si substrate can significantly reduce the defect density (*i.e.* stacking fault) between the SiC deposit and the Si interface. And thus the formation of single crystal β–SiC(100) is favored. Furthermore, the porous nature on the top surfaces of Si(100) substrates could provide the

surface–energy anisotropy in the early stage of CVD process [15]. That is, films with the orientation that minimize the interfacial free energy should grow preferentially (*e.g.* β–SiC(100) in this study). The amount of strain due to lattice constant mismatches in the early stage of CVD process were also believed to be released by the porous nature of the Si(100) substrates. Therefore the formation of β–SiC(100) films with a single crystal matrix and a preferred orientation of (100) from β–SiC at 1150° C and 1100° C, respectively, were favored. The same phenomenon was also described for the CVD β–SiC films on Si(100) substrates by using cold wall reactors [16,17].

4.5 SUMMARY:

Epitaxial β–SiC(100) thin films with a single crystal matrix having smooth surfaces were grown at 1150° C in a hot wall LPCVD reactor by using MTS as the precursor for a short deposition time (12.5 min). As far as we know, this is the lowest temperature used to grow single crystal β–SiC in a hot wall reactor and by using MTS.

As the deposition time increased, the rotational β–SiC(100) crystals and polycrystalline β–SiC were observed on the top surface of the previously deposited matrix of single crystal β–SiC(100). The (100) orientation from polycrystalline β–SiC can only be grown with the deposition times shorter than 75 min in this study. Further increased the deposition time (time > 75 min), the appearance of the polycrystalline β–SiC(111) layers on the top surface of the polycrystalline β–SiC(100) film was observed.

At a lower deposition temperature (*i.e.* 1100° C), poor surface morphology

and no single crystal β–SiC deposit can be obtained for the deposition time as short as 12.5 min. However, the highly preferred orientation from {100} planes of β–SiC was preserved up to the deposition time of 150 min. The (111) orientation of the β–SiC thin films was observed at the deposition of 200 min in this study.

4.6 REFERENCES:

1. C.C. Chiu, S.B. Desu, and C.Y. Tsai, J. Mat. Res., **8**, 2617 (1993).
2. B.W. Sheldon, T.M. Besmann, K.L. More, and T.S. Moss, J. Mat. Res., **8**, 1086 (1993).
3. F. Langlais, F. Hottier, and R. Cadoret, J. of Crystal Growth, **56**, 659 (1982).
4. C.C. Chiu and S.B. Desu, J. Mat. Res., **8**, 535 (1993).
5. C.C. Chiu, C.K. Kwok, and S.B. Desu, in *Chemical Vapor Deposition of Refractory Metals and Ceramics* II, edited by T.M. Besmann, B. M. Gallois, and J.W. Warren, Mat. Res. Soc. Symp. Proc. vol **250** (Materials Research Society, Pittsburgh, PA) p. 179 (1992).
6. D.G. Schimmel, in *Quick Reference Manual for Silicon Integrated Circuit Technology*, edited by W.E. Beadle, J.C.C. Tsai, and R.D. Plummer (John Wiley & Sons, Inc., New York, NY), p. 5–9 (1985).
7. R.C. Newman and J. Wakefield, in *Solid State Physics in Electronics and Communication*, edited by M. Desirant and J.L. Michels, p 319 (1960).
8. K.A. Jacobson, J. Electrochem. Soc., **118**, 1001 (1971).
9. D.J. Cheng, W.J. Shyy, D.H. Kuo, and M.H. Hon, J. Electrochem. Soc., **134**, 3145 (1987).

10. M.G. So and J.S. Chun, J. Vac. Sci. Technol., **A6**, 5 (1988).

11. C.H. Carter, Jr., R.F. Davis, and S.R. Nutt, J. Mat. Res., **1**, 811 (1986).

12. H.J. Kim, R.F. Davis, X.B. Cox, and R.W. Linton, J. Electrochem. Soc., **134**, 2269 (1987).

13. N. Bécourt, J.L. Ponthenier, A.M. Papon, and C. Jaussaud, Physica B, **185**, 79 (1993).

14. M. Shigeta, Y. Fujii, K. Furukawa, A. Suzuki, and S. Nakajima, Appl. Phys. Lett., **55**, 1522 (1989).

15. T. Yonehara, H.I. Smith, C.V. Thompson, and J.E. Palmer, Appl. Phys. Lett., **45**, 631 (1984).

16. P. Liaw and R.F. Davis, J. Electrochem. Soc., **132**, 642 (1985).

17. K. Ikoma, M. Yamanaka, H. Yamaguchi, and Y. Shichi, J. Electrochem. Soc., **138**, 3028 (1991).

Chapter 5 was entitled

"Local equilibrium phase diagrams:
SiC deposition in a hot wall LPCVD reactor"
submitted to Journal of Materials Research

and

"Local equilibrium phase diagrams for SiC deposition
in a hot wall LPCVD reactor"
in *Metal–organic chemical vapor deposition of electronic ceramics*
Materials research society symposium proceedings, vol **335**
(Materials research society, Pittsburgh, PA, 1994)
(in press)

Chapter 5: LOCAL EQUILIBRIUM PHASE DIAGRAMS: SiC DEPOAITION IN A HOT WALL LPCVD REACTOR

5.1 ABSTRACT:

Traditional CVD phase diagrams, which neglect the depletion effects in a hot wall reactor and assume the gaseous species concentrations at the substrate are the same as input concentrations, are at best valid for cold wall reactor. Due to the constant change of gaseous species concentration along the length of the reactor, traditional CVD phase diagrams do not accurately predict the phases in the deposit on the substrate in a hot wall CVD system. In this paper, a new approach to calculate the local equilibrium CVD phase diagrams at the substrate is presented by coupling the depletion effects in a hot wall reactor to the equilibrium thermodynamic computer codes SOLGASMIX–PV. The deposition of SiC using the gas system of methyltrichlorosilane (MTS) – hydrogen (H_2) under low pressures was chosen for this study. Differences between the new CVD phase diagrams and the traditional CVD phase diagrams, for this gas system, were discussed. The calculated CVD phase diagrams were also compared with the experimental results both from our own experiment and from the literature. The local equilibrium phase diagrams predicted the deposition of a single phase of SiC much better than those without the consideration of the depletion effects. The experimental regions for depositing the single phase SiC are larger than the calculated local phase diagrams. This is attributed to the higher linear velocity of the gas flux under low pressure and the polarity of the Si carrying intermediate species.

5.2 INTRODUCTION:

Chemical vapor deposition (CVD) working under reduced pressure conditions and a hot wall reactor is currently used in semiconductor industry to manufacture microelectronic devices because of its high wafer throughput rate, improved layer thickness homogeneity, and the elimination of contamination from the susceptor by using a very low deposition pressure [1]. Although lots of models have been developed to study the CVD phase diagrams, all of the calculated phase diagrams are based on the cold wall assumptions in which the precursor concentrations at the substrate are assumed to be the same as those at the inlet of the reactor [2–4]. For a hot wall reactor, the temperature profile is contineously increasing from the inlet of the reactor to the position where the substrates located. Thus it is expected that the precursors will undergo some chemical reactions (*i.e.* depletion effects) along the reactor, which exhaust the precursor concentrations and generate some intermediate gaseous species. Moreover, the other kinetic factors such as thermal diffusion and thermal convection of the gas flux were also believed to play a role in the depletion effects. Therefore, with the constant changes in the reactive gaseous species along the length of hot wall CVD reactor because of the depletion effects, it is apparent that the local gaseous species concentrations at the substrate are significantly different from the input concentrations. This phenomenon will be more obvious under a higher deposition temperature [5]. Thus the current reported phase diagrams are apparently not suitable to study in hot wall reaction conditions [2–4]. Although various models have been proposed to study the hot wall CVD processes [6–9], none of them involve the study of the local CVD phase diagrams at the substrate under various processing conditions, which are of fundamental importance

in understanding and optimizing the processes.

For the present study, a new approach was presented to calculated the local CVD phase diagrams in a hot wall reactor, which combined the depletion effects with the equilibrium thermodynamic calculation. The stchematic diagram for this approach is depicted in Fig. 5.1; the depletion effects were considered before performating the equilibrium thermodynamic calculation to obtain the local CVD phase diagrams. Detailed analytical method is described in next section.

The deposition of silicon carbide (SiC) from the MTS–H_2 mixture in a hot wall reactor under low pressures was chosen to study the local equilibrium CVD phase diagrams. Silicon carbide prepared by chemical vapor deposition (CVD) has become a technologically important material in structural and electronic applications because of its outstanding properties [10–12]. Among various types of the CVD process, as stated above, the one operating at low pressure and at a hot wall reactor (hot wall CVD) is widely used in semiconductor industry to manufacture the microelectronic devices. In addition, composite structures utilizing this process to deposit the SiC matrix are being developed as a solution to high temperature materials needs [13].

In this paper, a model for studying the phase diagrams of hot wall CVD materials is proposed. Comparisons between the CVD phase diagrams for depositing SiC developed based on both the hot wall and cold wall assumptions are emphasized. Experimental results were also used to verify the calculated results.

5.3 METHOD OF CALCULATION:

In the hot wall CVD process, the reactive species are consumed or generated

The approach to calculate local phase diagram in a hot wall reactor

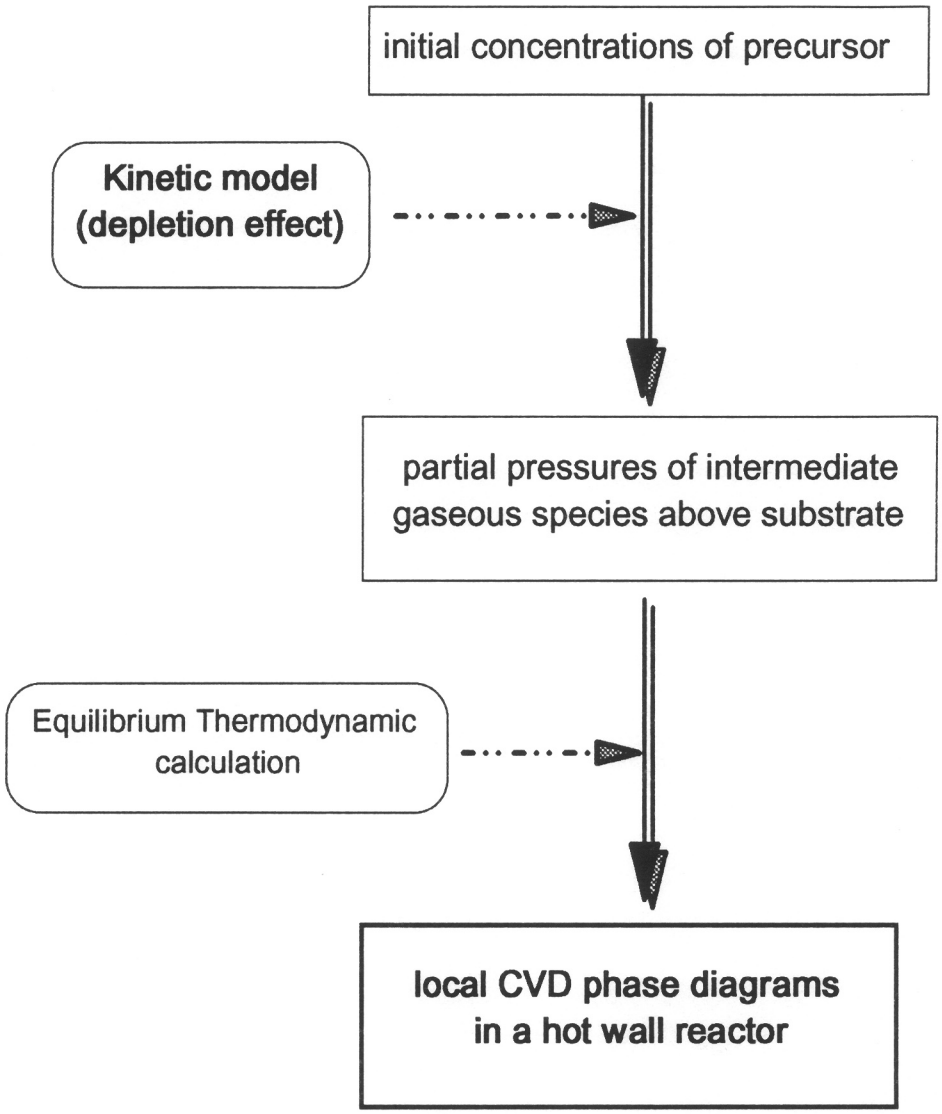

Figure 5.1: The schematic of the method of calculation.

along the CVD reactor. In order to include this hot wall factor into the calculations of the CVD phase diagrams for SiC deposition, a kinetic model for this deposition process [14,15], which considers both the transport phenomena and deposition mechanism of the MTS–H_2 CVD system, was used to calculate the spatial dependence of the gaseous species concentrations.

As shown in Fig. 5.1, in the kinetic model, the steps involved in the deposition of SiC from MTS/H_2 precursors are assumed to be: (i) gas phase decomposition of the MTS molecules into two major intermediates, one containing silicon (IP_{Si}) and the other containing carbon (IP_C), as well as gaseous byproducts (BP), (ii) adsorption of the intermediate species onto the surface sites of the growing film, and (iii) reaction of the adsorbed intermediates to form silicon carbide. Detailed description of the calculations was shown elsewhere [14].

For the present study, the kinetic analysis of silicon carbide deposition, in a hot wall CVD reactor, is first introduced to identify the partial pressures of the intermediate species (IP_{Si} and IP_C) and gaseous byproducts (BP) over the position where the substrate is located. Then, equilibrium thermodynamic calculations were performed at this position to calculated the CVD phase diagram for this hot wall reactor.

The thermodynamic analysis in the present study was conducted with a modified form of the computer program SOLGASMIX–PV to calculate the equilibrium composition of the system [16]. The procedures are based on free–energy minimization under given conditions of temperature, total pressure and, the input gas concentrations. Detailed descriptions of the calculation were reported by Eriksson [17] and White [18].

As mentioned above, for a hot wall CVD reactor, the MTS precursor will

decompose into some gaseous intermediate species while transporting from the entrance of the furnace to the substrates [19–21]. It was reported that the concentrations or the partial pressures of the gaseous species in a hot wall reactor can be predicted from the equilibrium calculations assuming no condensed phases present [1,20]. In these concentrations, the reactants are the same as those at the entrance of the furnace (*i.e.* no intermediate species and gaseous byproducts). However, these equilibrium calculations without the formation of condensed phases from thermodynamic analysis can only predict the partial pressures or concentrations for silicon bearing (IP_{Si}), carbon bearing (IP_C) species, and the gaseous byproducts (BP) in a hot wall CVD reactor. The experimentally determined concentrations of MTS along the reactor were much larger than those calculated from the equilibrium thermodynamic calculations assuming no condensed phases present, especially at high temperatures (T > 1200 K) [20]. Moreover, the concentrations of the MTS precursor and the intermediate gaseous species were also dependent on the thermal profile and the geometry of the reactor. Thus the analysis of the CVD system by merely using the equilibrium thermodynamic analysis is insufficient to understand the partial pressures or concentrations for each gaseous species in a hot wall reactor without considering the kinetic factors.

For the present study, the partial pressures of MTS, the intermediate species (IP_{Si} and IP_C), and the gaseous byproducts (BP) in the gas phase above the substrate were obtained from the kinetic analysis stated above. Since the CVD processes were believed to be controlled by the surface reactions under low pressure [15], it is also assumed that, above the substrate, the partial pressures of the gas species (MTS, IP_{Si}, IP_C, and BP) in the boundary layer are the same as those in the gas phase. And the reactions in the boundary layer above the substrate come to a

rapid equilibrium, forming molecules which represent the most stable distribution. Before the thermodynamic analysis with the present of condensed phases, the orders and the ratios for the intermediate species (IP_{si} and IP_c), and the gaseous byproducts (BP) above the substrate in the gas phase were obtained by assuming no condensed phases formed under equilibrium conditions and with the initial H_2/MTS ratio at the entrance of the furnace. Since the kinetic analysis can only gives the total pressures of IP_{si}'s ,IP_c's, and BP's, the individual real partial pressure of each IP_{si} ,IP_c and BP was obtained from the kinetic analysis and from the ratios of equilibrium thermodynamic calculation assuming no condensed phases. Then the equilibrium calculations were performed with the presence of the condensed phases in obtaining the CVD phase diagram in a hot wall reactor. In this study , 59 gas species and 6 condensed phases were considered, as listed in Table 5.1. The free energies, entropies, and enthalpies of formation of the species are available in SOLGASMIX–PV [16], JANAF thermochemical table [22], and Ref. [23]. Since the cubic form, β–SiC, was more stable than the hexagonal polytypes for the temperatures considered, only one polymorph of SiC (*i.e.* cubic form β–SiC) was considered in the calculation. In most cases the results are presented as CVD phase diagrams as a function of temperature and H_2/MTS ratios in the input gas for a specific system pressure. The calculated CVD phase diagrams were compared with the data from our own experimental results and from the literatures for the hot wall type of reactor under 10 Torr and from 1000 to 1500 K. Detailed experimental procedure was described elsewhere [15,24,25].

Table 5.1:

Intermediate Gaseous Species Considered in MTS-H_2 Gas System in a Hot Wall Reactor

IP_c	IP_{si}	BP
C, CCl, CCl_2, CCl_3, CCl_4, CH, CH_2, CH_3, CH_3Cl, CH_4, C_2, C_2Cl_2, C_2H, C_2H_2, C_2H_3, C_2H_4, C_3, N-C_3H_7, I-C_3H_7, C_3H_8, C_4, N-C_4H_{10}, I-C_4H_{10}, C_5, C_5H_6, C_6H_6, C_7H_8, C_8H_{16}, N-C_8H_{18}, I-C_8H_{18}, O-$C_{12}H_9$, $C_{12}H_{10}$	Si, SiCl, $SiCl_2$, $SiCl_3$, $SiCl_4$, SiH, $SiHCl_3$, SiH_2Cl_2, SiH_3Cl, SiH_4, Si_2, Si_3	Cl, Cl_2, H, HCl, SiC, SiC_2, SiC_4H_{12}, Si_2C, SiC_3H_9Cl, $SiC_2H_6Cl_{12}$, $SiCH_6$
34 species	**12 species**	**11 species**

Condensed Species Considered in MTS-H_2 Gas System in a Hot Wall Reactor

$C_{(graphite)}$, $C_7H_{8(l)}$, $C_8H_{8(l)}$, $Si_{(s)}$, $Si_{(l)}$, β-$SiC_{(s)}$

5.4 RESULTS AND DISCUSSION:

The CVD phase diagrams without considering the effects of the kinetic factors, which are valid for cold wall configuration, are shown in Fig. 5.2 for the system of MTS/H_2 for various pressures. As can be seen in Fig. 5.2, β–SiC would be deposited under a wide variety of conditions. Carbon would be codeposited with β–SiC under small values of H_2/MTS. In fact, according to Minato et al. [4], silicon would be codeposited with β–SiC at very high H_2/MTS values (>1000) at 0.1MPa from about 1300 to 1800 K. It is also depicted in Fig. 5.2 that the boundaries between β–SiC and β–SiC + graphite move toward smaller values of H_2/MTS with increasing deposition pressure. Thus, for a cold wall CVD reactor and MTS–H_2 gas system, a large quantity of H_2 carrier gas is required to deposit β–SiC along ,especially at lower pressures.

The experimental results of the present study together with the calculated CVD phase diagrams neglecting the depletion effects from a hot wall reactor are shown in Fig. 5.3. As shown in Fig. 5.3, the deposit compositions of the present experimental results were β–SiC. However, the calculated CVD phase diagrams indicated that the deposit compositions at thermodynamic equilibrium were graphite+β–SiC under small H_2/MTS ratios for the considered deposition pressures (1.8, 5, and 8 Torr). And the region for graphite+β–SiC expands toward higher values of H_2/MTS ratios above 1100 K with decreasing deposition pressure. Thus these equilibrium phase diagrams without considering the depletion effects in a hot wall reactor can only predict the experimental deposit composition with higher deposition pressures, higher H_2/MTS ratios ,and lower temperature for the present study.

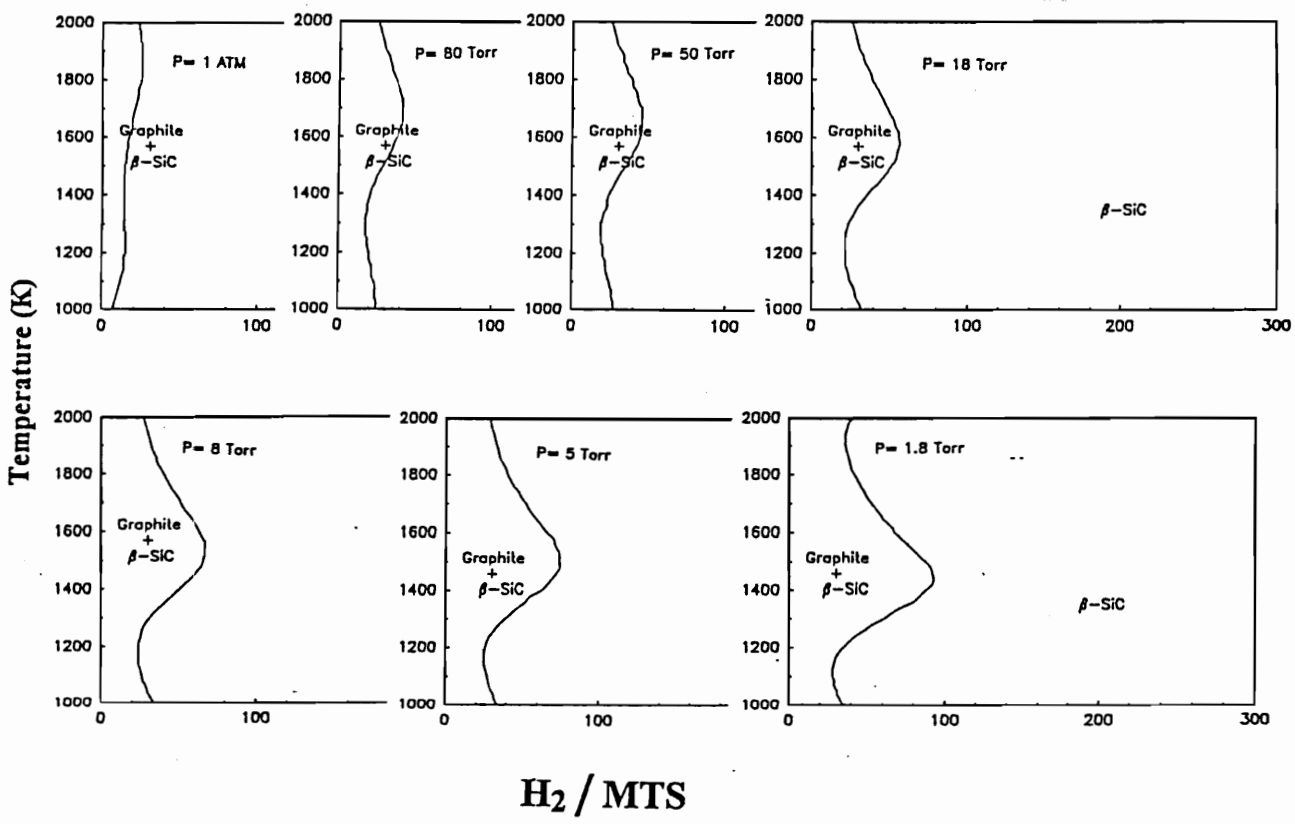

Figure 5.2: CVD phase diagrams for CH_3SiCl_3–H_2 gas system without the consideration of the depletion effects for various pressures.

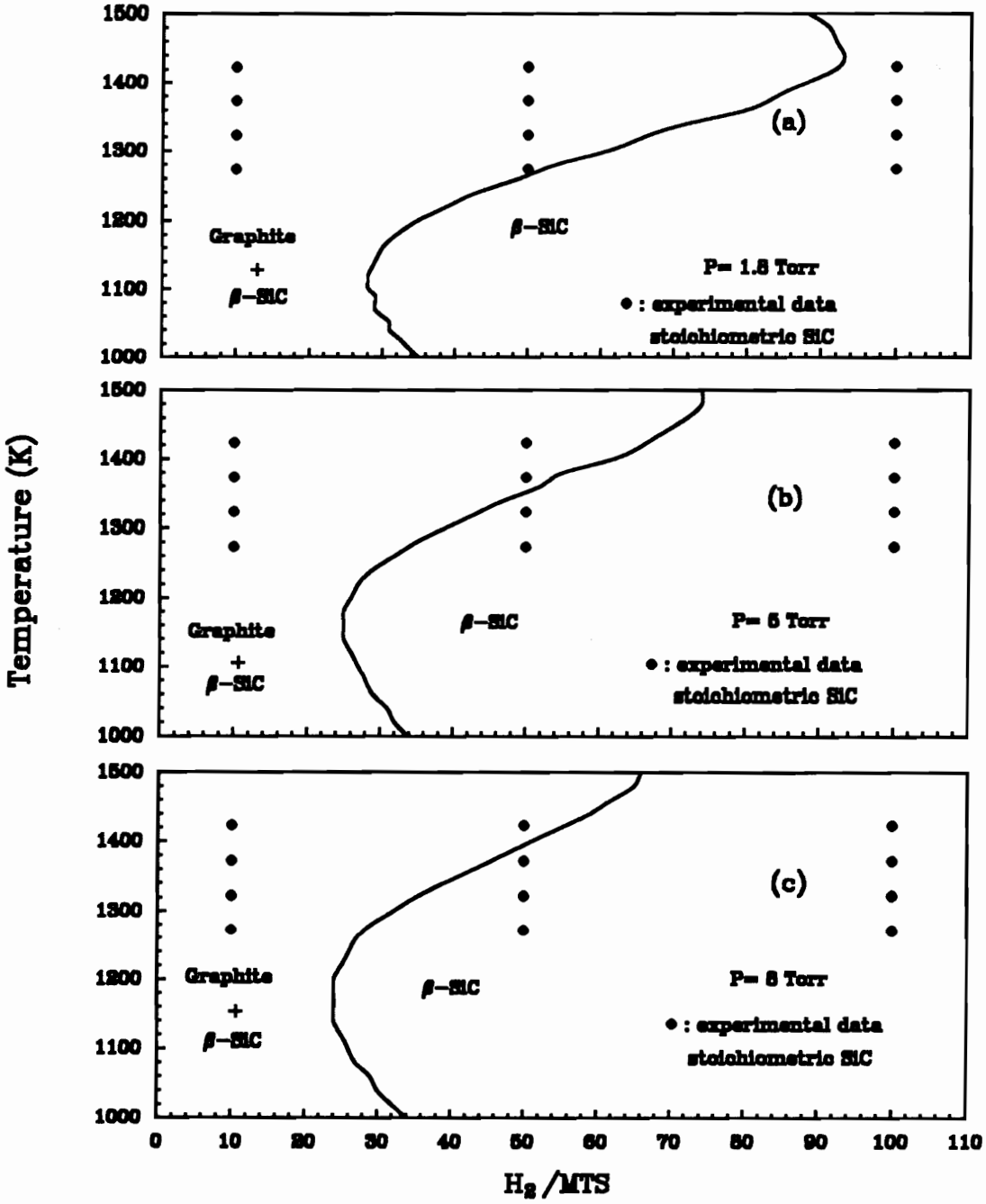

Figure 5.3: Comparison of the experimental results from a hot wall reactor with the calculated CVD phase diagrams without considering the depletion effects for (a) 1.8 Torr, (b) 5 Torr, and (c) 8 Torr.

In contrast to Fig. 5.3, the CVD phase diagrams for MTS–H_2 system in a hot wall reactor and the comparison with the experimental results are given in Fig. 5.4. In comparison with the results from the cold wall CVD reactors (Figs. 5.2 and 5.3), the boundaries between graphite+β–SiC and β–SiC essential are not influenced by the depletion factor from the hot wall reactor at temperatures lower than 1100 K. This is because the depletion effect was not prominent under lower deposition temperatures. However, it is clear that the boundaries between graphite+β–SiC and β–SiC move toward smaller values of H_2/MTS with increasing deposition temperature (T > 1100K) and pressure. The regions for Si+β–SiC and/or Si are also obtained with increasing deposition pressures and at high temperatures (*e.g.* Figs. 5.4(b) and 5.4(c)). With increasing temperature, the compositions of the deposit phases seem to be more dependent on the deposition pressure than those for cold wall reactor (Figs. 5.2 and 5.3) under the range of temperature and H_2/MTS ratios considered in this study. As shown in Fig. 5.4, the regions containing the deposition or codeposition of Si are to be moved toward lower temperatures and low H_2/MTS ratios with increasing deposition pressure. This is because of the depletion effect inherited from the hot wall reactor, which is more significant with increasing deposition temperature and pressure. Therefore, β–SiC was expected to be codeposited with Si at higher deposition pressure in a hot wall CVD reactor. The codeposition of Si with SiC is also evidenced by the experimental results obtained from the literatures using MTS–H_2 gas system as the SiC precursor in a hot wall reactor [26–29].

Since the calculated boundaries between graphite+β–SiC and β–SiC move toward smaller values of H_2/MTS as shown in Fig. 5.4, the experimental data at 1.8, 5, and 8 Torr agree much better than those without the consideration of

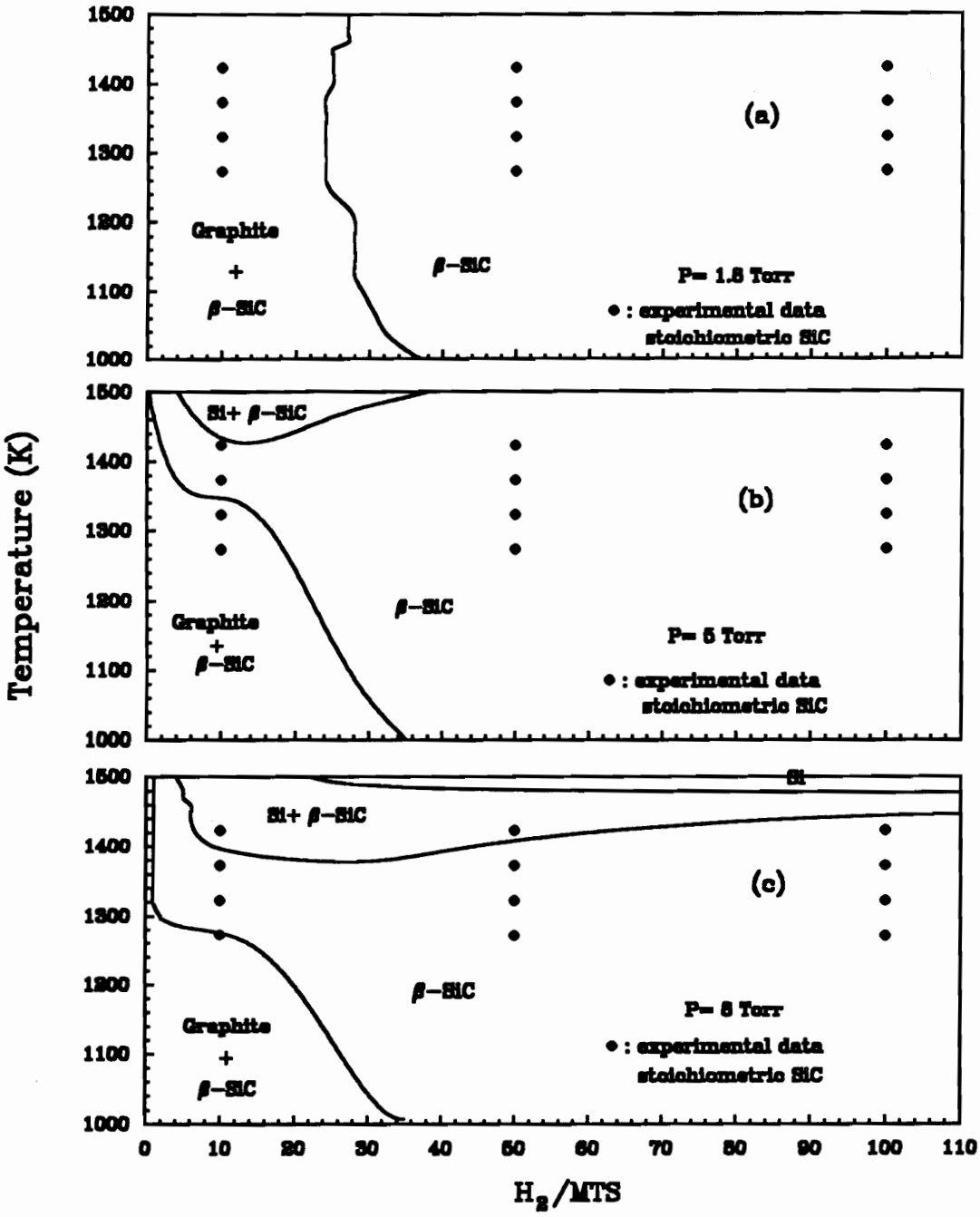

Figure 5.4: Comparison of the experimental results from a hot wall reactor with the calculated CVD phase diagrams with considering the depletion effects for (a) 1.8 Torr, (b) 5 Torr, and (c) 8 Torr.

depletion factors, especially under high H_2/MTS ratios (Figs. 5.2 and 5.3). However, for lower deposition pressures of 1.8 and 5 Torr (Figs. 5.4(a) and 5.4(b)), the experimental boundaries between the regions of graphite+β–SiC and β–SiC appear to be located at the lower values of H_2/MTS ratios and temperatures. The boundary between β–SiC and Si+β–SiC also seems to be moved toward the region of calculated region for Si+β–SiC at 8 Torr (Fig. 5.4(c)). The same phenomenon is also depicted in Fig. 5.5 which shows the calculated phase diagram and the experimental results at 10 Torr from Motojima et al [29]. These indicate that the deposition of single–phase β–SiC is not only influenced by the thermodynamic equilibrium factor but also by the dynamic ones. According to Fischman et al. [2], the expansion of single phase β–SiC toward the region of graphite+β–SiC at lower H_2/MTS ratios can be explained by a higher rate of deposition of silicon than carbon because the primary intermediate species carrying Si are polar molecules, whereas the primary molecules bearing carbon are nonpolar. On the other hand, the shift of the boundaries between β–SiC and Si+β–SiC toward the region for Si+β–SiC was believed to be due to the suppression of the deposition of free Si under high linear velocity of gas flux at low deposition pressures and high temperature. Therefore, as shown in Fig. 5.6, the experimental regions for single phase of β–SiC should be larger than those from the calculated CVD phase diagrams at low pressure and in hot wall reactor.

5.5 SUMMARY:

A new model considering both the depletion effects and equilibrium thermodynamics was proposed to calculated the CVD phase diagrams in a hot wall

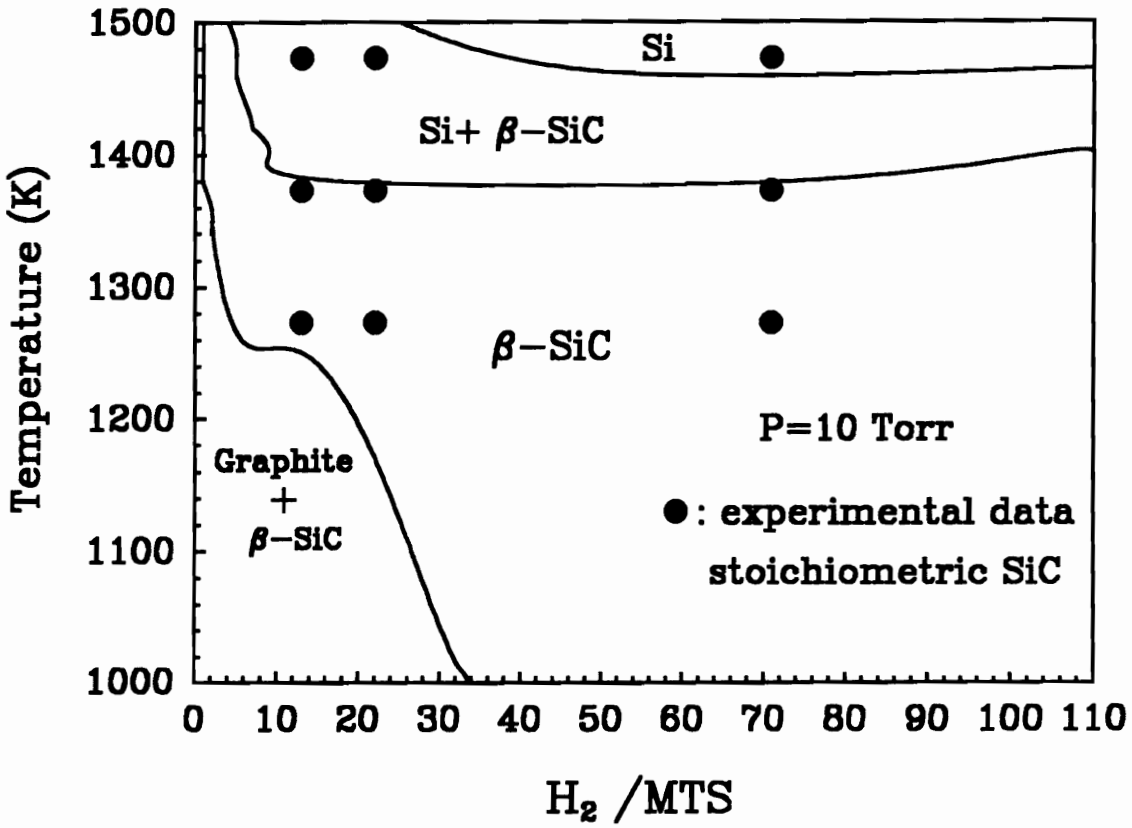

Figure 5.5: Comparison of the local CVD phase diagram with the experimental results quated from Ref. 27 at 10 Torr.

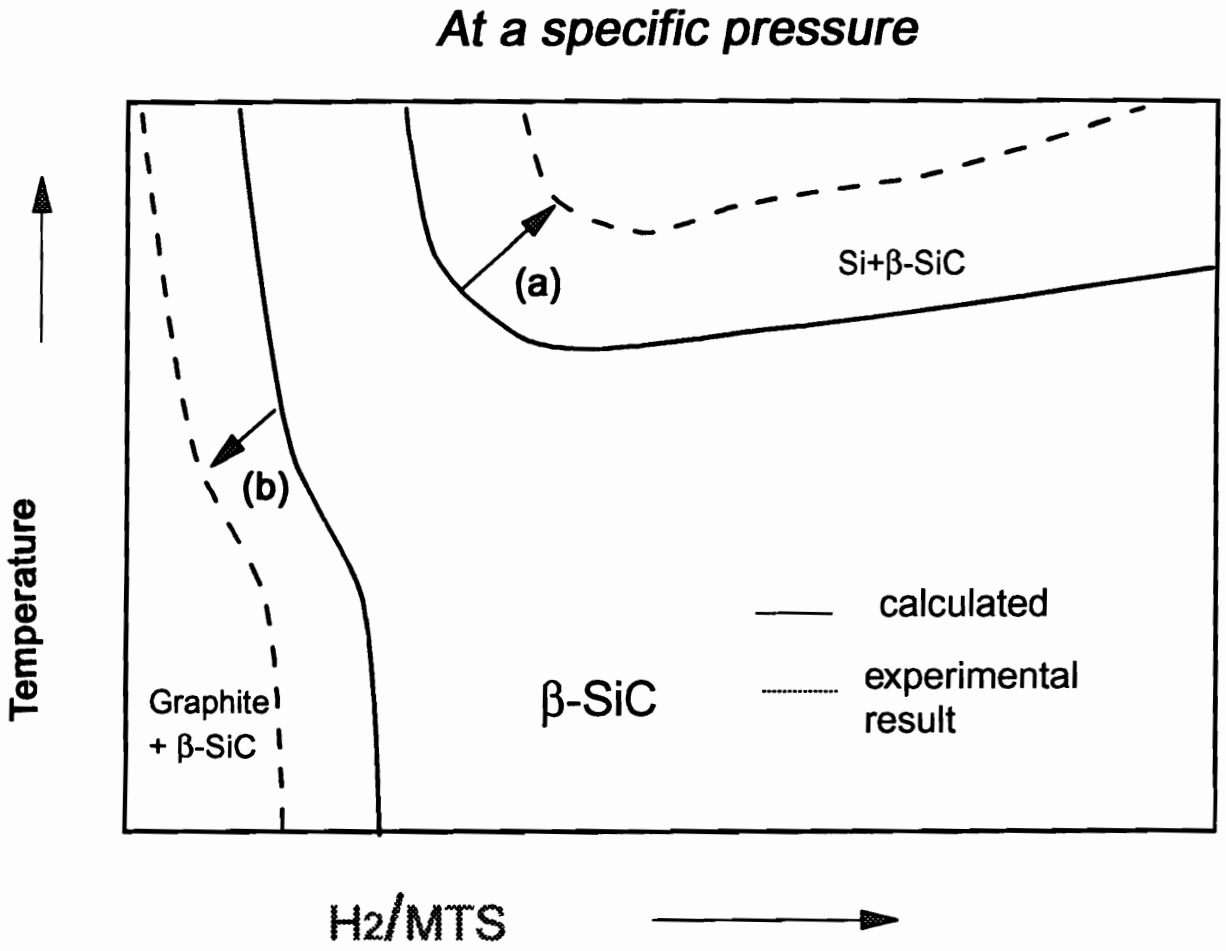

Figure 5.6: The schematic local CVD phase diagram representing the effects of (1) high velocity of gas flux and (2) polarity of the Si carrying interimediate species on the boundaries between regions.

reactor. For the deposition of SiC from MTS–H_2 gas system, in comparison with the CVD phase diagrams without considering the depletion effects, the calculated equilibrium CVD phases diagrams in a hot wall CVD reactor showed better agreement between the calculated and experimental results and depicted that the composition of the deposit was strongly influenced by the deposition pressure. It is also shown that Si starts to deposit or codeposit with SiC with increasing deposition temperature and pressure because of the depletion effects. The discrepancies between the calculated and experimental results were probably attributed to a high linear velocity of the gas flux at low pressure and polarity of the Si carrying molecules.

5.5 REFERENCES:

1. F. Langlais, F. Hottier, and R. Cadoret, J. Cryst. Growth, **56**, 659 (1982).
2. G.S. Fischman and W.T. Petuskey, J. Am. Ceram. Soc., **68**, 185 (1985).
3. A.I. Kingon, L.J. Lutz, P. Liaw, and R.F. Davis, J. Am. Ceram. Sco., **66**, 558 (1983).
4. K. Minato and K. Fukuda, J. Nuclear Mater., **149**, 233 (1987).
5. S.A. Gokoglu, in *Chemical Vapor Deposition of Refractory Metal and Ceramics II*, edited by T.M. Besmann, B.M. Gallois, and J.W. Warren (Mater. Res. Soc. Symp. Proc. vol. **250**, Mater. Res. Soc., Pittsburgh, PA, 1992), p. 18.
6. F. Langlais, C. Prebenge, B. Tarride, and R. Naslain, J. de Physique, Colloque c5, supplément au n° 5, Tome 50, C5–93 (1989).

7. D. Neuschütz and F. Salehomoum, in *Chemical Vapor Deposition of Refractory Metal and Ceramics II*, edited by T.M. Besmann, B.M. Gallois, and J.W. Warren (Mater. Res. Soc. Symp. Proc. **250**, Mater. Res. Soc., Pittsburgh, PA, 1992), p. 41.

8. F. Langlais and C. Prebende, in *Prec. 11th Int. Conf. on CVD*, edited by K.E. Spear and G.W. Cullen (The Electrochem. Soc., Pennington, NJ, 1990), p. 686.

9. S.A. Gokoglo and M.A. Kuczmarski, in *Proc. of the 12th Int. Symp. on Chemical Vapor Deposition 1993*, edited by K.F. Jeusen and G.W. Cullen (The Electrochem. Soc., Inc., Pennington, NJ, Proc. vol. **93–2**), p. 392.

10. J. Schlichting, Powder Metall. Int., **12**[3], 141 (1980), contined in [4], 196 (1980).

11. R.C. Marshall, in *Silicon Carbide–1973*, edited by R.C. Marshall, J.W. Faust, Jr., and C.E. Ryan, University of South Carolina Press, Columbia, SC, 1974.

12. M. Matsunami, S. Nishino, and T. Tanaka, J. Cryst. Growth, **45**, 138 (1978).

13. D.P. Stinton, A.J. Caputo, and R.A. Lowden. Am. Ceram. Soc. Bull., **65**, 347 (1986).

14. C.Y. Tsai, S.B. Desu, and C.C. Chiu, J. Mater. Res., **9**, 104 (1994).

15. C.C. Chiu, S.B. Desu, and C.Y. Tsai, J. Mater. Res, **8**, 2617 (1993).

16. B.W. Sheldon, in Solgasmix–PV for the PC, ORNL, Oct., 1989.

17. G. Eriksson, Acta Chem. Scand., **25**, 2651–2658 (1971).

18. W.B. White, W.M. Johnson, and G.B. Dantzig, J. Chem. Phys., **28**, 751 (1958).

19. T.M. Besmann, B.W. Sheldon, T.S. Moss III, and M.D. Kaster, J. Am. Ceram. Soc., **75**, 2899 (1992).

20. T.M. Besmann and M.L. Johnson, in *Proc. 3rd Int. Symp. on Ceramic Materials and Components for Engine*, Las Vegas, NV, 443–456 (1988).

21. J.N. Burgess and T. Lewis, Chem. and Industry, **19**, 76 (1974).

22. JANAF Thermochemical Tables, 3rd Edition, J. Phys. Chem. Reference Data, vol **14**, 1985.

23. Z.J. Chen and S.B. Desu, unpublished paper.

24. C.C. Chiu and S.B. Desu, J. Mater. Res., **8**, 535 (1993).

25. C.C. Chiu, S.B. Desu, G. Chen, C.Y. Tsai, and W.T. Reynolds, Jr., submitted to J. Mater. Res.

26. T.M. Besmann, B.W. Sheldon, and M.P. Kaster, Surface and Coating Technol., **43/44**, 167 (1990).

27. W. Schintlmeister, W. Wallgram, and K. Gigl, High Temp.–High Pressures, **18**, 211 (1986).

28. D.H. Kuo, D.J. Cheng, W.J. Shyy, and M.H. Hon, J. Electrochem. Soc., **137**, 3688 (1990).

29. S. Motojima and M. Hasegawa, J. Vac. Sci. Technol., **A8**, 3763 (1990).

Chapter 6: SUMMARY

The deposition of β–SiC thin films on Si(100) substrates has been systematically investigated by using the MTS–H_2 gas mixture in a horizontal, hot wall LPCVD reactor. The results of the present research are summarized as follows:

1. The procedure to form SiC buffer layers with smooth or porous morphology on Si(100) surfaces was developed. Optimum smooth SiC buffer layers with a thickness of 35Å was obtained from the chemical conversion of the Si(100) surface at a temperature of 1050° C for 60 minutes by using C_2H_2 and H_2. The reaction was highly active and resulted in the formation of porous morphology at a lower temperature (*e.g.* 1000° C) and a shorter time without the presence of H_2. The Si–rich converted SiC layers indicated that the Si atoms were supplied faster to the interface between C_2H_2 and the converted SiC layer than the C atoms. The presence of defects provided effective paths for the Si out–diffusion in the carburization process. A possible process for the formation of defects was also proposed.

2. With the formation of a smooth SiC buffer layer at 1050° C, stoichiometric and polycrystalline β–SiC thin films with smooth surfaces were successfully grown on Si(100) at the same temperature (1050°) by using a MTS–H_2 mixture in a hot wall CVD reactor. The deposited β–SiC thin films were also found to show a preferred orientation of β–SiC(111). Defect free Si substrates and smooth topography were favored by using lower MTS concentrations and/or lower deposition pressures. The stoichoimetric composition of the deposited film was also attributed to the lower deposition pressures which suppressed the formation of gaseous intermediate species and Cl radicals. The occurrence of the etching on

Si(100) substrates at higher MTS concentrations and deposition pressures was likely due to the presence of Cl radicals from the decomposition of MTS molecules while transporting from the entrance of the furnace to the substrate. Etching on Si(100) substrates at the temperature higher than that for buffer layer procedure (*i.e.* 1050° C) could be due to the out–diffusion of Si atoms and the presence of Cl radicals. A kinetic model was proposed and predicts very well with the experimental data by analyzing the deposition rates and the hot wall CVD process using the finite element method (FEM).

3. On porous Si(100) substrate, epitaxial β–SiC(100) thin films with a single crystal matrix and smooth surfaces were grown at 1150° C in a hot wall LPCVD reactor from the MTS–H_2 gas mixture for a short deposition time (12.5 min). This is the lowest temperature, which has been reported, used to grow single crystal β–SiC thin films in a hot wall reactor and using MTS as a precursor. Rotational β–SiC(100) crystals and polycrystalline β–SiC were formed on the top surface of the previously deposited matrix of single crystal β–SiC with increasing deposition time. The preferred orientation from (100) planes from polycrystalline β–SiC can only be grown with the deposition times shorter than 75 minutes. Further increased the deposition time (> 75 min), polycrystalline β–SiC(111) layer was observed. Poor surface morphology and polycrystalline β–SiC deposit can only be obtained at a lower deposition temperature (*i.e.* 1100° C). The highly preferred orientation (100) planes from β–SiC could be observed up to the deposition time of 150 minutes at this temperature. The (111) orientation from β–SiC was obtained at the deposition time of 200 minutes at 1100° C.

4. A new method for the calculation of CVD phase disgrams in a hot wall reactor was proposed by coupling the equilibrium thermodynamics to depletion effects. For the deposition of SiC from the MTS–H_2 gas system, the calculated CVD phase diagrams from this new method showed better agreement with the experimental results than the traditional CVD phase diagrams which do not consider the depletion effects in a hot wall reactor. It is also shown from the calculated CVD phase diagrams that the composition of the depsoit was strongly influenced by the deposition pressure and Si starts to deposit or codeposit with SiC at higher deposition temperatures and pressures. The disagreement with the experimental results were probably due to a high linear velocity of the gas flux at low pressure and the polarity of the intermediate Si carrying molecules.

VITA:

The author was born in Taiwan on March 30, 1963. Upon graduating from The High School of National Taiwan Normal University, he entered National Cheng Kung University, Tainan, Taiwan. He received his Bachelor of Science degree in Metallurgy and Materials Engineering in June, 1985. Since then, he served in the ROC army as a second lieutenant until August of 1987. In 1988, he joined Virginia Tech in Blacksburg to start his graduate work in Pb–based relaxor dielectric materials under the supervision of Dr. Seshu B. Desu. He received his Master of Science degree in Materials Engineering in 1990. And then he continued his Ph.D. work in chemical vapor deposition (CVD) of SiC in the same group.

He is a member of the American Ceramic Society and Materials Research Society.

Chienchia Chiu